



CZECH TECHNICAL UNIVERSITY IN PRAGUE
FACULTY OF BIOMEDICAL ENGINEERING
Department of Natural Sciences

Time-resolved luminescence spectroscopy of core-shell nanodiamonds
Časově rozlišená luminiscenční spektroskopie core-shell nanodiamantů

Master Thesis

Study programme: Biomedical and Clinical Technology
Study branch: Instruments and Methods for Biomedicine

Thesis supervisor: Ing. Dalibor Pánek, Ph.D.
Co-Supervisor: Ing. Vladimíra Petráková, Ph.D.

Bc. Milan Adelt

Kladno, May 2017

Diploma thesis assignment

(Master project thesis assignment)

Student: **Bc. Milan Adelt**
Study branch: Instruments and Methods for Biomedicine
Title: **Time-resolved luminescence spectroscopy of core-shell nanodiamonds**
Title in Czech: Časově rozlišená luminiscenční spektroskopie core-shell diamantových nanočástic

Instructions for processing:

Diamond nanoparticles (ND) can be modified to contain very stable luminescent point defects termed Nitrogen-Vacancy centers (NV). Luminescent ND can be distinguished in the cellular environment from the cell autofluorescence by a substantially longer luminescence lifetime of NV centers (typically around 15 ns). This can be used to advantage in a development of new intracellular reporters or biosensors based on ND. One of the most common way of preparation of ND is milling crystals synthesized by a high pressure and high temperature (HPHT) method which produces nanoparticles of various shapes and sizes but also a number of point defects which can alter energy state structure of NV centers. Luminescence of NV centers is sensitive to surface modifications and, moreover, to interactions with immediate environment of nanoparticles. Characterization of heterogeneity of ND luminescence and detailed understanding of the influence of the surrounding environment on luminescence are therefore necessary for a practical use of ND in a biomedical research. Develop a methodology for evaluation of heterogeneity of luminescence properties of ND using single-particle time-resolved luminescence measurements. Discuss the dependence of the ND luminescence lifetime on the surrounding environment.

References:

- [1] Vladimíra Petráková, Andrew Taylor, Irena Kratochvílová, František Fendrych, Jiří Vacík, Jan Kučka, Jan Štursa, Petr Cígler, Miroslav Ledvina, Anna Fišerová, Peter Kneppo, Miloš Nesládek, Luminescence of Nanodiamond Driven by Atomic Functionalization: Towards Novel Detection Principles, *Advanced Functional Materials*, Vol. 22, 2012, February, 812-819 s., DOI:10.1002/adfm.201101936
- [2] Asma Khalid, Kelvin Chung, Ranjith Rajasekharan, Desmond W.M. Lau, Timothy J. Karle, Brant C. Gibson, Snjezana Tomljenovic-Hanic, Lifetime Reduction and Enhanced Emission of Single Photon Color Centers in Nanodiamond via Surrounding Refractive Index Modification, *Scientific Reports*, Vol. 5, 2015, 11179 s., DOI: 10.1038/srep11179
- [3] V. Petrakova, V. Benson, M. Buncek, A. Fiserova, M. Ledvina, J. Stursa, P. Cigler, M. Nesladek, Imaging of transfection and intracellular release of intact, non-labeled DNA using fluorescent nanodiamonds, *Nanoscale*, Vol. 8, 2016, 12002 s., DOI: 10.1039/c6nr00610h

Validity of assignment until date: 20.08.2018

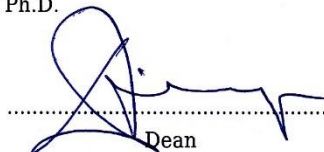
Supervisor of diploma thesis: Ing. Dalibor Pánek, Ph.D.

Consultant of diploma thesis: Ing. Vladimíra Petráková, Ph.D.



Head of Department

In Kladno, 08.02.2017



Dean

Katedra přírodovědných oborů

Akademický rok: 2016/2017

Zadání diplomové práce

Student: **Bc. Milan Adelt**
Studijní obor: Přístroje a metody pro biomedicínu
Téma: **Časově rozlišená luminiscenční spektroskopie core-shell diamantových nanočástic**
Téma anglicky: Time-resolved luminescence spectroscopy of core-shell nanodiamonds

Zásady pro vypracování:

Diamantové nanočástice (ND) mohou být upraveny tak, aby obsahovaly velmi stabilní luminiscenční bodové poruchy, centra dusík-vakance (NV). Luminiscenční ND lze v buněčném prostředí odlišit od buněčné autofluorescence zejména na základě podstatně delší doby života luminiscence center NV (typicky okolo 15 ns). Toho lze s výhodou využít při vývoji nových intracelulárních reporterů či biosenzorů založených na ND. Nejběžnější způsob přípravy luminiscenčních ND je mletím krystalů připravených syntézou za vysokého tlaku a vysoké teploty (HPHT), při které vznikají nanočástice o různých tvarech a velikostech, ale i množství bodových poruch, které mohou měnit strukturu energetických stavů center NV. Luminiscence center je navíc ovlivněna povrchem nanočástic a tedy interakcí s bezprostředním okolím nanočástic. Charakterizace vlastní heterogenity luminiscence ND a detailní porozumění vlivu prostředí na luminiscenci jsou tudíž nezbytné pro praktické využití ND v biomedicínském výzkumu.

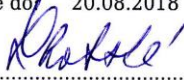
Navrhnete metodiku pro posouzení heterogenity luminiscenčních vlastností ND s využitím časově rozlišených měření luminiscence jednotlivých ND. Diskutujte závislost doby života luminiscence ND na vlastnostech prostředí, ve kterém se částice nacházejí. Stejnou metodiku použijte pro charakterizaci luminiscence core-shell ND, tj. ND zapouzdřených v oxidu křemičitém.

Seznam odborné literatury:

- [1] Asma Khalid, Kelvin Chung, Ranjith Rajasekharan, Desmond W.M. Lau, Timothy J. Karle, Brant C. Gibson, Snjezana Tomljenovic-Hanic, Lifetime Reduction and Enhanced Emission of Single Photon Color Centers in Nanodiamond via Surrounding Refractive Index Modification, Scientific Reports, Vol. 5, 2015, 11179 s., DOI: 10.1038/srep11179
- [2] Vladimíra Petráková, Andrew Taylor, Irena Kratochvílová, František Fendrych, Jiří Vacík, Jan Kučka, Jan Štursa, Petr Cígler, Miroslav Ledvína, Anna Fišerová, Peter Kneppo, Miloš Nesládek, Luminescence of Nanodiamond Driven by Atomic Functionalization: Towards Novel Detection Principles, Advanced Functional Materials, Vol. 22, 2012, February, 812-819 s., DOI:10.1002/adfm.201101936
- [3] V. Petrakova, V. Benson, M. Buncek, A. Fiserova, M. Ledvina, J. Stursa, P. Cigler, M. Nesladek, Imaging of transfection and intracellular release of intact, non-labeled DNA using fluorescent nanodiamonds, Nanoscale, Vol. 8, 2016, 12002 s., DOI: 10.1039/c6nr00610h

Vedoucí: Ing. Dalibor Pánek, Ph.D.
Konzultant: Ing. Vladimíra Petráková, Ph.D.

Zadání platné do: 20.08.2018


vedoucí katedry / pracoviště


děkan

V Kladně dne 05.01.2017

Annotation

This diploma thesis presents the study of fluorescent lifetime heterogeneity of nitrogen-vacancy centres in fluorescent diamond nanoparticles. The thesis also introduces the methodology developed for measurement and evaluation of heterogeneity of luminescence properties of nanodiamonds using single-particle time-resolved luminescence measurements based on Time Correlated Single Photon Counting (TCSPC). The dependence of the luminescence lifetime of nanodiamonds on refractive index of the surrounding environment is discussed as well. Same method is applied on core-shell nanodiamonds of the same type, coated in silica shells of various thicknesses, created by a novel approach, which allows a comparison with the source diamond nanoparticles. First part of the thesis includes theoretical overview of nanodiamond material and its classification, fluorescent nitrogen-vacancy defects and their fluorescence properties as well as their synthesis. Following part of the thesis describes used experimental methods and measurements procedures in single-particle measurements. Optimal measurement conditions and methodology of sample preparation and substrate purification are demonstrated and evaluated to meet requirements such as single nanodiamond crystal distribution. Then the number of NV centres in measured particles was studied through observation of photon antibunching. Multiple NV centres in examined nanodiamonds were observed. Single-particle measurements were performed on greater populations of selected nanodiamonds in order to determine and assess fluorescence lifetime heterogeneity of nanodiamonds. Effect of the change of refractive index of surrounding media on fluorescence intensity and lifetime was investigated. The influence of refractive index of surrounding media on fluorescence intensity of NV centres showed to be a function of various defined factors. It was confirmed that fluorescence lifetime of nanodiamonds decreases in presence of the surrounding environment with increasing refractive index.

Key Words: Nanodiamonds, fluorescence, fluorescence lifetime, refractive index, TCSPC, nitrogen-vacancy

Anotace

Tato diplomová práce uvádí studii zabývající se heterogenitou doby života fluorescence center dusík-vakance ve fluorescenčních diamantových nanočásticích. Práce dále uvádí metodologii vytvořenou pro měření a vyhodnocení heterogenity luminiscenčních vlastností nanodiamantů s využitím jedno-částicových časově rozlišených luminiscenčních měření založených na časově korelovaném čítání jednotlivých fotonů (TCSPC). Rovněž je diskutována závislost doby života luminiscence nanodiamantů na indexu lomu okolního prostředí. Stejná metoda je aplikována na tzv. core-shell nanodiamanty shodného typu, obalené ve vrstvě oxidu křemičitého (silica), vytvořené novou metodou, což umožňuje přímé srovnání se zdrojovými diamantovými nanočásticemi. První část diplomové práce obsahuje teoretický přehled o nanodiamantovém materiálu a jeho klasifikaci, fluorescenčních poruchách dusík-vakance a jejich fluorescenčních vlastnostech, včetně jejich syntézy. Následující část popisuje použité experimentální metody a měřicí postupy v měření na jednotlivých částicích. Jsou představeny a vyhodnoceny optimální podmínky a metodologie přípravy vzorků a čištění substrátu za účelem splnění požadavků jako je přítomnost jednotlivých nanodiamantových krystalů na substrátu. Byl studován počet NV center ve zkoumaných částicích pomocí antibunchingu fotonů. Byla zjištěna přítomnost více NV center ve zkoumaných nanodiamantech. Měření na jednotlivých částicích byla provedena na větší populacích nanodiamantů za účelem určení a posouzení heterogenity doby života fluorescence. Dále byl zkoumán vliv indexu lomu okolního prostředí na intenzitu a dobu života fluorescence nanodiamantů. Vliv indexu lomu okolního prostředí na fluorescenční intenzitu nanodiamantů je funkcí více definovaných faktorů. Bylo potvrzeno, že doba života fluorescence nanodiamantů se snižuje s rostoucím indexem lomu okolního prostředí.

Klíčová slova: Nanodiamanty, fluorescence, doba života fluorescence, index lomu, TCSPC, dusík-vakance

Acknowledgement

It is my great pleasure to express my sincere thanks to my supervisor Dr. Dalibor Panek, for all the given advices, trust, support, motivation and knowledge passed on me during my work on this thesis. I would also like to thank him for all the time he devoted to me and most valuable guidance which helped me to complete my experiments and data analysis.

I would like to thank to my co-supervisor Dr. Vladimira Petrakova for introducing me to the world of nanodiamonds and chance to work on this topic.

Further, I would like to thank to my fellow colleagues from our nanogroup for their cooperation and discussions over the topic and related problematics.

It is my great pleasure to express my thanks to Dr. Petr Cigler and Jan Vavra from Institute of Organic Chemistry and Biochemistry of the CAS for their help in the beginning of the project and for providing us with nanodiamond samples.

Declaration

I hereby declare that I have completed this thesis with the topic Time-resolved luminescence spectroscopy of core-shell nanodiamonds independently and I have attached a full list of used references and citations.

I do not have a compelling reason against the use of the thesis within the meaning of Section 60 of the Act No.121/2000 Coll., on copyright, rights related to copyright and amending some laws (Copyright Act).

In Kladno, date.....

.....
students signature

Table of contents

List of symbols	6
List of abbreviations	8
List of figures	10
1. Introduction	13
1.1. Aims of the thesis	15
2. Theoretical background	16
2.1. Nanodiamonds	16
2.1.1. Crystal structure	16
2.1.2. Classification of nanodiamonds	17
2.1.3. Synthesis of nanodiamonds	19
2.1.3.1. Detonation diamonds	19
2.1.3.2. CVD diamonds	20
2.1.3.3. High-pressure high-temperature diamonds (HPHT)	21
2.2. Coloration and fluorescent defects in diamond	23
2.2.1. Nitrogen-vacancy centres	23
2.2.2. Generation of NV centres	26
3. Experimental methods and instrumentation	27
3.1. Fundamentals of measurement methods	29
3.1.1. Confocal Microscopy	29
3.1.2. Contact angle measurement	30
3.1.3. Fluorescence Spectroscopy	31
3.1.4. Time correlated single photon counting (TCSPC)	33
3.1.4.1. TCSPC instrumentation	35
3.1.4.2. Timing electronics and acquisition modes	37
3.1.4.3. Timing resolution and convolution integral	39
3.1.4.4. Least -Squares Analysis	41
3.1.4.5. Analysis of multi-exponential decays	43
3.1.4.6. Intensity decay law	43
3.1.5. Fluorescence lifetime imaging microscopy (FLIM)	45
3.2. Instrumentation used in the thesis	46
3.3. Sample preparation	47
3.3.1.1. Substrate purification	47
3.3.1.2. Sample preparation and contact angle measurement	49
3.4. Measurement procedure	57

3.4.1.	Single particle imaging and decay measurement	57
3.4.1.1.	Scattering of excitation light on nanodiamonds.....	57
3.4.1.2.	Motion drift of the particle.....	58
3.4.1.3.	Diffraction limited resolution	60
3.4.1.4.	Determination of excitation frequency	62
3.4.1.5.	Instrument Response Function acquisition	66
3.4.1.6.	Fluorescence decay measurement.....	68
3.4.2.	Photon antibunching.....	69
3.4.3.	Measurement of single particle saturation intensity	70
4.	Results and discussion	71
4.1.	Number of NV centres in measured particles	71
4.2.	Assessment of heterogeneity of fluorescence lifetime	74
4.2.1.	Single-particle fluorescence decay analysis	74
4.2.2.	Analysis of fluorescence decay heterogeneity of nanodiamonds	75
4.2.2.1.	Fluorescence decay analysis of uncoated nanodiamonds NDs104.....	76
4.2.2.2.	Fluorescence decay analysis of silica coated nanodiamonds JV39-1	77
4.2.2.3.	Fluorescence decay analysis of silica coated nanodiamonds JV39-4.....	78
4.2.3.	Absorption cross section estimation	80
4.3.	Effect of the change of refractive index of surrounding media on fluorescence lifetime and intensity	84
4.3.1.	The correct choice of „Average“ fluorescence lifetime	89
5.	Conclusions and perspective	92
	References	95

List of symbols

Symbol	Unit	Meaning
B	T	Magnetic field (induction)
c	$\text{m}\cdot\text{s}^{-1}$	Speed of the light
CoM		Centre of mass
D	Hz	Zero field splitting
D_k		Deviations under decay curve
E_{photon}	J	Energy of single photon, in fluorescence saturation measurements
f_i	%	Fractional steady-state intensities in a multi-exponential intensity decay
h	J·s	Planck's constant
I_{MAX}	counts	Maximum obtainable intensity count rate, in fluorescence saturation measurements
$I_c(t_k)$		Fitted function
$I(0)$		Intensity at time zero
$I(P)$	counts	Count rates for the given emitter, in fluorescence saturation measurements
$I(t)$	counts	Impulse response function
k_e	s^{-1}	Decay rate of the excited state
$L(t_k)$	counts	Decay intensity
m_s		spin states
n		Refractive index
$N(t_k)$	counts	Number of counts per channel, in time-correlation single-photon counting
NA		Numerical aperture
n_d		Number of data points, in nonlinear least square analysis

n_i		Number of detected photons, in centre of mass calculation
P	W	Excitation power
p		Number of floating parameters
P_{SAT}	photons·m ⁻² ·s ⁻¹	Saturation intensity
S		Spin multiplicity
SNR		Signal-to-noise ratio
t	s	Time of acquisition
t_i	s	Time channel, in centre of mass calculation
t_k	s	Time of excitation
α_i	counts	Pre-exponential factors in a multi-exponential intensity decay
γ	rad·s ⁻¹ T ⁻¹	Gyromagnetic ratio
$\gamma_{l/v}$	N·m ⁻¹	Liquid-vapour tension
$\gamma_{s/l}$	N·m ⁻¹	Solid-liquid surface tension
$\gamma_{s/v}$	N·m ⁻¹	Solid-vapour tension
Δ	m	Diffraction limit
θ_γ	°	Contact angle
λ	m	Wavelength of the excitation laser beam
ν		Number of degrees of freedom
σ^2		Variance
σ_A	m ²	Optical cross section for absorption
τ	s	Fluorescence lifetime
τ_i	s	Fluorescence lifetime of i -th decay component
τ_{AVG}^A	s	Amplitude average fluorescence lifetime
τ_{AVG}^I	s	Intensity average fluorescence lifetime
χ^2		Goodness of fit

List of abbreviations

Abbreviation	Meaning
ADC	Analogue to digital converter
AFM	Atomic force microscopy
B	Boron
BP	Band pass filter
C	Carbon
CH	Channel information
CVD	Chemical vapour deposition
FCS	Fluorescence correlation spectroscopy
FLIM	Fluorescence lifetime imaging microscopy
FTIR	Fourier transform infrared spectroscopy
FWHM	Full width at half maximum
HPHT	High pressure high temperature
IR	Infrared
IRF	Instrument response function
LCU	Laser coupling unit
LP	Long pass
M	External marker
N	Nitrogen
NCD	Nano-crystalline diamond
ND	Nanodiamond
NIR	Near-infrared
NLLS	Nonlinear Least Squares
NV	Nitrogen-vacancy
OD	Optical density, grey filter
PEI	Polyethylenimine
PEI-ND	Polyethylenimine-nanodiamond complex
PGA	Programmable gain amplifier
PL	Photoluminescence
PMT	Photomultiplier
ROI	Region of interest
SIMS	Secondary ion mass spectroscopy
SP	Short pass filter
SPAD	Single photon avalanche diode
TAC	Time-to-amplitude converter
TCSPC	Time-correlated single photon counting
TEM	Transmission electron microscopy

TEOS	Tetraethyl orthosilicate
TTTR	Time-tagged time-resolved
UNCD	Ultra-nanocrystalline diamond
UV	Ultraviolet part of electromagnetic spectrum
VIS	Visible part of electromagnetic spectrum
WD	Window discriminator
ZPL	Zero phonon line

List of figures

Figure 1: Diamond crystal structure . Dark circular objects represent carbon atoms linked with bonds, forming cubic crystal structure. ^[2]	16
Figure 2: Characteristics and diversification of diamond types.	18
Figure 3: The arrangement of dopants in diamond lattice with respect to the classification. C-carbon atoms which form diamond lattice, N-nitrogen atoms in several ways of aggregation, B-boron dopants. Modified from [23].....	19
Figure 4: Diamond CVD model. a) Decomposition of methane to methyl radicals and hydrogen to obtain source for diamond growth and b) generation of place for carbon addition. ^[22]	20
Figure 5: CVD diamond structure with bonded nitrogen atoms. ^[22]	21
Figure 6: Schematic view of diamond crystal lattice with a) NV centres ^[3] and b) fluorescence spectrum of nanodiamond ^[30] . Black lines in b) indicate zero-phonon lines of NV0 (576 nm) and NV – (638 nm) centres.....	24
Figure 7: Three level energy diagram of NV centre with detailed energy level scheme of triplet ground (³ A) and excited (³ E) states, metastable (¹ A) state and diagram depicting effect of magnetic field on energy levels of the ground state. D is zero-field splitting and 2γB is Zeeman splitting, where γ is gyromagnetic ratio, B is magnetic field. Wiggly arrows indicate radiative transitions and straight lines strong and weak nonradiative decay via singlet state. Modified from [7]	25
Figure 8: Block diagram of the experiment.....	28
Figure 9: A schematic of laser scanning confocal microscope. ^[33]	30
Figure 10: Illustration of contact angles for situations with a) hydrophilic (small values of contact angle) and b) hydrophobic surfaces (high values of contact angle). ^[34]	31
Figure 11: Jablonski diagram. Horizontal lines represent electronic states. Solid vertical lines represent radiative transitions and absorption. Dotted lines illustrate radiationless transitions. S ₁ and S ₂ are singlet states and T ₁ triplet state. Modified from [36].....	33
Figure 12: The principle of time-resolved fluorescence measurement of start-stop times with TCSPC. ^[38]	34
Figure 13: Principle of TCSPC and fluorescence decay acquisition. a) Principle of TCSPC ^[37] and b) histogram of start-stop times measured with TCSPC ^[38] . Pulses in the middle of a) are pulses from a discriminator generated as an indication of photon arrival ...	34
Figure 14: The effect of dead time and pile-up effect on the TCSPC histogram. a) effect of dead time of the detector on data acquisition and b) distortion of the histogram due to pile-up effect. ^[38]	35
Figure 15: A schematic of TCSPC device and arrangement of individual components ^[37] S is sample, CFD is constant fraction discriminator, TAC is time-to-amplitude converter, WD is window discriminator, PGA is programmable gain amplifier, ADC is analogue-to-digital converter	36
Figure 16: A principle of Time-Tagged Time-Resolved measurement. Start-stop times (t), arrival time of photon with respect to the start of the experiment (T), channel information dependent on fluorescence properties of the photon (CH), external marker characterizing the movement of the scanner (M). ^[38]	37
Figure 17: A principle of T3 mode. ^[39]	38
Figure 18: A principle of T2 mode function. ^[39]	39

Figure 19: Convolution of the impulse response function $I(t)$ with a) excitation pulses or b) lamp profile $L(t_k)$. ^[37]	40
Figure 20: Example of the real fluorescence decay of nanodiamond (upper set of curves) fitted with four-exponential model and residuals (lower black horizontal curve) representing goodness of the fit.	44
Figure 21: A schematic of the used confocal setup. [courtesy of Katerina Zambochova, modified]	46
Figure 22: FLIM scan 20x20 μm of untreated coverslip with related fluorescence lifetime histogram.	48
Figure 23: FLIM scan 20x20 μm of coverslip cleaned in the sonicator with related fluorescence lifetime histogram.	48
Figure 24: FLIM scan 20x20 μm of coverslip cleaned in the sonicator and etched with NaOH with related fluorescence lifetime histogram.	48
Figure 25: A schematics of arrangement of diamond nanoparticles according to the substrate. NDs are deposited on a) oxidized substrate, which leads to the clustering due to same polarity of NDs and the substrate, and b) polymer-coated substrate, which electrostatically binds negatively charged NDs and stabilizes their position on the substrate. Purple corrugated layer coating the blue coverslip represents positively charged Polyethylenimine.	50
Figure 26: Contact angles of water droplets on various substrates. Water droplets on the A) non-treated substrate, B) oxygen-terminated substrate, C) Polyethylenimine-coated substrate. ^[30]	51
Figure 27: FLIM scans (10x10 μm) of PEI before (left) and after (right) irradiation with high excitation power. Red-marked region indicates photobleached area and subsequent elimination of fluorescent molecules.	52
Figure 28: An example of FLIM scan of diamond sample before (left) and after (right) photobleaching of fluorescent molecules of non-diamond character. Green dots in the photobleached area represent fluorescence emitting nanodiamonds.	53
Figure 29: An example of FLIM scan of sample JV39-1 (silica coated) with overall lifetime histogram.	54
Figure 30: Representation and structure of investigated source nanodiamonds NDs104 (left) and silica coated JV39-1 (right)	54
Figure 31: Example of FLIM scan 10x10 μm of JV39-1 showing required distribution of NDs prepared from 0,0032 mg/ml ND solution from the determined optimal range concentrations.	55
Figure 32: Comparison of fluorescence decays of NDs104 with a) indicated distortion of the curve peak caused by the scattering and b) reduction of the fluorescence signal due to the BP filter 635 ± 10 . Black curve indicates fluorescence decay of the particle with the use of BP 635/10 nm filter and orange indicates fluorescence decay with the contribution from the scattered light recorded with SP 750 nm.	57
Figure 33: Motion drift of the observed NDs during the long measurement supplemented with a decreasing time trace signal due to the drift.	58
Figure 34: Position of the cross indicator on the particle a) in the beginning of the measurement	59
Figure 35: Diffraction-limited FLIM scan of NDs104 (60 nm single crystal). The highlighted area indicates a diffraction limited-spot which represents observed ND particle.	61

Figure 36: Example of fluorescence decay of not fully relaxed NV centre.....	63
Figure 37: Comparison of dependencies of fluorescence intensity on excitation power for excitation frequency 1 MHz.....	63
Figure 38: Fluorescence lifetime histograms of fluorescent beads and uncoated diamonds NDs104 for selected excitation frequencies. Upper figures represent lifetime histogram and FLIM image of fluorescent beads, lower figures represent the same for multiple ND (NDs104).....	65
Figure 39: The on-axis beam spot of the back scattered light displayed on the video camera.	67
Figure 40: Example of instrument response function for the MicroTime 200 system (see 3.2.). Left: semi-logarithmic scale, right: linear scale.....	68
Figure 41: Typical setup for antibunching measurements. ^[43]	69
Figure 42: a) FLIM scan of NDs104 diamonds with marked measured particles. Second order correlation curve measured for b) cluster of nanodiamonds, c) + d) nanodiamonds with stronger emission, e) nanodiamond with weaker emission.....	72
Figure 43: Example of fluorescence decay of NDs104.....	74
Figure 44: Fluorescence decay heterogeneity a) and mean decay curve b) with indicated standard deviations of NDs104.....	76
Figure 45: Structured arrangement of silica embedden nanodiamonds JV39[courtesy of Dalibor Panek].....	77
Figure 46: Fluorescence decay heterogeneity a) and mean decay curve b) with indicated standard deviations of JV39-1.....	77
Figure 47: Fluorescence decay heterogeneity a) and mean decay curve b) with indicated standard deviations of JV39-4.....	78
Figure 48: Comparison of fluorescence decays of silica coated nanodiamonds (JV39-1, JV39- 4).....	79
Figure 49: Example of measured saturation curve data for JV39-4 with fitted curve.	80
Figure 50: Plot of dependence of laser power (532 nm, 20 MHz, 99%) on intensity [au]. [courtesy of Katerina Zambochova].....	81
Figure 51: Structured arrangement of NDs104 in a) air and b) water environment. [courtesy of Dalibor Panek].....	84
Figure 52: Example of FLIM scans with marked ND particles measured on air and later in water. Each measured particle marked with red arrow and related number was measured in air and later in water.	85
Figure 53: Fluorescence decay curves of ND particles and mean decay curves. Individual fluorescence decay curves for NDs104 measured on air a) and in water b) with plot of mean decay curves c) with indicated standard deviations.	85
Figure 54: Time trace signals of diamonds NDs104 measured on air and in water.	86

1. Introduction

With the development of modern scientific, medical and industrial methods, science and medicine gained not only new and useful information that allowed us deeper understanding of physiology of living organisms at the molecular level, but also new means for therapy and diagnostics. With these findings, it was suddenly possible to utilize and combine knowledge from many different fields of science and find a biomedical use of materials and chemical compounds where it was not possible before. New chemical and fabrication methods allowed to shrink these materials up to nanometre scale and discover their previously hidden features which were not apparent in their macroscopic form. This gave a foundation to a field of science nowadays called nanotechnology.

The typical example of such materials are certain semiconductors whose valence and conduction bands can be split into discrete energy levels by their shrinking. This principle is used to create nanometre luminescent semiconductors termed quantum dots. Quantum dots have the ability to emit photostable luminescence upon appropriate excitation. The great advantage of quantum dots is that the wavelength of their luminescence can be altered by their size which allows to accurately control their excitation and emission.^[1] Therefore, quantum dots represent a very useful tool widely used for biomedical applications, such as particle tracking or bioimaging. A great handicap of using quantum dots in biomedicine is their cytotoxicity.^[2]

The need to find a material which would be suitable for labelling and imaging while meeting the requirements, such as biocompatibility, stable luminescence or appropriate detection feature, led scientist to diamond. Mankind was always enthusiastic about diamonds and later, with the discovery of their outstanding mechanical features, they started to be used in industry as cutting and sharpening tools. Unique features of diamond are the proof that not only chemical composition but also an arrangement of atoms in the material holds the great importance.

In a recent few decades, there has been a rapid development in the production of nanomaterials. Fabrication methods such as chemical vapour deposition (CVD), detonation method or high-pressure high-temperature synthesis made synthesis of diamond nanocrystals possible. The shrinking enabled to create nanodiamond (ND) which inherits many excellent features of bulk diamonds, such as superior hardness, simple carbon chemistry, high biocompatibility and nontoxicity which makes them valuable tools for applications in biomedicine^[3,4] Their great advantage is the presence of various fluorescent color centres and lattice defects where some of them are useful as single photon sources. One of the most

commonly studied defect is termed nitrogen-vacancy (NV) centre composed from a vacancy and adjacent nitrogen atom. An important feature of NV centres is the ability to emit stable photoluminescence (PL) without negative effects such as photobleaching and photoblinking under normal conditions.^[4] Wavelengths of their fluorescence (550 nm – 750 nm, maximum around 700 nm) are also well separated from the emission range of cell autofluorescence. This and high quantum yield predetermines nanodiamond as a suitable marker for long term observations without suffering a photodegradation which is often a case of many fluorophores.^[5] Should we compare nanodiamonds with fluorescent dyes, fluorescent dyes are usually synthesized for a specific task or environment with the wide variability of excitation and emission wavelengths and quantum yields. Fluorescent dyes are also likely to photodegrade under the continuous excitation producing toxic residues.

This Thesis focuses on another remarkable feature of NV centres which is their fluorescence lifetime. The fluorescence lifetime of NV centres is noticeably longer (up to 25 ns) than observed in commonly used fluorescent dyes or probes (units of ns) ^[5-7]. Moreover, the fluorescence lifetime of NDs is widely heterogeneous and has been widely studied in dependence on various parameters, such as nitrogen content^[10,11], surface modifications^[12,13], refractive index (n)^[14-18], shape and size as a key information towards creation of ultimate fluorescent sensors for biology and cellular markers^[3-4,6-8], drug delivery and transfection of nuclei acids^[9], environment ^[14-16,18], electromagnetic field^[19]. For this reason, sensing capability of NV centres combined with unique chemical properties of diamond make nanodiamonds a very promising alternative to fluorescent dyes and quantum dots, since they can be utilized bare or modified in a wide spectrum of environments and applications.

Especially dependence of PL lifetime of NV centres on surrounding refractive index is quite a challenging topic assuming sensing a cellular environment in biomedical applications. As the PL lifetime of NDs vary according to their surroundings or cover, it can be assumed that the lifetime depends on changes in not only refractive index of the surrounding chemical environment but also on the thickness of the shell in which nanodiamonds are embedded in (core-shell systems). It was found that changes in the local refractive index affects the emission rate of NDs^[16]. In recent years there have been several experiments ^[14-16,18] which tried to solve this question and provide a valuable insight in this problematic and some ^[11,20-21] also tried to describe this dependence numerically.

1.1. Aims of the thesis

Use of nanoparticles in sensoric applications is conditioned by a suitable detection feature that provide information about the environment which nanoparticles are supposed to probe. Nanodiamonds possess such detection feature – fluorescence which, despite of many other excellent features, predetermines them for probing surrounding chemical environments usually containing many different chemical compounds with various properties.

This work is mainly interested in one particular property – refractive index of the surrounding environment and its effect on fluorescence lifetime behaviour of nanodiamonds. For fluorophores, this was described by Strickler and Berg. For nanodiamonds, it remains unclear whether they would react on changes in surrounding refracting index the same way or differently.

The main motive for realization of the presented thesis is to solve this question in our conditions.

Main aims of the thesis are to develop a methodology for evaluation of heterogeneity of luminescence properties of nanodiamonds using single-particle time-resolved luminescence measurements and to discuss the dependence of the ND luminescence lifetime on the surrounding environment. Specified constitutive aims are:

- Determine optimal conditions for single-particle measurements.
- Perform single-particle measurements on greater populations of selected diamond nanoparticles.
- Assessment of fluorescence lifetime heterogeneity of nanodiamonds.
- Confirm decrease of fluorescence lifetimes for silica embedded nanodiamonds.

Based on above mentioned knowledge and requirements, this work focuses on development of the uniform and reliable methodology for sample preparation of diamond nanoparticles in a given form and given conditions. This would enable to measure and evaluate heterogeneity of fluorescence lifetime of single diamond nanocrystals using time-resolved measurements. The same approach will be used to characterize and evaluate luminescence of core-shell nanodiamonds embedded in silica shells. The final goal is to determine the dependence of the fluorescence lifetime of NV centres in diamonds on refractive index of their surrounding environment and thickness of the shell in which nanodiamonds are embedded in.

2. Theoretical background

2.1. Nanodiamonds

2.1.1. Crystal structure

Diamond is a form of carbon which crystal lattice is formed by carbon atoms established periodically and bound to each other covalently to create face centred cubic crystal structure (Figure 1). This arrangement results in extraordinary features, such as superior hardness and Young's modulus, biocompatibility, high thermal conductivity, optical properties and fluorescence, chemical stability and many others^[5,11]. These features being inherited by nanodiamonds make them a suitable material for nanoscale applications in many fields of industry and science.

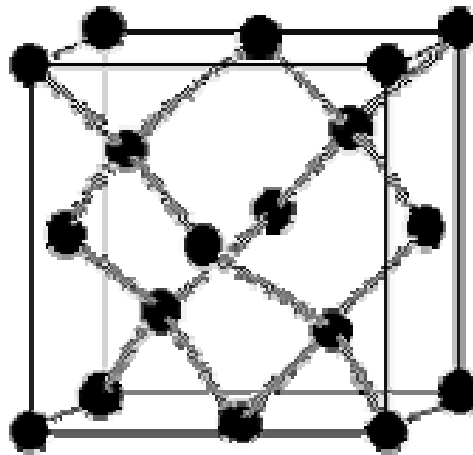


Figure 1: Diamond crystal structure . Dark circular objects represent carbon atoms linked with bonds, forming cubic crystal structure.^[2]

Especially in biology and biomedicine, biocompatibility and fluorescence allow us to use nanodiamonds as a tool for bioimaging and biosensoric applications.^[4,7,22]

The coloration and ability to emit fluorescence is based on presence of specific impurities and dopants in diamond structure. Many diamond defects are known and were investigated in terms of their structure, physical and optical properties^[7]. One of the most common defects in diamond are luminescent nitrogen-vacancy centres.

2.1.2. Classification of nanodiamonds

The unique properties of diamond originate from impurities and content of i.e. non-carbon elements. A typical foreign element which can be usually present in diamond is nitrogen which can drastically alter the properties of diamond crystal with even a slightest change in its content.^[22] Therefore, it is important to know its concentration with the highest possible accuracy to be able to correctly evaluate measured properties.

Impurities can be found in natural or synthetic diamonds since these are never completely pure. There are lattice impurities formed by incorporation of foreign atoms replacing carbon atoms or inclusions which do not replace carbon atoms but are interstitial as separate particles, such as magnesium, silicates or aluminium. The two most frequently present impurities are boron and nitrogen which fit good within the diamond structure and have the most significant effect on diamond properties while other elemental impurities are present in a very small concentrations and their effect is uncertain or negligible.^[22]

Diamonds, in general, are divided into two main groups –types I and II. Each group differs in a content of nitrogen and boron impurities and are further divided according to the arrangement of nitrogen atoms as shown in Figure 2. The presence of nitrogen impurities correlates to a certain characteristics of diamond (coloration, IR absorption, etc.). Leading information for identification of diamonds and their properties is thus their chemical composition which is different for natural and synthetic diamonds. The list of several common lattice defects can be found in [23]. The most common methods used to determine diamond types are Fourier Transform Infrared Spectroscopy (FTIR) and Secondary Ion Mass Spectroscopy SIMS.^[23]

The largest group are type I diamonds which are characteristic by a presence of nitrogen (N) atoms in their structure, high enough to be measured by IR absorption (7-20 μm)^[23]. This group further subdivides into two other groups – Ia (98 % of natural diamonds) and Ib (<0,1 % of natural diamonds) where Ia contains aggregated nitrogen atoms (0,1 % of N) and Ib has N atoms isolated in a form of single substitutional nitrogen atoms (0,05 % of N).^[22, 24]

Ib nanodiamonds are a predominant product of High Pressure High Temperature (HPHT) synthesis and allow to produce vacancies in a high rate containing only a few hundreds ppm (parts per million) of nitrogen. The single substitutional N produces absorption in a visible region starting at approximately 500 nm and gives the diamond yellow coloration.^[24] Ia nanodiamonds contain aggregated N atoms which, in aggregated form, are deep electron

donors. Ia type can be further divided into two sub-forms. If N atoms aggregate in a group of two and are well separated from other N groups, they are termed IaA or A aggregates, and in case there are four N atoms grouped symmetrically surrounding a vacancy, they are termed IaB or B aggregates (Figure 3).^[24,25]

Type II diamonds occur rarely in nature and are also divided into two subgroups – IIa and IIb. Type II diamonds, unlike type I, do not contain a sufficient amount of nitrogen to be detected by IR spectrometry. IIa group is characteristic with absence or negligible concentration of nitrogen (few ppm of N)^[22] and boron impurities while IIb diamonds contain boron impurities in a place of carbon atoms. Doping IIb diamonds by boron can induce semiconductive properties^[22]. IIb nanodiamonds are very rare in nature.^[23]

The different character of various color centres and defects in diamond lattice allow to distinguish I and II types of diamond with absorption in UV region based on the content of nitrogen impurities. Type I diamonds strongly absorbs in short-wave UV (225 – 320 nm) while type II is almost completely transparent for UV radiation.^[24]

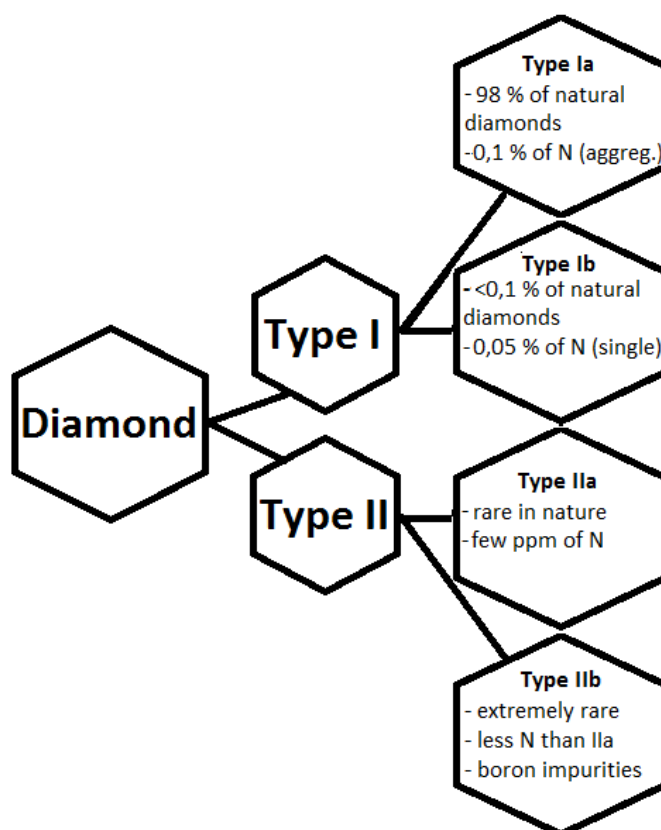


Figure 2: Characteristics and diversification of diamond types.

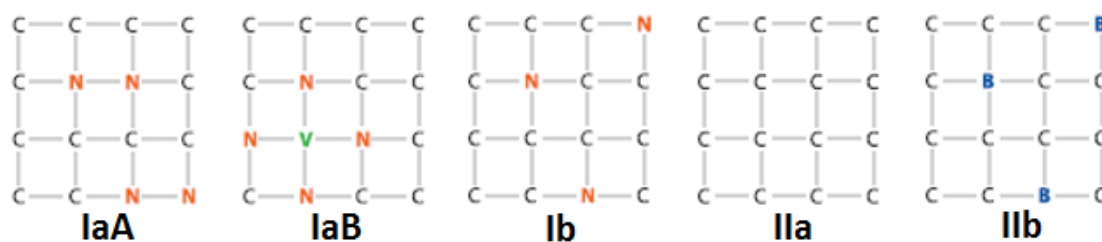


Figure 3: The arrangement of dopants in diamond lattice with respect to the classification. C-carbon atoms which form diamond lattice, N-nitrogen atoms in several ways of aggregation, B-boron dopants. Modified from [23]

2.1.3. Synthesis of nanodiamonds

Diamonds can be synthesized in many forms, such as bulk crystals, nanocrystals or thin films. The smallest form of diamond allows to create lattice defects is nanodiamond. There are several ways how to synthesize diamond nanocrystals and each of them is based on a different principle with a different purity and yield of the final product. Preparation method has a notable effect on the structure and properties of the final product – nanodiamonds^[5,6,7]. Nowadays, we know three basic methods of diamond synthesis – Detonation method, Chemical vapour deposition, High pressure high temperature.

2.1.3.1. Detonation diamonds

The first method is the detonation method based on a controlled detonation of explosives (trinitrotoluene or hexogen) in a closed chamber filled with an inert gas. Molecules of explosives provide source of carbon and energy necessary for the conversion.^[5] Detonation nanodiamonds are usually small (5 nm) spherical particles which is advantageous for biosensing^[7] but also contain a lot of impurities which is, on the other hand, a great disadvantage in terms of biocompatibility and luminescent properties^[5]. The high amount of impurities is mostly sp^2 carbon (graphite), in a form of a thin layer around the sp^3 carbon (diamond), and metal-, oxide-like impurities originating from igniter in the chamber. Another negative feature of the detonation method is that nanodiamonds are difficult to disaggregate which is necessary to remove trapped impurities.^[7] Amount of graphite, created by the conversion of sp^3 carbon to sp^2 , can be reduced by a quick cooling after the detonation through non-oxidising cooling medium or by annealing at 400 – 430 °C^[6]. Reaggregation can be carried out using sonication or ball milling and purification of a detonation soot using liquid oxidants, such as HNO_3 or various mixtures of H_2SO_4 ^[6].

2.1.3.2. CVD diamonds

Chemical vapor deposition (CVD) is another approach toward creation of thin diamond layers^[6,26], monocrystalline diamonds^[7] or nano-crystalline (NCD) and ultra-nanocrystalline diamond (UNCD)^[25]. Nano-crystalline diamonds have rather unusual properties than single-crystal diamonds and can be deposited in submicron thicknesses on various substrates. These features make CVD diamonds applicable for micro-electronics, optical coating, electrochemistry and bioelectronics.

NCD and UNCD are entirely different forms of diamond crystals as far as the size of the grain and the type of plasma are concerned. UNCD is grown from Ar-rich plasma and its grains are 5-15 nm large and independent on the thickness of the film. NCD are prepared from hydrogen-rich plasma with grains of size below 100 nm which is comparable with the thickness of the film.^[25]

Diamond CVD is a low-pressure process carried out in a high temperature 700-1000 °C which produces diamond coatings that alter surface properties of the substrate (Si, SiO₂, SiC). Substrate is exposed to volatile precursors which react with each other and decompose to give the desired material. This process is often accompanied by creation of secondary volatile products which are removed from the reaction space by a flow of carrier gas or vacuum. CVD diamonds are prepared on the plate from a mixture of, for example, methane which decomposes to methyl radical and hydrogen (Figure 4a). The mixture is dissociated by microwaves, laser or dielectric discharge. Methyl radical which is created in the first part of the reaction is a source compound in generating growth of diamond. Activation of diamond is completed by a removal of surface-bonded hydrogen atoms by atomic hydrogen (Figure 5). Second reaction includes reaction of activated carbon radicals with the carbon-hydrogen in the gas phase to serve as a place for carbon addition (Figure 4b).^[6,23]

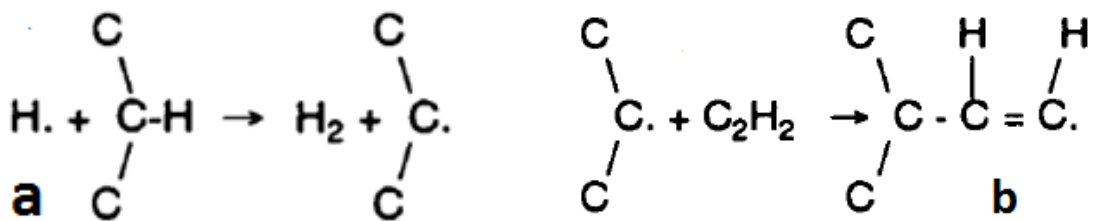


Figure 4: Diamond CVD model. a) Decomposition of methane to methyl radicals and hydrogen to obtain source for diamond growth and b) generation of place for carbon addition.^[22]

Moreover, hydrogen (or oxygen, OH radicals^[6]) is continuously etching sp^2 carbon and stabilizing sp^3 carbon during the growth (graphite is removed while diamond remains). That is very promising feature for electrochemistry where sp^2 carbon influences electrode stability^{[19],[22]}

Appropriate selection of the reactive mixture and annealing significantly affects quality of the sample.

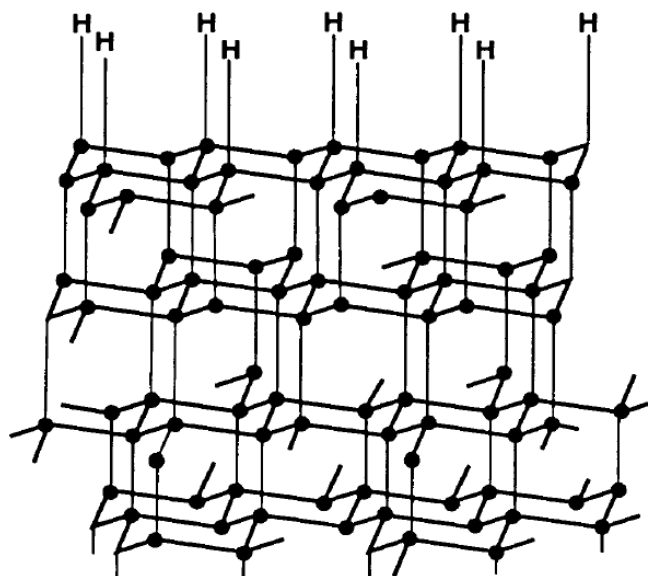


Figure 5: CVD diamond structure with bonded nitrogen atoms.^[22]

2.1.3.3. High-pressure high-temperature diamonds (HPHT)

High-pressure high-temperature (HPHT) technique is based on growing diamonds at a high temperature and pressure surrounding the core (germinal centre) simulating natural conditions. Source material is graphite which is transformed into diamond through chemical and physical processes. High pressure is generated in a tapered piston which attains diamond stability at high temperature of approximate range from units to dozens of GPa. During the synthesis, required temperature depends on the type of diamond but usually reaches about 2000 °C. Temperature and pressure must be carefully chosen to keep the sample thermodynamically stable and ensure metal catalysts to be molten. Metal catalysts are for example chromium, iron, cobalt or platinum, and are used to induce the growth. HPHT nanodiamonds are usually larger than detonation nanodiamonds with less amount of sp^2 carbon^[6] but their main advantage is low concentration of lattice defects^[27] which is important for sensing applications.^[26]

However, ultrasmall luminescent HPHT NDs of size 1 nm (much smaller than detonation nanodiamonds) can also be created via combination of annealing at 450 °C and centrifugation.^[27] These ultrasmall nanodiamonds are very promising tool for cellular sensing due to their more effective penetration through the cell membrane.^[27] Nitrogen atoms which form NV centres come from the residual gas in the HPHT reactor and carbon source material. N is implanted into crystals during their growth. HPHT created diamonds are almost all type Ib which is a nature-rare type containing single substitutional nitrogen atoms^{[6]. [26]}

2.2. Coloration and fluorescent defects in diamond

Until now there are more than hundred known color centres/luminescent defects discovered in diamond which have been extensively studied in a matter of spin, optical or charge properties. Especially nitrogen defects are of particular importance since they are the most abundant impurities and significantly alters optical or mechanical properties of the diamond crystal.^[28] Coloration origins from a nitrogen in different aggregations. Diamonds can be colored artificially by irradiation with particles or high-energy ions. Final coloration is dependent not only on the overall content of internal defects but also on the light under which diamonds are observed.^[29] Occurrence and formation of nitrogen in diamond lattice was described earlier in 2.1.2..

Several lattice defects which contribute to the coloration of diamond can be distinguished using UV-VIS spectroscopy to measure absorption or fluorescence. Among the most frequently occurring ones are, for example, NV centres which will be discussed later, N2 (zero phonon line (ZPL) at 478 nm) and N3 (ZPL at 415 nm) centres where N2 centre is usually part of N3 centre which consists of three nitrogen atoms surrounding vacancy and is partially responsible for yellow coloration and blue luminescence after UV excitation.^[23] Term zero phonon line represents in emission spectrum the energy difference between the lowest vibrational level of the excited electronic state and the ground energy state.^[9] Another type of color centres are H centres (H3, H2). H3 centre (ZPL at 503,2 nm) is an uncharged defect which consists of vacancy surrounded by two nitrogen atoms ($[N - V - N]^0$). H2 centre (ZPL at 986 nm) has similar arrangement as H3 but it is negatively charged ($[N - V - N]^-$). H2 and H3 centres are both evidence of HPHT treatment and are responsible for yellow (H3) or, when combining their effects, green color.^[23] Due to developments in thin film technology and crystal growth it is possible to incorporate various dopants into the diamond lattice during the growth and create also silicon or nickel related centres.

2.2.1. Nitrogen-vacancy centres

The nitrogen-vacancy centres (NV) are one of the most intensively studied defects we can find in Ib diamond lattice (Figure 6a). NV centre is artificially fabricated luminescent point defect which exhibits some very promising fluorescence properties. Several optical centres in diamond may exist in more than one charged state ^[24]. It is the same for NV centres in diamond where they exist in two charge states. First state is the negatively charged (NV^-)

and the second is neutral (NV^0). NV^- centre emits stronger luminescence than NV^0 as shown on fluorescence spectrum in Figure 6b.^[5-7]

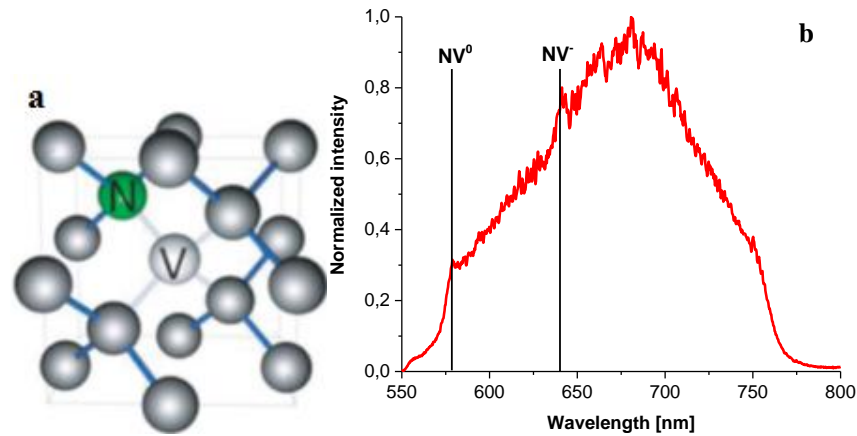


Figure 6: Schematic view of diamond crystal lattice with a) NV centres^[3] and b) fluorescence spectrum of nanodiamond^[30]. Black lines in b) indicate zero-phonon lines of NV^0 (576 nm) and NV^- (638 nm) centres.

NV^0 and NV^- spectra exhibit in fluorescent spectrum of diamond two characteristic peaks with zero phonon lines on wavelengths 576 nm (2,156 eV) (NV^0) and second on a strong optical transition at 638 nm (1,945 eV) (NV^-) (Figure 6b) with emission maximum around 680 nm. The broad emission band in red/NIR predetermines diamond for bioimaging application since the emission wavelengths are well separated from the emission region of cell autofluorescence.^[5,8,24] Effective excitation can be achieved using excitation light of wavelengths below 640 nm since the excitation band is in range 480 – 580 nm with maximum around 550 nm.^[31] Emission intensity is then proportional to the number of NV centres present in the particle. NV centres hold one extraordinary feature which is stable luminescence without photoblinking or photobleaching under continuous excitation.^[4] This applies for either bulk diamond or ultrasmall 5nm diamond particles.^[32] Moreover, nitrogen-vacancy centres are set apart from other defects by its spin state dependent luminescence, so their luminescence can be modulated by a magnetic field^[7]. Also, their fluorescence quantum yield is very high, approximately 70-80%^[7].

Electronic structure of NV centre is composed of six electrons which are provided by three carbon atoms near the vacancy and nitrogen atom. Sixth electron is usually captured from the lattice forming charge state NV^- . Almost all experiments are based on NV^- , because NV^0 or positively charged state NV^+ are not magneto-optically active^[7] and have

weaker fluorescence (see Figure 6b). Both NV^- and NV^0 are sensitive on electrical charges on the surface of the particle. If charged molecules are attached, they interact with shallow NV centres in the particle which results into changes in luminescence by changing the electron occupation of NV charged states.^[9]

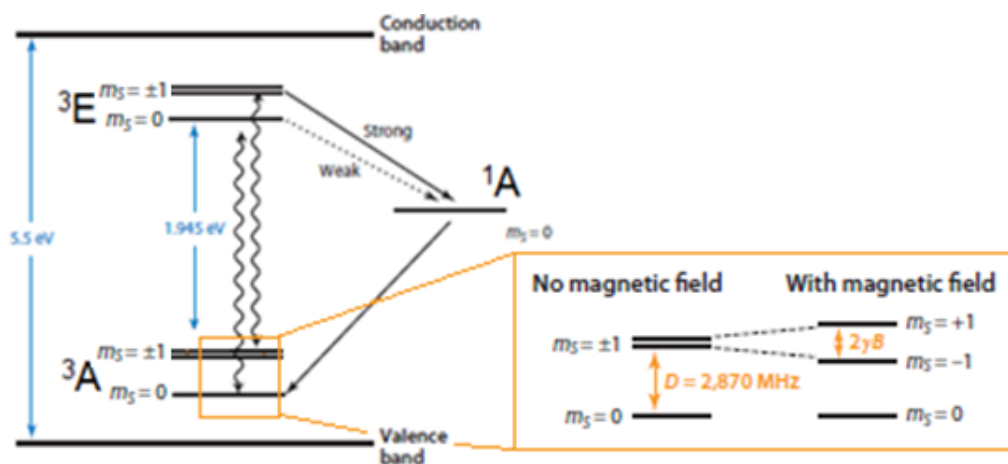


Figure 7: Three level energy diagram of NV centre with detailed energy level scheme of triplet ground (3A) and excited (3E) states, metastable (1A) state and diagram depicting effect of magnetic field on energy levels of the ground state. D is zero-field splitting and $2\gamma B$ is Zeeman splitting, where γ is gyromagnetic ratio, B is magnetic field. Wiggly arrows indicate radiative transitions and straight lines strong and weak nonradiative decay via singlet state. Modified from [7]

Energy structure of the NV centre can be described using energy-level diagram which consists of three electronic levels (Figure 7). Electronic levels are triplet (total spin $S=1$) ground 3A and excited 3E states and metastable singlet state 1A . The ground and excited states are split into three energy sublevels. The main radiative transition, between the ground state and excited state, is characteristic with red emission on wavelength 638 nm which is the wavelength typical for NV^- centre, as described above.

The average time which the fluorescent molecule spends in the excited state is termed fluorescence lifetime and is characteristic feature for every fluorophore. For nanodiamonds, fluorescence lifetime of their excited state is notably longer than lifetime of common biological fluorophores (or cell autofluorescence), depending on conditions and form of nanodiamond.^[5,7]

Another way of deexcitation is through the non-radiative transition from one of sub-energy levels of the excited triplet state to metastable singlet state. As indicated in Figure 7, this non-radiative transition is more preferential for spin states $m_s = \pm 1$ rather than $m_s = 0$.

The difference between transitions shows spin dependence of NV photoluminescence intensity and can be used for optical monitoring of NV spin state. Electrons can be excited from the lower $m_s = 0$ into the higher $m_s = \pm 1$ using excitation with resonance frequency 2,87 GHz (microwave). The energy level $m_s = \pm 1$ may split to $m_s = +1$ and $m_s = -1$ upon presence of magnetic field which affects NV photoluminescence and thus enables magnetic field detection, i.e. to use NV centre as a nanoscopic spin probe.^[7]

2.2.2. Generation of NV centres

Color centres exist due to the presence of the small concentration of nitrogen atoms in a single substitutional form incorporated inside crystal lattice during the growth process.

The first step in creation of NV centre is to create a vacancy. Vacancies are created by irradiation of nanodiamond with high-energy particles (protons, electrons, ions) to remove individual carbon atoms. Electrons with energy 1 – 2 MeV have been preferred because of high penetration depth up to 1 mm and a quick production of isolated vacancies. Neutrons and heavy ions, on the other hand, produce regions of multiple damage. Charged particles are used with energies around few MeV and despite their high energy they penetrate only in few μm depth (for example 5,5 MeV α particles penetrate into 14 μm).^[24]

Only creating vacancies is not sufficient due to low probability of bonding with nitrogen on its immediate place. To ensure formation of NV centre (through vacancy diffusion), irradiation is followed by a vacuum annealing at temperatures 600-800 °C. For temperatures ≥ 800 °C concentration of NV centres can be much enhanced.^[7] In type Ib diamond, higher temperatures than 800 °C (1000 °C – 1600 °C) cause great reduction of NV^- absorption due to conversion of single substitutional nitrogen into A aggregates accompanied by a production of N-V-N centres.^[24]

Annealing causes migration of vacancies and if the nitrogen atom is present in a close proximity, it traps vacancy and forms more stable NV centre although the sample depth is limited.^[27] Number of NV centres increases with the size of nanodiamond particles^[6] and can also be controlled by the energy of the particle beam or annealing duration. For example, lower energy and shorter annealing can be used to create nanodiamonds with less or even single NV centre, the latter with a very low probability.^[5-7]

3. Experimental methods and instrumentation

This section theoretically covers used methods and reports the overall description of methodology developed for sample preparation, experimental steps leading to the measurement of fluorescence decays of selected nanodiamonds and introduction and specification of instrumentation used for these tasks. All experiments were done at the Faculty of Biomedical engineering (FBME) of Czech Technical University in Prague (CTU). Results of individual sub-experiments are also reported.

Three diamonds system were investigated in this work; fluorescent nanodiamonds (60 nm) (NDs104), core-shell fluorescent nanodiamonds embedded in 50 nm thick silica shell (160 nm) (JV39-1) and core-shell fluorescent nanodiamonds embedded in 100 nm thick silica shell (260 nm) (JV39-4). Source material and modified nanodiamonds were provided by Institute of Organic Chemistry and Biochemistry in Prague. Both source diamond material and silica shells were fabricated by a novel approach for the purpose of their investigation and also to determine fluorescence lifetime heterogeneity of NV centres in various surrounding chemical environments.

This Chapter is divided into 4 main sections. Sections comprise of complex description of instrumentation, methods and experimental procedures used for the examination and development of the correct and reliable methodology utilized for evaluation of above presented problematics. Subsections contain findings which lead to the fulfillment of presented aims (see 1.1.).

Section 3.1. describes fundamentals of measurement methods, i.e. confocal microscopy, contact angle measurement, fluorescence spectroscopy, time-correlated single photon counting and fluorescence lifetime imaging microscopy.

Section 3.2. describes instrumentation used for performed experiments.

Section 3.3. contains the detail description of sample preparation which comprise of substrate purification and steps taken to find the optimal substrate modification which was preceded by ND sample preparation.

Section 3.4. contains measurement procedure including determination of appropriate excitation parameters, which has a crucial impact on the fluorescence behaviour of investigated nanodiamonds and their fluorescence decay, and single particle imaging and decay measurement which encompasses technical troubleshooting of effects which influence analysis

and acquisition of the data and which originate from the used physical equipment. This section also reports measurement of photon antibunching for determination of number of NV centres in measured particles and measurement of single particle saturation intensity.

For the transparency and orientation in the thesis a block diagram of the experiment was created (Figure 8).

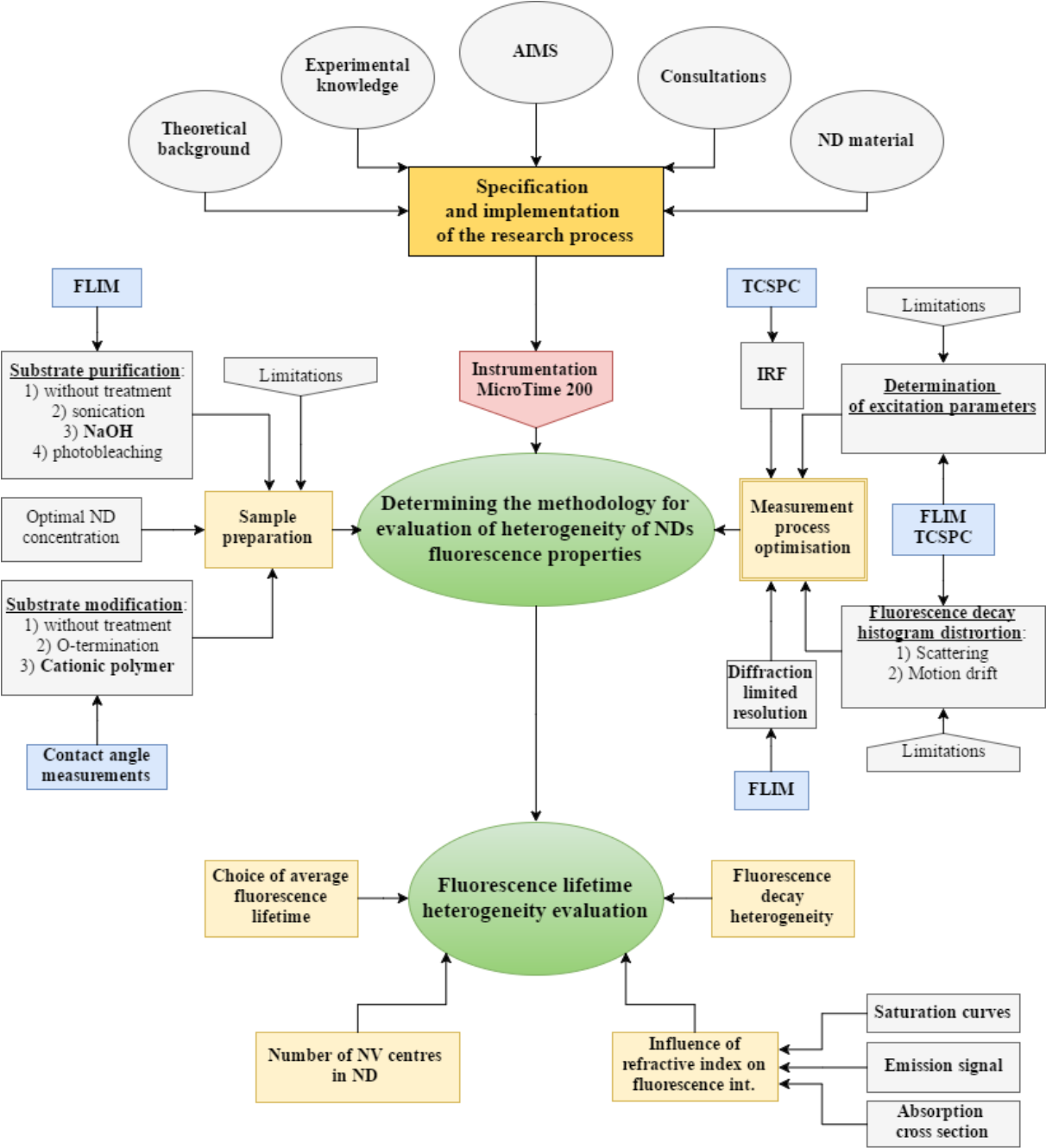


Figure 8: Block diagram of the experiment.

3.1. Fundamentals of measurement methods

3.1.1. Confocal Microscopy

Confocal microscopy is an optical microscopic method which represents a significant improvement of conventional optical microscopy. Confocal microscopy offers several advantages over conventional widefield microscopy, i.e., the capability to collect series of optical sections from a thick sample, reduction of background signal, ability to control depth of the field and elimination of the light which originates from a space out of the focal plane.^[33]

Positive characteristics of confocal systems enable to create a high-quality images of the observed specimen prepared for a conventional or fluorescence microscopic techniques. Therefore, it is one of the most important and widely used techniques for imaging in natural sciences in general.

Scanning confocal microscope is a microscope (Figure 9) which uses coherent light emitted by the excitation laser for the illumination of the observed object in a small volume at the focus of the objective. Laser light passes through the light source pinhole aperture and is reflected by a dichroic mirror. Then it passes through the microscope objective. Objective focuses the illumination light into a diffraction limited spot in the focal plane of the sample. Incident light is reflected, scattered or may excite fluorescence of the sample. The light from the specimen is then collected and led by the same objective again on the dichroic mirror. Dichroic mirror allows transmission only of the light emitted by the specimen of longer wavelengths than the excitation light. Light is transmitted by the dichroic mirror is focused at a confocal point at the detector pinhole aperture which also serves for elimination of the out-of-focus light and stray light. Out-of-focus light is the fluorescence emission emanating from above and below of the scanned focal plane and therefore is not confocal with the pinhole. Because only a small fraction of fluorescence is collected, sensitive detectors such as single photon counting photomultiplier or avalanche photodiode are usually used in this system.^[33]

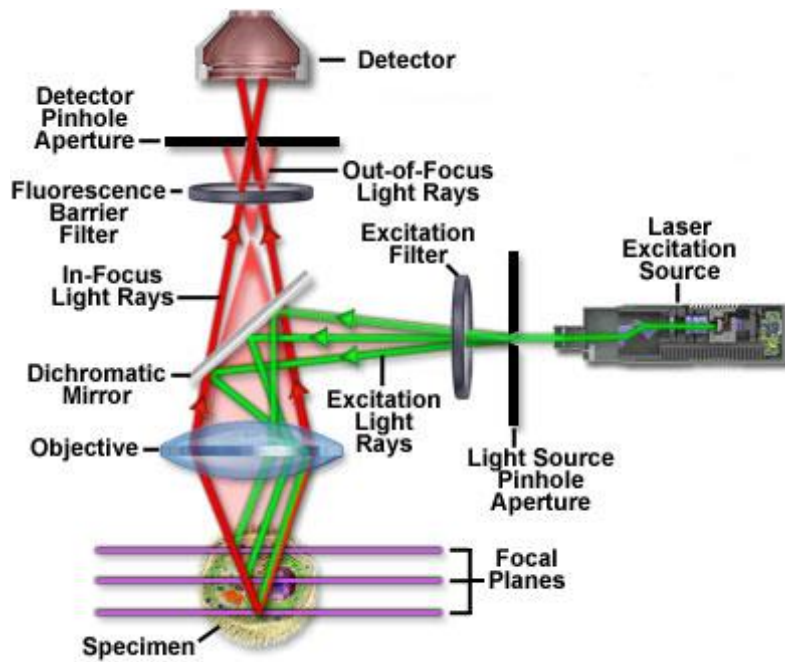


Figure 9: A schematic of laser scanning confocal microscope.^[33]

Resolution of confocal systems is determined by the wavelength of the excitation light, size of the pinhole aperture and numerical aperture of the objective (might be improved by immersion).

Imaging is accomplished by raster scanning of the laser beam or spatial shift of either observed specimen or microscope objective. Acquisition of a sufficient number of plane scans enables to create a 3D model of the sample and thus perform a volume analysis.

3.1.2. Contact angle measurement

Contact angle measurement serves as an experimental method to determine the hydrophobicity/hydrophilicity of solid surfaces or the surface tension between a solid material and a liquid surrounded by gaseous phase. Hydrophobicity/hydrophilicity can be evaluated with contact angle, which is developed on the interface of three phases (liquid, solid, gas). Contact is one of few directly measurable properties of the phase interface solid surface-liquid and provides quantitative information about the range of wettability of solid surfaces. Wettability is a property of liquids to adhere to a solid surface. The relationship between contact angle and wettability is inverse. A small value of contact angle corresponds to a high wettability.^[34]

The basic equation used to calculate the contact angle is the Young's equation (1)^[34]:

$$\gamma_{s/v} = \gamma_{s/l} + \gamma_{l/v} \cos \theta_Y \quad (1)$$

where $\gamma_{s/v}$ is solid-vapour tension, $\gamma_{s/l}$ is solid-liquid surface tension, and $\gamma_{l/v}$ is liquid-vapour tension, and θ_Y is the contact angle. The whole principle can be seen on Figure 10.

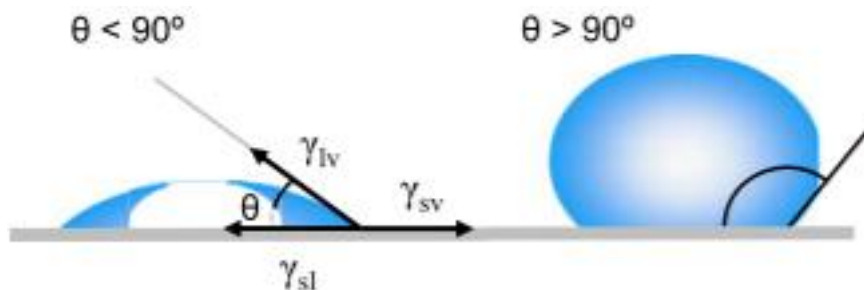


Figure 10: Illustration of contact angles for situations with a) hydrophilic (small values of contact angle) and b) hydrophobic surfaces (high values of contact angle).^[34]

The principle of this method resides in application of the drop of pure liquid (water) using micropipette on a solid sample, fixed in the measuring device. Camera and light source are positioned against each other with the sample positioned between.

3.1.3. Fluorescence Spectroscopy

Luminescence is a spontaneous light, not resulting from heat, which originates from a transition of excited molecule from its excited state to its ground state. Luminescence can be caused by many different ways of excitation, e.g. chemiluminescence (chemical excitation) or photoluminescence (optical excitation), which is generated by absorption of UV, visible or infrared light. As a result, excited fluorescent compound (fluorophore) loses its energy in a form of photon of visible part of spectrum.

The principle of photoluminescence (fluorescence, phosphorescence) can be described by Jablonski diagram (Figure 11). Jablonski diagram shows possible energy transitions that can occur between individual energy states of the fluorophore.

If the fluorescent specimen absorbs photons of light with frequency equal to the energy difference between excited and ground state, it is excited from the singlet ground state (S_0) to one of the singlet vibrational states of the excited electronic state (S_2). Absorption of light

is a very fast process (10^{-15} s). Excited molecule possesses an excess of energy after the excitation and loses this excess through radiationless processes termed vibrational relaxation (10^{-12} s) and then by internal conversion ($S_2 \rightarrow S_1$) ($10^{-6} - 10^{-12}$ s). Transitions between singlet states are „spin allowed“ and take place with higher probability than transitions involving singlet and triplet state. Vibrational relaxation always ends with the fluorophore on its lowest vibrational level of the excited electronic state (S_1). From this point, either fluorescence can occur upon relaxation to the ground state ($S_1 \rightarrow S_0$) or the molecule can undergo radiationless intersystem crossing ($S_1 \rightarrow T_1$) to the triplet state T_1 ($10^{-4} - 10^{-12}$ s) and continue with relaxation to the ground state, which is accompanied by the emission of phosphorescence.

Singlet states S_1 and S_2 are quantum states of the molecule where spins of electrons in the electron cloud are paired and compensate each other. Total spin is zero and spin multiplicity is, according to the $2S+1$, equal to 1 ($2 \cdot (1/2 - 1/2) + 1 = 1$) where S is total spin quantum number of electrons. Triplet state T is a quantum state of molecule where the total spin of electrons in the electron cloud after excitation is equal to 1. This is undermined by the change of spins of electrons to antiparallel state with multiplicity equal to 3 ($2 \cdot (1/2 + 1/2) + 1 = 3$).^[35]

Fluorescence is characteristic by a very short duration, usually in order of nanoseconds. Because fluorescence mostly occurs from the lowest vibrational level of the excited electronic state (information of energy states structure of the molecule), either fluorescence wavelength or fluorescence lifetime are very useful tools for characterisation and identification of chemical compounds in biomedicine.^[35]

Because phosphorescence originates from the transition starting at the triplet state, there is a much lower probability of occurrence than it is in case of fluorescence which originates from singlet state. This is because the triplet state is „spin forbidden“. Excited molecule resides in the triplet state much longer before it decays to the ground state ($10^{-3} - 10^0$ s) and therefore, the duration of phosphorescence is longer than we can see during fluorescence emission.

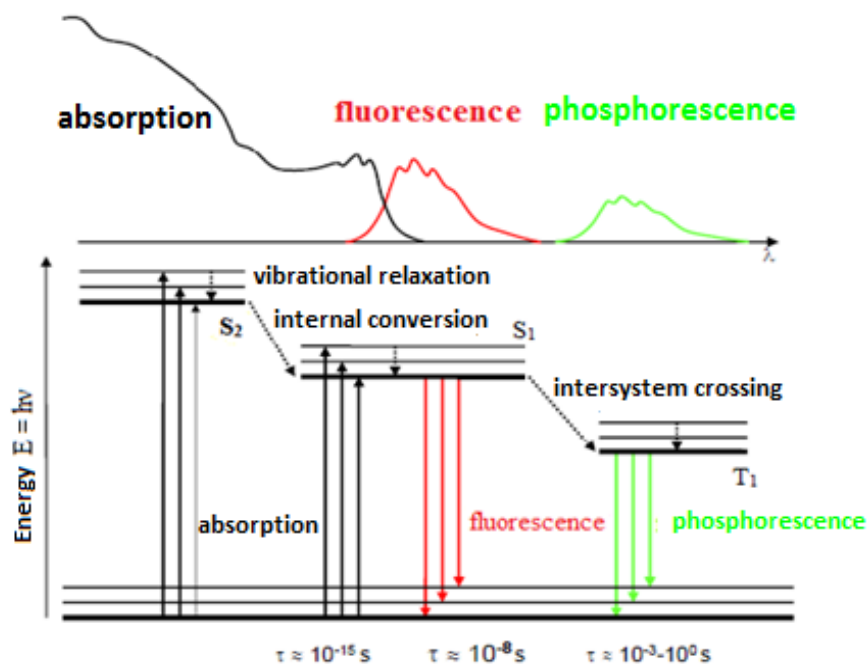


Figure 11: Jablonski diagram. Horizontal lines represent electronic states. Solid vertical lines represent radiative transitions and absorption. Dotted lines illustrate radiationless transitions. S_1 and S_2 are singlet states and T_1 triplet state. Modified from [36]

Fluorescence emission is always shifted to higher wavelengths (lower energies), with respect to the excitation wavelength, as a result of the radiationless loss of energy during vibrational transitions. This shift in emission spectrum is termed Stokes shift.

Presented diagram describes energy states structure well for organic fluorophores (molecules). It should be noted that energy structure of nanodiamonds (nanoparticles) is slightly different. Ground and excited energy states are both triplets, meaning that absorption and radiative deexcitation occurs between triplet and not singlet states (see 2.2.1).

3.1.4. Time correlated single photon counting (TCSPC)

Time correlated single photon counting (TCSPC) is a time-resolved method of fluorescence spectroscopy used for determination of fluorescence lifetime. This method has a potential use in many applications using fluorescence for characterisation of fluorescent substances, their molecules and behaviour. TCSPC can be carried out in a time or a frequency domain. This work is restricted to the time-domain measurement. More information about frequency domain can be found in [37].

Molecules of the fluorophore are excited by a series of short laser pulses and the time between the excitation (time reference) and arrival of the single fluorescence photon

on a detector is precisely registered (Figure 12). Single photon sensitive detectors, such as single photon avalanche diode (SPAD) or photomultiplier (PMT) are used for this purpose.

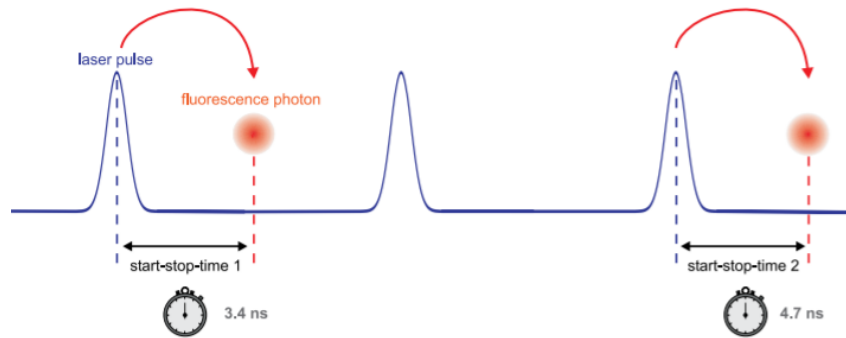


Figure 12: The principle of time-resolved fluorescence measurement of start-stop times with TCSPC.^[38]

From Figure 12 it is clear that fluorescence photons might not be detected after each excitation but it can be described in terms of probability. The probability of photon detection in each excitation cycle must be actually quite low, approximately 1 fluorescence photon for 100 excitation pulses. This is carried out in order to prevent detection of more than 1 fluorescence photon after 1 excitation pulse because the electronics is unable to detect more than one photon in each cycle (dead time: 10 μ s – 120 ns)^[38]. This process is repeated over many cycles until the sufficient amount of data is acquired.

Every detected delay time is saved and sorted into histogram of the occurrence of emission photons over time after excitation pulse (Figure 13).^[38]

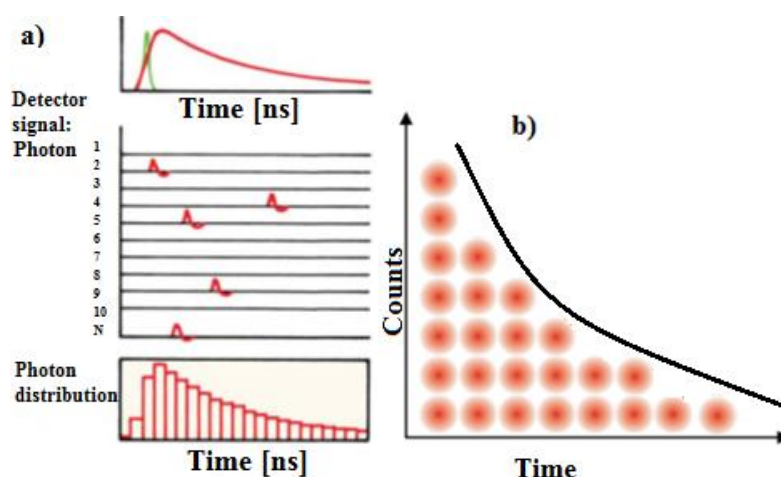


Figure 13: Principle of TCSPC and fluorescence decay acquisition. a) Principle of TCSPC^[37] and b) histogram of start-stop times measured with TCSPC^[38]. Pulses in the middle of a) are pulses from a discriminator generated as an indication of photon arrival

Arrangement of individual photons under the curve in Figure 13b shows that the highest probability of photon detection is in the beginning of acquisition. As mentioned before, the probability of photon detection with respect to the number of excitation pulses must be very low in order to prevent distortion of the histogram to shorter times of photon arrivals (Figure 14b). This necessity comes from the limitation of the detector which, after photon detection, requires approximately few nanoseconds to recover (dead time) (Figure 14a). If there is more than one photon in one excitation cycle, the detector would register only the first one and would not “consider” the following ones, which would lead to a false (over-representation) representation of collected data and affect the calculated lifetime. This effect is termed “pile-up” effect. However, modern electronics can nowadays collect even multiple photons per cycle.^[38]

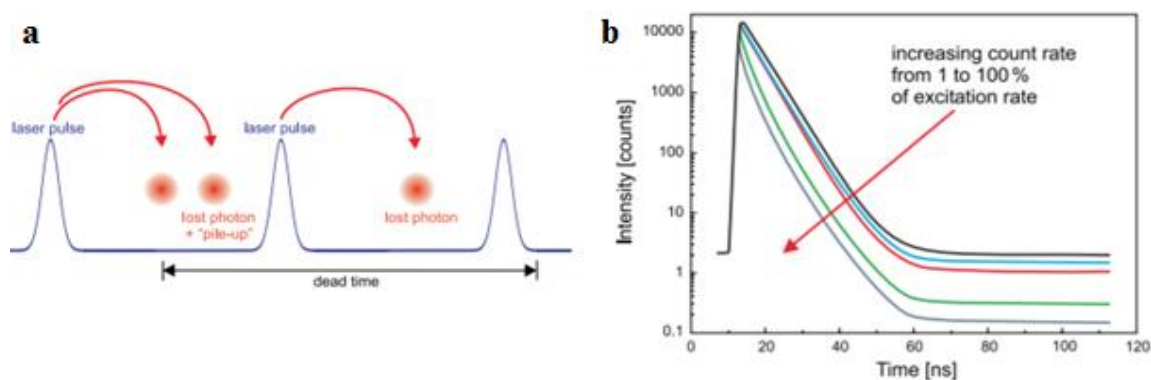


Figure 14: The effect of dead time and pile-up effect on the TCSPC histogram. a) effect of dead time of the detector on data acquisition and b) distortion of the histogram due to pile-up effect.^[38]

To prevent pile-up effect, it is desirable to measure with the count rate at the detector 1 % – 15 % of the excitation rate (for example 1 fluorescence photon in 20 to 100 excitation pulses).^[38] This is an issue of the detector and question of count rate the detector can handle.

3.1.4.1. TCSPC instrumentation

Schematic arrangement of the TCSPC components can be seen in Figure 15. Required START signal is provided by the pulsed excitation laser electronics in a moment when each excitation pulse is released and STOP signal is generated by the discriminator according to the signal from the detector at the moment of photon arrival.

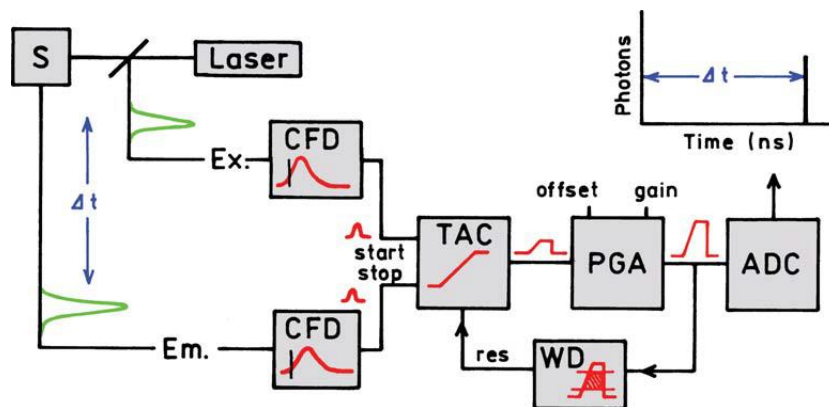


Figure 15: A schematic of TCSPC device and arrangement of individual components ^[37] S is sample, CFD is constant fraction discriminator, TAC is time-to-amplitude converter, WD is window discriminator, PGA is programmable gain amplifier, ADC is analogue-to-digital converter

Both signals, from the laser and the time-delayed (Δt) from the sample, pass through constant fraction discriminator (CFD) which accurately measures arrival times of fluorescence photons. In time-to-amplitude converter (TAC), the voltage ramp is generated linearly with time (ns) until the fluorescence photon (from the second channel) arrives or reaches the threshold value in case photon does not arrive. If the photon does not arrive, TAC is reset. TAC holds the value of the generated voltage proportional to the time delay between excitation pulse and fluorescence signal. TAC can also work in a reversed mode where the start signal is represented by the fluorescence photon and the next excitation pulse serves as the stop signal.

Reverse mode is more convenient for the TAC because it operates only when the fluorescence photon arrives (1:100). In the previous mode, TAC could be constantly in the reset mode (generated voltage needs to be reset to zero before each start pulse arrival) due to a high repetition frequency of the excitation laser. Nevertheless, nowadays is the fast electronics more commercially available and thus the fast measurement in the „direct mode“ does not mean a serious complication during TCSPC measurement. The TAC signal is low, so it must be amplified in a programmable gain amplifier (PGA). To suppress noise and false readings, window discriminator (WD) compares whether the signal from the PGA is within the restricted voltage range. If the signal is not in the range, WD will suppress the signal. The analogue-to-digital converter (ADC) converts the analogue value provided by the PGA and converts it to the digital form which is stored into the histogram as the single “time-delay” event. The histogram (Figure 13) is then formed after many repetitions of above described cycle.^[37]

3.1.4.2. Timing electronics and acquisition modes

As described in 3.1.4.1., start-stop timing components are essential for the TCSPC acquisition. In order to correctly maintain and store the information about photon arrivals in temporal patterns, these events are stored as discrete records. Additionally, the timing electronics performs time-tagging which means that photon arrival time of each photon is recorded with respect to the start of the measurement (Time-tagged Time-Resolved; TTTR) (Figure 16).^[38]

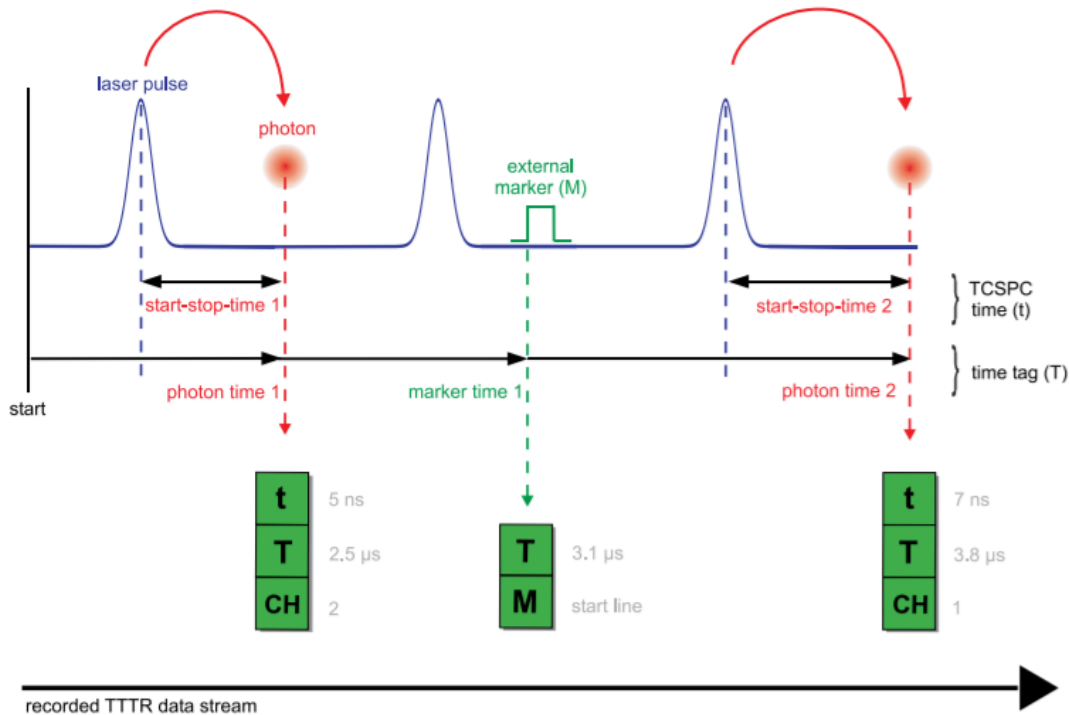


Figure 16: A principle of Time-Tagged Time-Resolved measurement. Start-stop times (t), arrival time of photon with respect to the start of the experiment (T), channel information dependent on fluorescence properties of the photon (CH), external marker characterizing the movement of the scanner (M).^[38]

Here the start-stop events are not sorted into histogram but are directly stored together with the time-tagged information (T) representing macroscopic information about arrival time of the photon with respect to the start of the experiment. Channel information (CH) is also recorded (depending on set-up) to provide information about, for example, wavelength of the photon. To create a FLIM image, electronics also add external markers (M), which carry information about position of the scanner, into the TTTR data stream. This enables 2D or 3D image reconstruction. Precise collection of all events of interest is an issue for the detection electronics and its ability to perform temporal analysis on even picosecond scale, in order to be able to collect as many dynamic effects of fluorescent molecules as possible.^[38]

There are two different time-tagging modes, T2 and T3 mode, which broaden the range of possible applications. There is a variety of detectors that can operate in T2 and T3 mode but these modes are not the same and slightly differ between detectors.

T3 mode (Figure 17) uses sync signals from the mode locked excitation laser operating with high repetition frequency (up to dozens of MHz) which makes T3 mode similar to TTTR. T3 mode uses sync signals in a separate channel instead of using second clock. Time-tagging is done by simply counting these sync pulses. T3 mode also uses special markers which are recorded when the counter overflows, which greatly enlarge the time span that can be recovered in a full resolution. This function enables to precisely determine to which sync signal arrived photon belongs to and thus with precise information about sync periods, the arrival time of the photon with respect to the overall time of the measurement can be reconstructed.^[39]

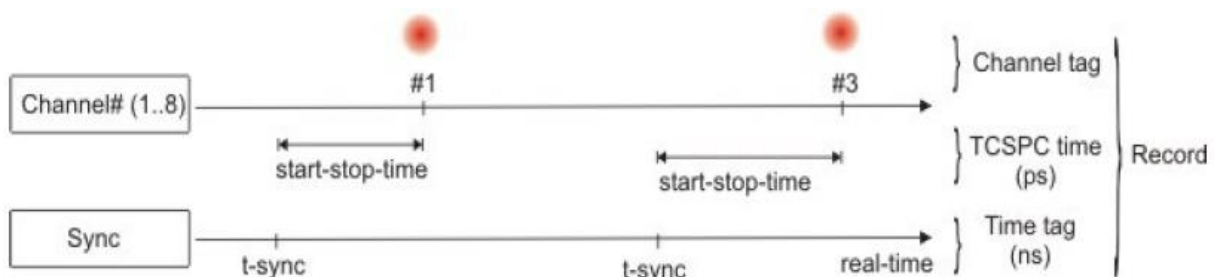


Figure 17: A principle of T3 mode.^[39]

T2 mode uses all channels for recording arrival photons independently (Figure 18). When an event is recorded, system generates information about on which channel the photon signal occurred and arrival time of the photon with respect to the start time of the measurement. In case of overflow, T2 mode uses overflow markers as well. Dead times exist only in individual channels but not across channels which is highly advantageous since it enables to do cross correlations across channels down to zero lag time, and perform measurements such as Fluorescence Correlation Spectroscopy (FCS).^[39]

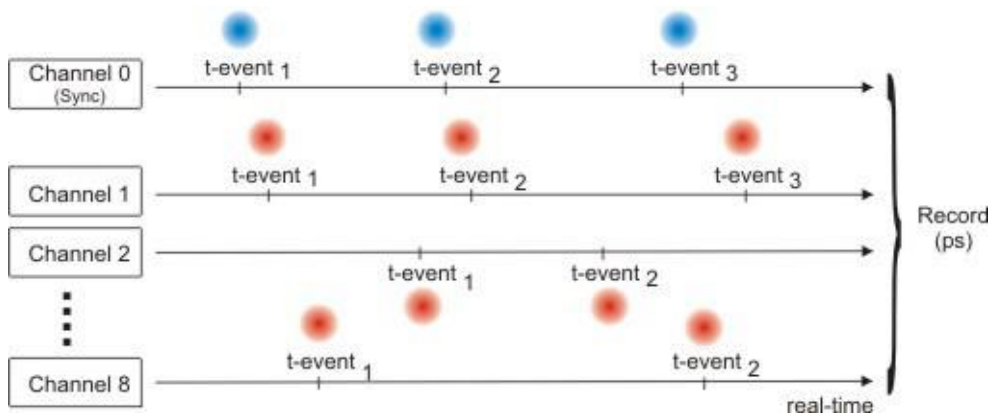


Figure 18: A principle of T2 mode function.^[39]

3.1.4.3. Timing resolution and convolution integral

The timing precision of the TCSPC system is determined by a function which represents the response of the instrumentation on the zero lifetime sample, Instrument Response Function (IRF).^[37] IRF can be collected by measuring the response of the detector on scattered excitation light (from a scattering medium) or from the fluorescent dye which is strongly quenched and has ideally mono-exponential fluorescence decay and short lifetime. IRF can be also described as a convolution of all components of the TCSPC system. The shape of IRF varies according to the instrumentation but in case of ideal system (infinitely sharp excitation pulse and infinitely accurate detector), the IRF would be infinitely narrow.^[37,38]

The timing resolution is mostly a matter of the detector and timing electronics and can be described by the Full Width at Half Maximum (FWHM) of the IRF. In real case, there are many influences on the IRF, such as thermal noise, interference, amplitude noise or timing jitter of electronics.^[38]

In ideal case we would observe the impulse response function $I(t)$ (Figure 19a), after the excitation with δ pulses, and a δ IRF. If the sample is excited by the series of excitation pulses, the intensity of the impulse response function increases proportionately to the height of the excitation δ pulses. The measured decay $N(t_k)$ is the sum of individual exponential decays generated by excitation pulses.

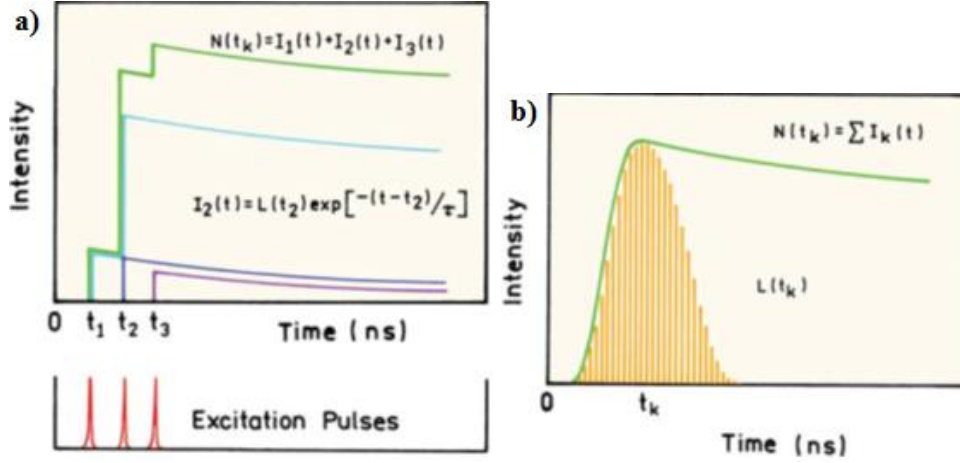


Figure 19: Convolution of the impulse response function $I(t)$ with a) excitation pulses or b) lamp profile $L(t_k)$.^[37]

This could be described by the equation (2):

$$I_k(t) = L(t_k)I(t - t_k)\Delta t \quad (t > t_k), \quad (2)$$

Where t_k is the time of excitation in which the impulse response function $I_k(t)$ of intensity $L(t_k)$ occurs, $t - t_k$ is the timing interval in which the photons are detected (start at $t = t_k$) and Δt is the width of the timing channel. As mentioned earlier, the measured decay curve $N(t_k)$ is the sum of individual decays $I(t)$:

$$N(t_k) = \sum_{t=0}^{t=t_k} L(t_k)I(t - t_k)\Delta t \quad (3)$$

For small values of the width of the channel, equation (3) can be rewritten to integral form for $t_k = t - \mu$:

$$N(t) = \int_0^t L(t - \mu)I(\mu)d\mu \quad (4)$$

Experimentally measured intensity at time t is the sum of intensities for all excitation pulses that occur until time t and new intensity decays occur when there is non-zero excitation intensity $L(t_k)$ (Figure 19b). That is why the intensity decay ($N(t)$) takes on the shape of IRF. In reconvolution analysis, the goal is to fit measured data (determine impulse response function $I(\mu)$), knowing IRF, with some analytical model, so that the difference between calculated

parameters, such as lifetime (τ) or intensity fractions, would differ from measured data minimally. Basically, assumed decay law $I(t)$ is convoluted with $L(t_k)$, and results are compared with $N(t_k)$ (iterative reconvolution for fitting the data). Fitted function can be described as an expected time profile for the recorded intensity decay with respect to the IRF or a convolution of the impulse response function (intensity decay law) with the IRF.^[37]

3.1.4.4. Least -Squares Analysis

Least-squares analysis (NLLS – Nonlinear Least Squares) serves in TCSPC as an analytical tool for a rapid estimation of the fluorescence lifetimes. Except for fitting data, least squares also serve for determining the goodness of fits and parameter values of the model with the highest possible probability of being correct.^[37]

The goal of NLLS is to test whether the fitting model is consistent with the measured data and determine parameter values of the model that provide the best matching results between measured data $N(t_k)$ and calculated decay $N_c(t_k)$ by minimizing the goodness-of-fit parameter χ^2 . If data satisfy several assumptions (as follows) the least squares provide the best estimation for parameter values. These assumptions are^[37]:

1. All the experimental uncertainty is in the dependent variable (y-axis).
2. The uncertainties in the measured values (dependent variable) have a Gaussian distribution, centered on the correct value.
3. There are no systematic errors in the dependent (y-axis) or independent (x-axis) variables.
4. The assumed fitting function is the correct mathematical description of the system.
Incorrect model yields incorrect parameters.
5. The datapoints are independent observations.
6. A sufficient number of data points is recorded so that the parameters are overdetermined.

The goodness-of-fit parameter χ^2 is given by:

$$\chi^2 = \sum_{k=1}^n \frac{[N(t_k) - N_c(t_k)]^2}{\sigma^2} \quad (5)$$

Parameter χ^2 is the sum of the squares deviations between the measured $N(t_k)$ and expected values $N_c(t_k)$, each divided by the square deviations expected for the number

of detected photons. The value of χ^2 is a minimum when the measured and expected values are closely matched. In TCSPC analysis the standard deviation is known from Poisson statistics and can be calculated from the number of measurements (photon counts) by the expression: $\sigma_k = \sqrt{N(t_k)}$. This expression is true only if the counting statistics is the only source of uncertainty in the data.^[37] Moreover, photon counts might be also used to determine signal-to-noise ratio (SNR) which is also given by the Poisson statistics: $SNR = \sqrt{N(t_k)}$.^[45] We can see that with increasing number of detected photos the SNR increases as well.

Therefore, for TCSPC the denominator in equation (5) can be replaced by $N(t_k)$:

$$\chi^2 = \sum_{k=1}^n \frac{[N(t_k) - N_c(t_k)]^2}{N(t_k)} \quad (6)$$

But it is clear that χ^2 is number-of-data-points-dependent and therefore the equation (6) can be expressed as follows:

$$\chi_R^2 = \frac{\chi^2}{n_d - p} = \frac{\chi^2}{\nu}, \quad (7)$$

Where n_d is number of data points, p is the number of floating parameters, and ν is a number of degrees of freedom. Under normal circumstances n_d is usually much larger than p , so $n_d - p$ is close to n_d . In case of only random errors, χ_R^2 is expected to be unity because the average of χ_R^2 per datapoint should be one, otherwise it is much larger than unity (model does not fit the data correctly).^[37]

By combining (6) and (7) χ_R^2 can be expressed as^[37,46] :

$$\chi_R^2 = \frac{1}{\nu} \sum_{k=1}^n \frac{[N(t_k) - N_c(t_k)]^2}{N(t_k)} = \frac{1}{n - p} \sum_{k=1}^n \left[\frac{\text{actual deviation}}{\text{expected deviation}} \right]^2 \quad (8)$$

Judging the goodness of the fit is possible from observing residuals (Figure 20) which represent (graphically) the difference between measured and the fitted data. Accepting the fitting model might be difficult because even a small systematic error might give the appearance that the more complex model is needed even if the simpler one is adequate.^[37] Visual control is therefore always recommended.

3.1.4.5. Analysis of multi-exponential decays

If we encounter a sample containing more than one source of detected fluorescence, mono-exponential fit would cause mismatch between fitted function and measured fluorescence data.

Deviations (D_k) under decay curves (Figure 19) represent difference between measured and calculated data:

$$D_k = \frac{I(t_k) - I_c(t_k)}{\sqrt{I(t_k)}} \quad (9)$$

Where $I(t_k)$ is decay data, $I_c(t_k)$ is fitted function and $\sqrt{I(t_k)}$ is a standard deviation.^[37]

Deviations and residuals (or weighted residuals according to standard deviation of each data point) are additional information which serve for the visual representation of the goodness-of-fit and are usually plotted as the dependence of $I(t_k)$ on t_k . For a good fit we can observe random and symmetrical distribution of these values around zero with the mean value near unity.^[37]

3.1.4.6. Intensity decay law

For a mono-exponential fluorescence decay to the ground state of the fluorescent molecule, we can assume intensity decay as:

$$I(t) = I(0)e^{-t/\tau} \quad (10)$$

Where $I(t)$ is the intensity at time t , $I(0)$ is the intensity at time zero (upon excitation), t is a time of acquisition and τ is fluorescence lifetime of the fluorophore defined as the time in which the fluorescence intensity decays into I/e (37 %) of its original value.

Mono-exponential fluorescence decay is much simpler and often rare case. Usually, more complicated multi-exponential decays are measured. Here the equation (10) changes into sum of individual single exponential decays:

$$I(t) = \sum_{i=1}^n \alpha_i e^{-t/\tau_i} \quad (11)$$

In equation (11) α_i are amplitudes of individual components at $t = 0$, τ_i are decay times and n is the number of components. This expression can be applied either on a mixture

of fluorophores (each displays one of the τ_i) or a single fluorophore with more complex decay. Meaning of α_i is different for both cases. In case of single fluorophore with a complex decay, assuming the same radiative decay rate in each environment, the α_i represents (fluorescence intensity of the given component) the fraction of molecules in each conformation at $t = 0$, which represents the ground-state equilibrium. This is more complex in a mixture of fluorophores due to a dependence of α_i on concentrations, absorption, quantum yields or their intensities. Presented multi-exponential model is one of the most powerful models which can be used to fit almost any intensity decay no matter the complexity.^[37]

Fractional contribution f_i of i -th decay component to the overall steady-state intensity can be calculated from the knowledge of values α_i and τ_i .

$$f_i = \frac{\alpha_i \tau_i}{\sum_j \alpha_j \tau_j} \quad (12)$$

From the equation (12), we can see that the intensity is usually weaker for the shorter lifetimes because the term $\alpha_i \tau_i$ decreases. In terms of graphical representation of a decay, the factor $\alpha_i \tau_i$ is proportional to the area under the decay curve for each decay time.^[37]

An example of the real fluorescence decay and fit is show on Figure 20.

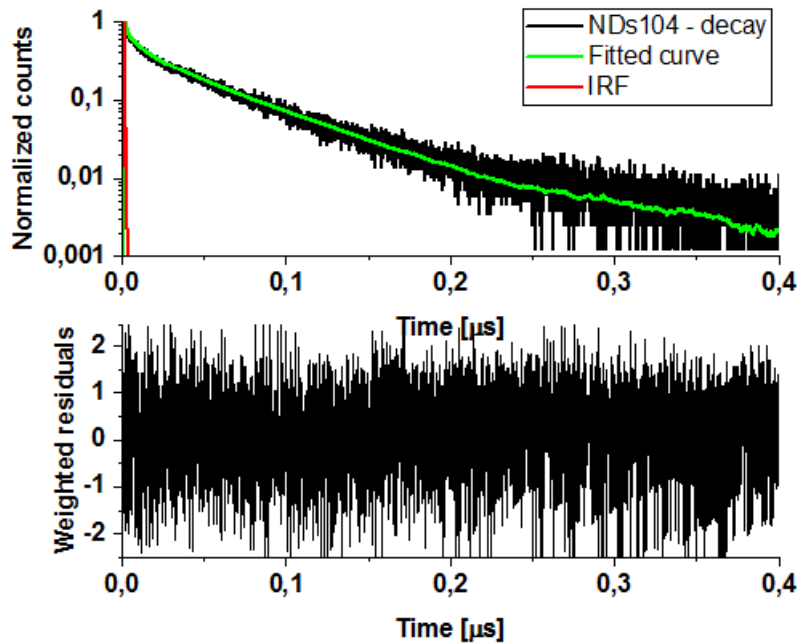


Figure 20: Example of the real fluorescence decay of nanodiamond (upper set of curves) fitted with four-exponential model and residuals (lower black horizontal curve) representing goodness of the fit.

3.1.5. Fluorescence lifetime imaging microscopy (FLIM)

Fluorescence lifetime imaging microscopy (FLIM) is fluorescence imaging technique based on resolving fluorescence lifetime of photons collected in each pixel of an image. FLIM is often extension of confocal microscope described above. As mentioned before, fluorescence lifetime is defined as the average time which the molecule of the fluorophore spends in the excited state before its return to the ground state. The contrast in the recorded FLIM image is therefore based on the fluorescence lifetime of individual fluorophores.^[40]

As the fluorescence lifetime does not depend on the concentration of the fluorophore, absorptivity of the sample, excitation intensity, this technique is more robust than usual intensity measurements. On the other hand, fluorescence lifetime is dependent on the fluorophore's surrounding environment and hence is pH, ion presence, energy acceptor dependent.^[41] Also, FLIM requires longer acquisition time and at least order of magnitude more signal than in conventional intensity based imaging.^[42]

The FLIM image is generated by assigning photons to different pixels by storing absolute arrival times of the photons additionally to the relative arrival times with respect to the laser pulse. Line and frame marker signals from the scanner are recorded to sort the time stream of photons into different pixels.^[38]

Based on above, FLIM is extremely useful technique for functional imaging of molecular or cellular dynamics.

3.2. Instrumentation used in the thesis

Experimental setup consists of inverted confocal microscope equipped with a piezo stage. Optical excitation of NV centres is done at 531 nm by a laser coupling unit (LDH-P-FA-530B, PicoQuant) with a picosecond pulsed diode laser (PDL 828 „Sepia II“, PicoQuant). The output of LCU is guided into the confocal microscope (IX73P2F, Olympus) via polarization maintaining single mode fibre. The laser beam is focused through the coverslip to a diffraction-limited spot in the sample, using 60x (water) immersion objective (UPlanSApo, Olympus) with a numerical aperture of 1,2. The same objective collects the fluorescence and guides the light through band-pass filter 635/10 nm (Edmundoptics). The detection is done by a single photon avalanche diode (SPAD) with single photon sensitivity (T-SPAD-100 (M), PicoQuant). Timing is measured using the multichannel TCSPC module HydraHarp 400 (PicoQuant) with picosecond resolution with TAC working in the direct (non-reverse) mode.

Fluorescence decay and saturation data were recorded in T3 acquisition mode because it allows high sync rates which cannot be handled in T2 mode due to dead time and to measure star-stop times for each detected photon. Antibunching measurements were carried out in T2 mode. The correlator can perform time-correlated single photon counting (TCSPC) measurements. Data were recorded and analysed in the software SymPhoTime 64.

A schematic of the described confocal setup is shown in Figure 21.

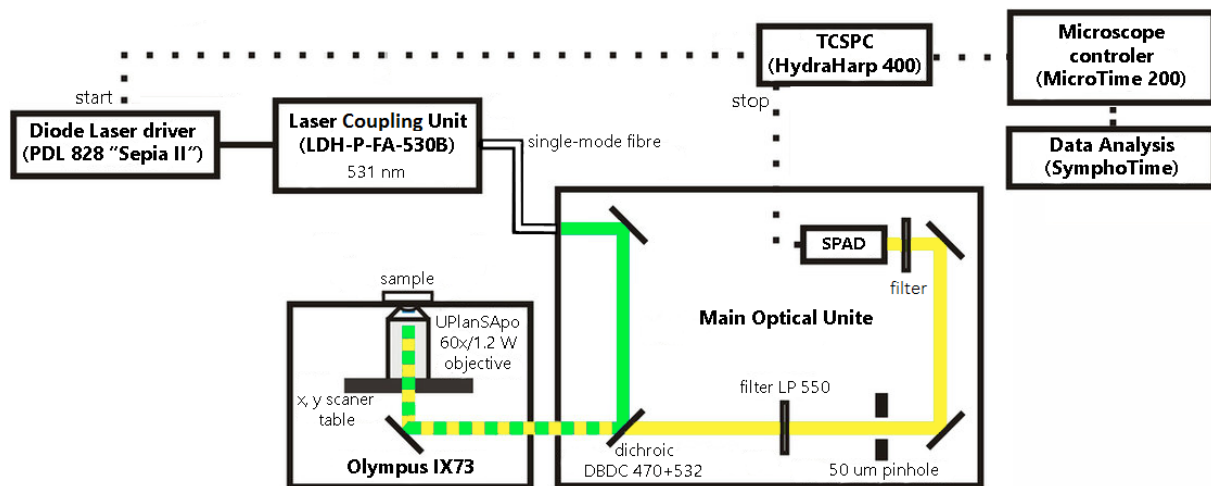


Figure 21: A schematic of the used confocal setup. [courtesy of Katerina Zambochova, modified]

3.3. Sample preparation

This part of the experiment was carried out to find a substrate and its (optionally) appropriate modification to ensure the lowest possible autofluorescence and other non-fluorescent contamination due to its possible negative effect on fluorescence emission of measured fluorescent nanodiamonds. In order to achieve reproducibility and reliability of samples during the measurement, several approaches have been performed and tested.

Substrate purification was performed for several purification procedures and was evaluated by fluorescence lifetime imaging microscopy. Sample preparation includes modification of glass substrate carried out in order to achieve a highly hydrophilic surface which prevents ND cluster formation and thus allows single-ND crystal distribution.

3.3.1.1. Substrate purification

The purity issue was partially solved treating microscope coverslips in the sonicator (E30H, Elmasonic) by placing them into the beaker filled with isopropyl alcohol (99,5%, 17550, Penta). The sonication lasted 15 minutes at temperature 60 °C. Coverslips were then washed by deionized water and sonicated again under same conditions. Another approach was using previously sonicated coverslips and alcohol solution of 20% sodium hydroxide (NaOH) to etch the surface of the substrate. The solution of 20% NaOH was prepared dissolving 13,05 g of NaOH pellets (71687 SIMGA, Sigma Aldrich) in 10 ml of demineralized water and then adding 70 ml of ethanol (96%, 70391, Penta). The solution was stirred and heated to 60 °C using magnetic stirrer (MSH-300, BioSan). After that, coverslips in the holder were placed into the beaker filled with prepared solution of 20% NaOH still stirring for several hours. Finally, coverslips were removed from the solution and carefully washed ten times with distilled water and stored in deionized water in a refrigerator. To evaluate and support importance of this step, described cleaning procedures were evaluated by FLIM, which was performed for untreated, sonicated and NaOH etched coverslips (Figures 22-24).

FLIM scanning was performed with repetition frequency 20 MHz using low excitation power 1,96 μ W sufficient to display short-lived fluorescence molecules (impurities) while not bleaching them. Filters used in this part were 550 nm LP and 750 nm SP with respect to the spectral range of emission of NDs (Figure 6b).

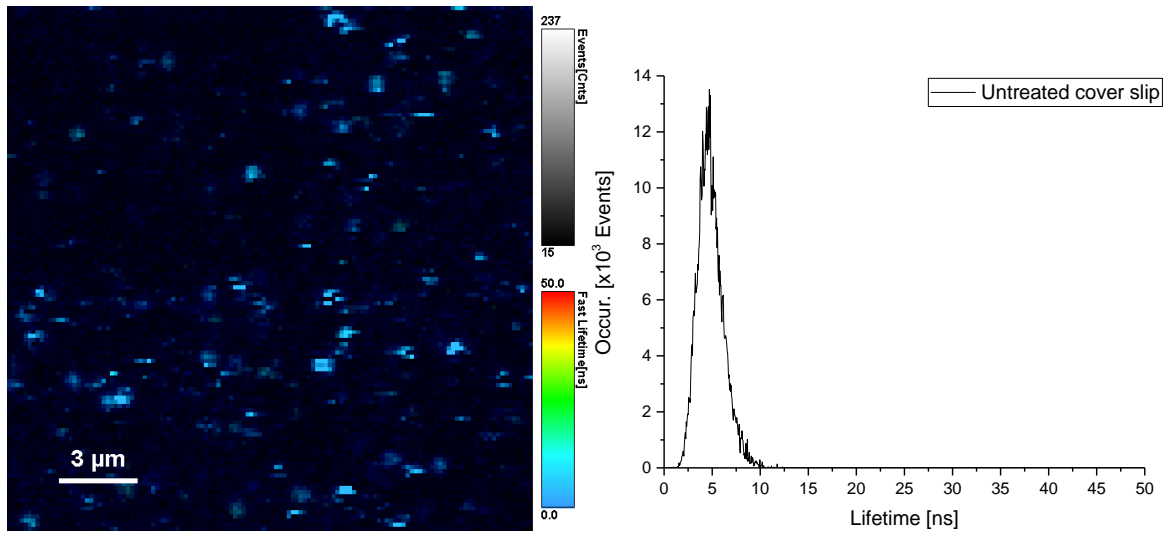


Figure 22: FLIM scan 20x20 μm of untreated coverslip with related fluorescence lifetime histogram.

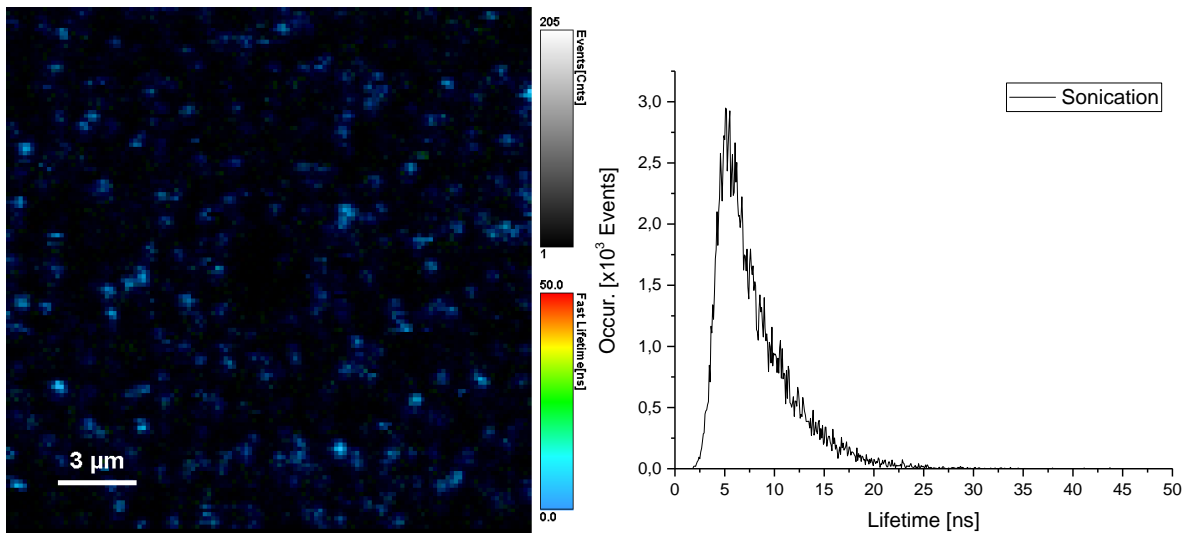


Figure 23: FLIM scan 20x20 μm of coverslip cleaned in the sonicator with related fluorescence lifetime histogram.

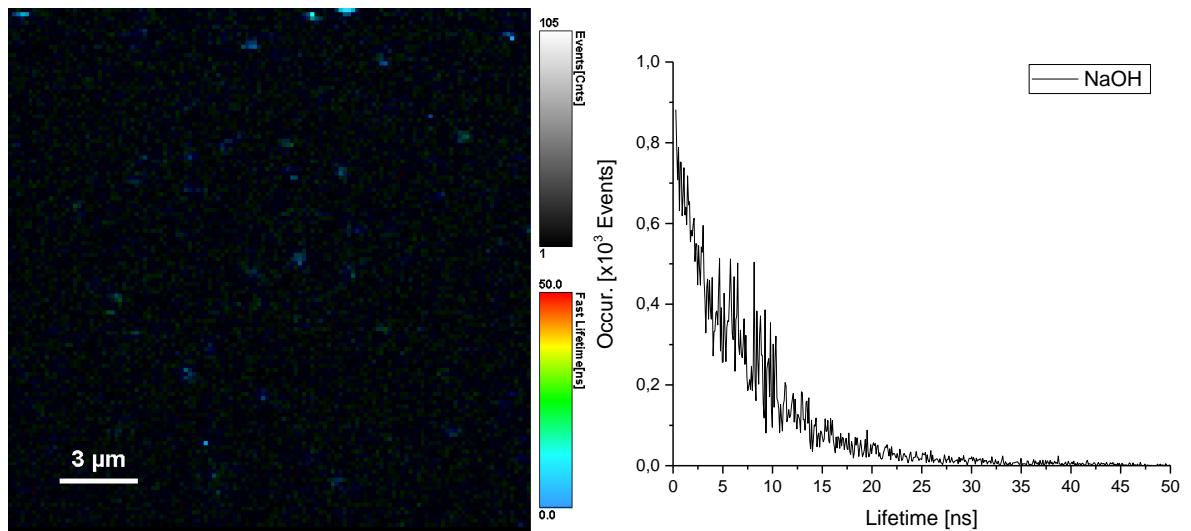


Figure 24: FLIM scan 20x20 μm of coverslip cleaned in the sonicator and etched with NaOH with related fluorescence lifetime histogram.

From detected occurrences of short-lived fluorescent impurities, it was found that untreated coverslips exhibited high fluorescent contamination (Figure 22) which clearly indicated the need of purification. Comparing fluorescence lifetime histograms in Figures 22-24, we can see that sonication of coverslips in isopropyl alcohol (Figure 23) showed an improvement by the factor of approx. 4,3 in reduction of fluorescent impurities compared to untreated coverslip. However, the result was not entirely satisfactory and more effective approach was needed. Etching sonicated coverslip with 20% NaOH (Figure 24) decreased the contamination more than 3 times in occurrences compared to sonicated coverslip. The overall decrease in contamination after etching was more than 14 times compared to untreated coverslip.

Not all the residual fluorescent contamination was eliminated by NaOH etching but it was the most successful method of all tested and provided hydrophilic surface of the substrate as a secondary effect which is regarded as a great advantage. Hydrophilicity of the substrate and its importance will be presented and highlighted in the following chapter.

It was shown that the untreated substrate was heavily contaminated by fluorescent impurities. Therefore, it was essential to clean it appropriately before the use. Impurities can be distinguished by their short fluorescence lifetimes. Two cleaning methods were tested. The first method was sonication of coverslip in isopropyl alcohol which shown not to be as effective as desired. The second method used 20% NaOH to etch the surface of the previously sonicated glass substrate and notably reduced the contamination.

Suggested improvement might be longer application of NaOH or its higher concentration. A selection of different chemicals (strong acids, e.g. piranha solution) could also lead to better results. Another possible way of purification of the substrate is treating glass substrate with oxygen plasma (O-termination). However, the device is not available in our laboratory, so plasma-cleaned substrates are not readily available. Also, O-termination slowly degrades which is where the advantage of NaOH lies. Coverslips can be stored in NaOH solution or in deionized/demineralized water (after NaOH treatment) for a very long time if conserved and sterilized in, for example autoclave.

3.3.1.2. Sample preparation and contact angle measurement

This section is dedicated to finding a suitable substrate, or rather its optimal modification, to ensure required distribution of diamond nanocrystals, i.e. evenly distributed single nanodiamonds with least possible clustering. This could be achieved using substrate, or its

modification, which would have high (or increased) wettability. NDs are applied on the substrate in the form of water-colloidal solution. A high wettability/hydrophilicity of the substrate causes water drop to spread across its surface which decreases the probability of clusters formation during the drying and washing process. This situation can be represented by the approximation of the sample arrangement in Figure 25.

Firstly, let's consider coverslip treated in oxygen plasma (O-termination) (Figure 25a) with a hydrophilic and negatively charged surface which brings an issue of the same mutual polarity of NDs and the surface. Their interaction is likely to result into clustering of NDs because NDs will not be held in the position and thus the distribution would not be uniform. The requirement is to have separated single diamond nanocrystals across the substrate's surface. This could be effectively achieved by addition of a thin layer of cationic polymer (Figure 25b) on the interface between NDs and the substrate. Such polymer would bind NDs through electrostatic interactions and form a PEI-ND complex.

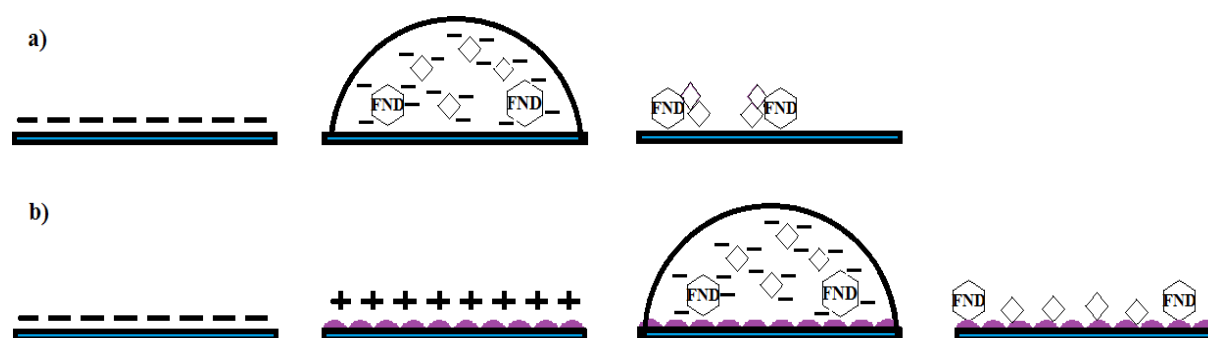


Figure 25: A schematics of arrangement of diamond nanoparticles according to the substrate. NDs are deposited on a) oxidized substrate, which leads to the clustering due to same polarity of NDs and the substrate, and b) polymer-coated substrate, which electrostatically binds negatively charged NDs and stabilizes their position on the substrate. Purple corrugated layer coating the blue coverslip represents positively charged Polyethylenimine.

The wettability of the glass substrate and its several modifications were examined and evaluated by a contact angle measurements where, for the high wettability, it is expected to measure low contact angles. The contact angle was measured for untreated, oxidized coverslip and coverslip covered by a thin layer of polymer Polyethylenimine (PEI). Polyethylenimine is a low molecular branched cationic polymer which was used to bind electrostatically negatively surface-charged^[9] NDs. PEI coating was created by addition of 150 – 200 μ l of Polyethylenimine of molecular weight 2000 g/mol (PEI 2000) on the glass

substrate (18x18 mm, 0,18 mm) and left for 10 minutes to attach to the substrate. After 10 minutes, the remaining (undried) PEI was carefully washed by deionized water from the wash bottle and substrate was left to dry out. After that, it was measured for contact angle.

Contact angles were measured on a home-built setup by applying 3 μ l of deionized water on the surface of all tested samples (Figure 26). Shape of the droplet was captured by the 13 Mpix digital camera, a light bulb as the light source. Contact angles were analysed by the software ImageJ.

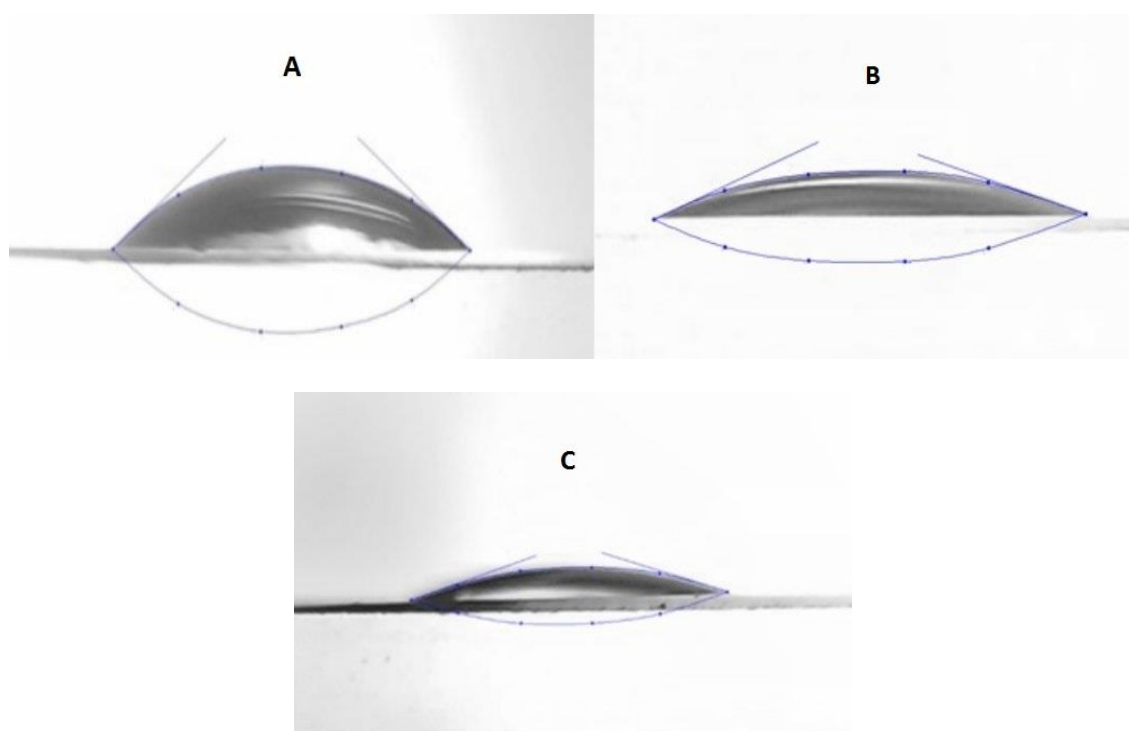


Figure 26: Contact angles of water droplets on various substrates. Water droplets on the A) non-treated substrate, B) oxygen-terminated substrate, C) Polyethylenimine-coated substrate.^[30]

Contact angles measured for three substrate modifications; untreated, O-terminated, PEI-coated coverslip were as follows 34,8 °, 17 ° and 12,5 °. Polymer Polyethylenimine significantly increased wettability (lowest measured contact angle) which makes it the most suitable modification of all tested. For this and following reasons, Polyethylenimine was added in the sample preparation procedure.

In the next step, Polyethylenimine was tested, before applying NDs, to evaluate its fluorescence contribution to overall fluorescence measured during ND fluorescence

acquisition. As shown on Figure 27, molecules of PEI are slightly fluorescent but can be photobleached using sufficiently high excitation power. The value of bleaching intensity may be almost arbitrary (high enough to eliminate undesirable luminescence) since we are dealing with nanodiamonds known to be highly photostable.

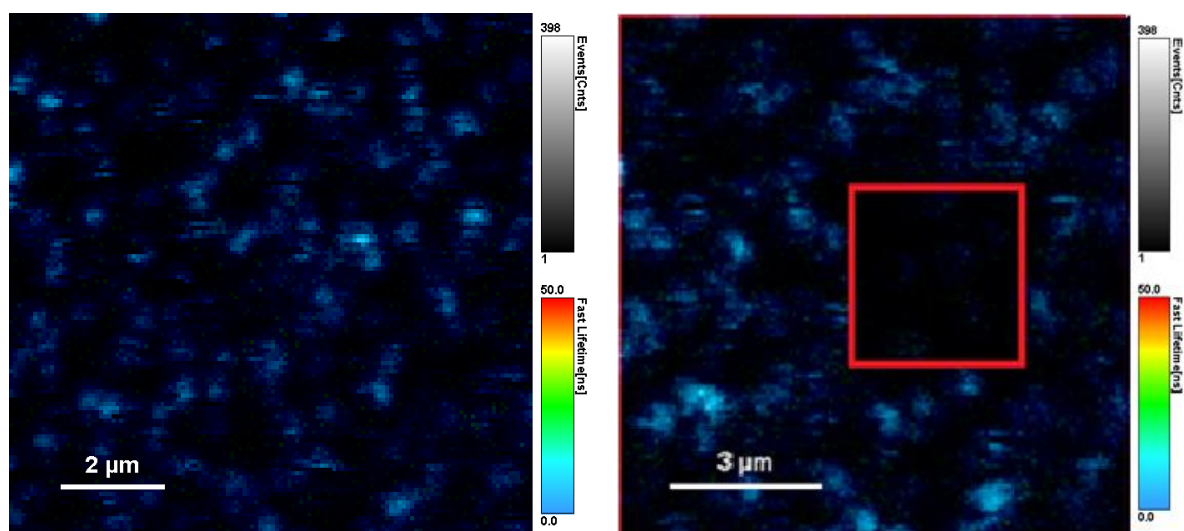


Figure 27: FLIM scans (10x10 μm) of PEI before (left) and after (right) irradiation with high excitation power. Red-marked region indicates photobleached area and subsequent elimination of fluorescent molecules.

From this step (including PEI deposition) any fluorescent impurities cannot be in our conditions eliminated any other way than by photobleaching because otherwise we would risk sample contamination or damage to PEI layer, and consequently to NDs distribution.

The final step in the sample preparation is application of ND solution on the substrate. 150 – 200 μl of ND solution was applied on the glass substrate coated with PEI 2000. ND solution was left 10 minutes for NDs to attach to PEI. Remaining solution of NDs was washed by deionized water from the wash bottle six times and left to dry out.

The fluorescence of NDs often cannot be visible during the first confocal scan since the unwanted fluorescence of PEI is stronger (Figure 28). Figure 28 (right) represents a typical confocal map of fluorescent nanodiamonds on the substrate. If the short-lived fluorescence on Figure 28 truly originates from PEI, it could mean that PEI forms not only bottom layer on the glass surface but also another surface layer over NDs that were attached to the substrate due to the water solubility of branched PEI 2000. Dried PEI layer might be partially dissolved by the water solution containing NDs, dropped on dried PEI, which would allow PEI molecules

to diffuse into the water droplet and descend onto already descended and attached NDs. This issue can be again quite effectively solved by photobleaching of PEI molecules because NDs are highly photostable and therefore will remain unaffected by higher excitation intensities. What remains after irradiation, are only easily distinguishable nanodiamonds with visible fluorescence emission.

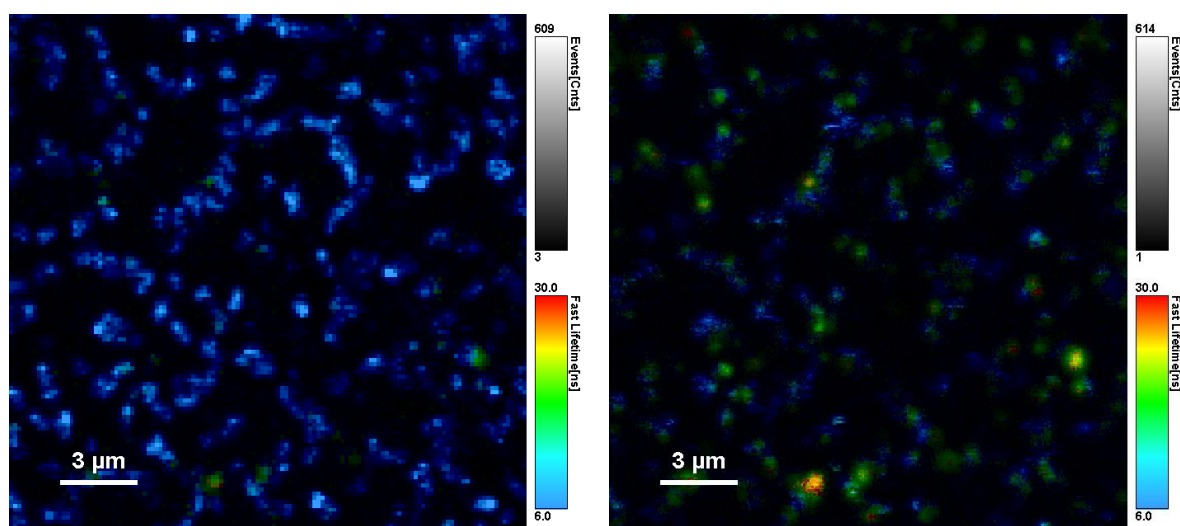


Figure 28: An example of FLIM scan of diamond sample before (left) and after (right) photobleaching of fluorescent molecules of non-diamond character. Green dots in the photobleached area represent fluorescence emitting nanodiamonds.

The excitation intensity used for bleaching (Figure 28 right) of non-diamond fluorescence was intentionally used lower than necessary for a complete cleaning of the observed area to show numerous NDs which were previously covered by non-ND fluorescence.

Unwanted fluorescence comes also from the immersion water, dust deposited on optical surfaces in the microscope body, or the glass coverslip. In the case of silica coated NDs, these are kept in a stock solution of ethanol which is diluted by deionized water to prepare samples. Impurities dissolved in the colloidal solution could then contribute to the short-lived fluorescence as well (lifetime histogram on Figure 29). Short-lived fluorescence in the lifetime histogram around 2,5 ns likely comprises of contributions from the polymer layer, optics, immersion, sample solution.

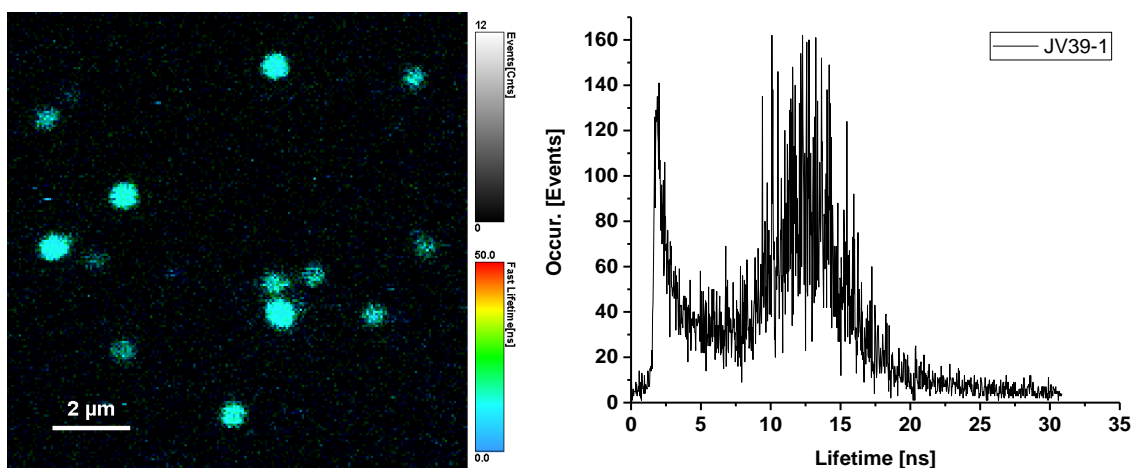


Figure 29: An example of FLIM scan of sample JV39-1 (silica coated) with overall lifetime histogram.

Three kinds of HPHT ND samples were used in this experiment, all provided by our colleagues from Institute of Organic Chemistry and Biochemistry of the CAS. First were 60-nm large source nanodiamonds NDs104 (Microdiamond, Switzerland MSY 0-0.05.). Vacancies were created by electron beam irradiation in microtron with energy 16,6 MeV and nitrogen-vacancy centres were created by a subsequent annealing at 900 °C for 1 hour.

Second were source diamonds embedded in 50-nm thick silica shell (total size 160 nm) (sample name: JV39-1), and third were source diamonds embedded in 100-nm thick silica shell (total size 260 nm) (sample name: JV39-4) (Figure 30). Characterisation of particles, i.e. overall size and confirmation of presence of single ND particle in each silica shell was done using TEM (unpublished data not shown).

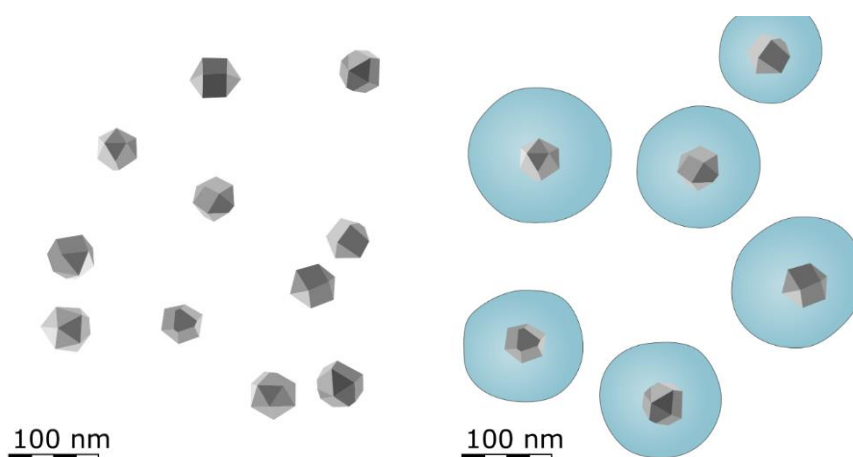


Figure 30: Representation and structure of investigated source nanodiamonds NDs104 (left) and silica coated JV39-1 (right)

The following part of this section will focus on determining the appropriate range of concentrations of FNDs solutions which is, with respect to the sample preparation method, the most favourable one in order to have adequately separated particles at least 1-6 μm without formation of clusters. Since three kinds of samples were measured, it was necessary to find such concentrations for source nanodiamond and coated nanodiamonds as well.

Samples of silica coated NDs were prepared from ethanol-based colloidal stock solution which was diluted in water to gain the target concentration. Ethanol is used for long-term storage of the silica-embedded NDs because the silica shell is not stable in aqueous solution. For samples NDs104 (60 nm), JV39-1 (160 nm) and JV39-4 (260 nm) were tested concentrations: 0,01 mg/ml, 0,005 mg/ml, 0,0035 mg/ml, 0,0032 mg /ml, 0,003 mg/ml, 0,0025 mg/ml, 0,002 mg/ml, 0,001 mg/ml. These initial concentrations were chosen according to previous experiments and preparation method described previously. The most satisfactory results were obtained for (optimal) concentrations in range from 0,0032 mg/ml to 0,0025 mg/ml (see example in Figure 31).

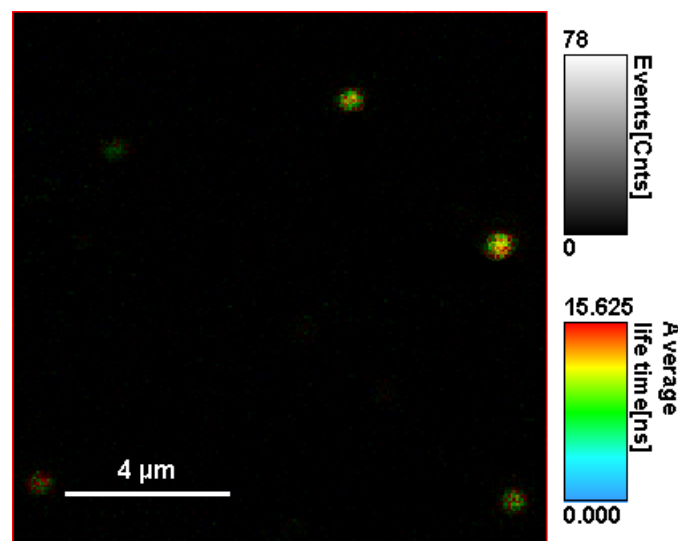


Figure 31: Example of FLIM scan 10x10 μm of JV39-1 showing required distribution of NDs prepared from 0,0032 mg/ml ND solution from the determined optimal range concentrations.

Concentrations of diamond solutions for all measured samples (uncoated NDs104 and two coated modifications JV39-1 and 4) were found to be, for the presented sample preparation and given requirements, in range 0,0032 mg/ml to 0,0025 mg/ml.

It should be mentioned that the distribution of nanodiamonds is not homogenous but might differ substantially area to area due to its dependence on the washing part of the sample preparation and time of incubation. Time of about 10 minutes of incubation ensures, to a certain extent, reproducibility. Washing might be additionally improved by submerging the sample into Petri dish filled with deionized water for a certain amount of time before using wash bottle. In case of washing, one should take into consideration that the described procedure works just fine but depends also on the angle of the coverslip that is being washed or the stream intensity from the wash bottle which might result into clustering of ND particles or unnecessarily wash some ND particles away.

It was found that substrate (glass coverslip) covered with thin layer of cationic polymer Polyethylenimine (PEI) exhibited the highest measured wettability and therefore, lowest contact angle (12,5 °). PEI electrostatically binds and mechanically stabilize negatively charged non-coated nanodiamonds. Then the fluorescence of PEI was observed and evaluated as a possible unwanted contributor to the detected NV fluorescence. This fluorescence was found to be short-lived and that it can be effectively photobleached using high excitation power. In this case, the excitation power is not limited due to high photostability of nanodiamonds.

3.4. Measurement procedure

This chapter comprise of technical troubleshooting and analysis of possible effects of critical parts of the instrumentation which were found to influence recorded fluorescence decay.

3.4.1. Single particle imaging and decay measurement

3.4.1.1. Scattering of excitation light on nanodiamonds

In the initial phase of the experiment, fluorescence decays were recorded with combination of two optical filters inserted behind the dichroic mirror, long pass (LP) filter with cut-off wavelength 550 nm and short pass (SP) filter with cut-off wavelength 750 nm, to obtain as much ND fluorescence signal as possible. This range (550-750 nm) covers the emission range of NDs quite well (Figure 6b) and LP 550 nm also blocks the laser light (531 nm) effectively, so it does not disturb detected fluorescence. However, acquired fluorescence decay curves suffered from distortion in the peak (Figure 32a) which probably originated from the light scattered on the diamond nanoparticles. This gravely influenced and altered results of the data analysis since scattered light adds apparent fast components to the recorded decay.

To eliminate this phenomenon, short pass filter 750 nm was replaced by the band pass filter 635 ± 10 nm which successfully eliminated the scattering but greatly reduced the fluorescence signal (Figure 32b) of almost one order of intensity. Due to 635 ± 10 nm band pass filter most of the NV^0 fluorescence is cut off and mainly NV^- fluorescence is detected (Figure 6b).

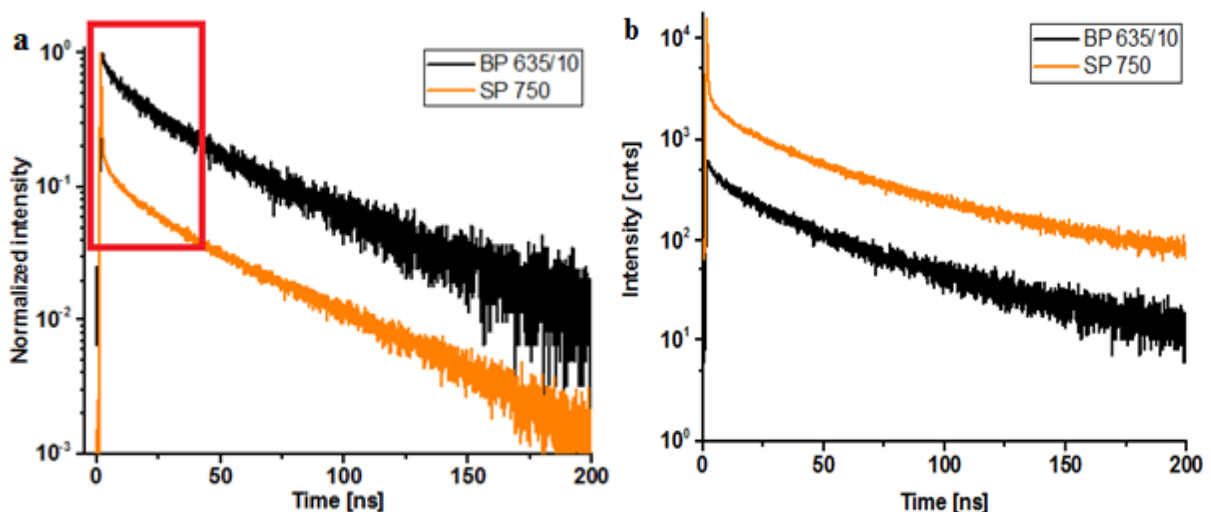


Figure 32: Comparison of fluorescence decays of NDs104 with a) indicated distortion of the curve peak caused by the scattering and b) reduction of the fluorescence signal due to the BP filter 635 ± 10 .

Black curve indicates fluorescence decay of the particle with the use of BP 635/10 nm filter and orange indicates fluorescence decay with the contribution from the scattered light recorded with SP 750 nm.

The shape of fluorescence decay after the elimination of scattering suggests multiexponential fluorescence decay of measured nanodiamond. In a logarithmic scale, monoexponential decay would have a form of a decreasing straight line which it is not in this case. Therefore, it is the issue of a multiexponential fluorescence decay. This fact and related causalities will be discussed later in this work.

3.4.1.2. Motion drift of the particle

Another distortion of recorded fluorescence decays occurred from the motion drift of the measured particle during the data acquisition (Figure 33). The drift is caused by the piezo-stage mounted on the microscope. Since FLIM or fluorescence decay measurements are often time-consuming tasks, the motion drift caused that the scan marker on the scanned particle was slowly changing its starting position from the centre of the particle and end up positioned on the background – out of the particle.

The drift causes two major problems which could lead to a degradation of measured data. First, the recorded fluorescence signal is being slowly reduced as the particle drifts and therefore, prolongs the time of acquisition necessary to obtain required amount of fluorescence counts. Second problem is that an irrelevant non-ND fluorescence and back-reflected light from the background is recorded and might overweight slow lifetime components hidden in the tail of the histogram. These issues consequently alter computed fluorescence lifetimes and have a great impact on the data analysis (curve fitting).

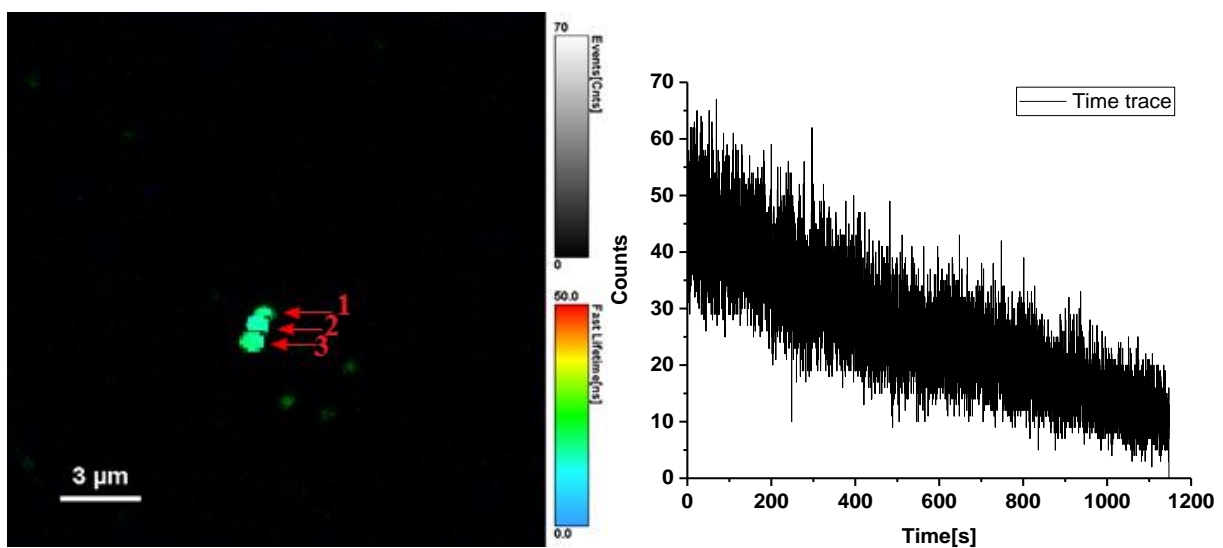


Figure 33: Motion drift of the observed NDs during the long measurement supplemented with a decreasing time trace signal due to the drift.

For the purpose of showing the drift a cluster of diamond particles was chosen due to its larger size which makes the drift more evident. The cluster changed its position during the 15-minute measurement from the position 1 to 2 which is approximately 0,25 – 0,5 μm and from the position 2 to 3 in another 15-20 minutes. This distance is of great importance because any of the measured particles (60 – 260 nm) would end up completely out of the measured point in about 15 minutes and would completely invalidate results. With respect to the drift, the time of acquisition must be shortened as much as possible while preserving the maximum amount of information sufficient for the correct analysis.

It was found that the maximum time about 10 – 12 minutes and positioning the marker not in the centre but slightly forward (still on the particle) in the direction of the drift (Figure 34a) will not disturb measured information.

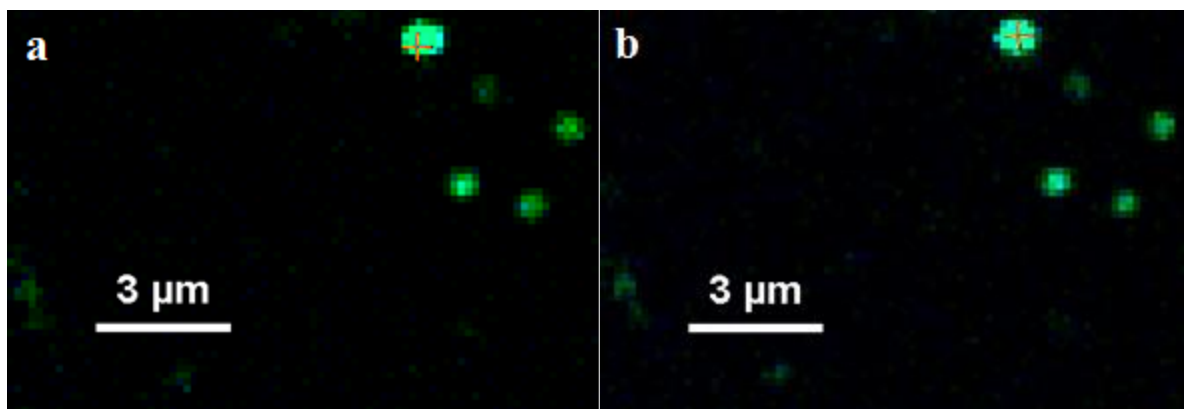


Figure 34: Position of the cross indicator on the particle a) in the beginning of the measurement

Figure 34 shows that placing the scan marker before the centre of the displayed particle at the beginning of the measurement will end up with the marker approximately in the centre of the particle (Figure 34b) where the maximal signal is detected. However, this is satisfactory for bigger clusters or smaller particles which provide sufficient fluorescence signal. Some particles may contain less (or only one) NV centres and emit weaker fluorescence signal. In this case, the particle could drift and be scanned over its entire surface, which would again result with the marker out of the particle (on the background).

Therefore, all measured particles were selected according to their count rate. The count rate threshold value was determined as 1000 counts/s collected from the centre of the particle at excitation power 2000 au (12,4 μW) which is the excitation power also used for following

fluorescence decay measurements. Excitation power 12,4 μW is the maximum power achievable at selected excitation frequency 1 MHz which was chosen with respect to the length of fluorescence decay of investigated NDs.

3.4.1.3. Diffraction limited resolution

Theoretical diffraction limit of the microscope and displayed size of particles on FLIM scans must be compared in order to verify that truly single particles are imaged. Measured particles (3.3.1.2.) have actual size 60 nm – 260 nm and appears as colored circular symmetrical spots on the dark background (Figure 35). Size of these spots is given by the diffraction limit of used confocal microscope. The diffraction limit indicates limitation of resolution of the microscope objective. The diffraction-limited resolution of the immersion objective with numerical aperture (NA) 1,2 and excitation wavelength 532 nm is given by following expression:

$$\Delta \approx 0,61 \frac{\lambda}{NA} = 0,61 \frac{532}{1.2} \doteq 270 \text{ nm} \quad (13)$$

Parameter Δ indicates the smallest theoretical resolvable distance assuming, that two point sources can be resolved (as two separate objects) when the centre of Airy disk of the first object overlaps the first dark ring in the diffraction (Airy) pattern of the second object. This rule is termed Rayleigh criterion.

Here, the calculated diffraction limit is approximately 270 nm. However, in reality, this limit is slightly larger. The highlighted area shows one of the best focussed/resolved FLIM scans of NDs104 our confocal system is capable of. According to the scale (0,3 μm), the size of the spot is around 300 nm which is larger than the calculated estimation 270 nm.

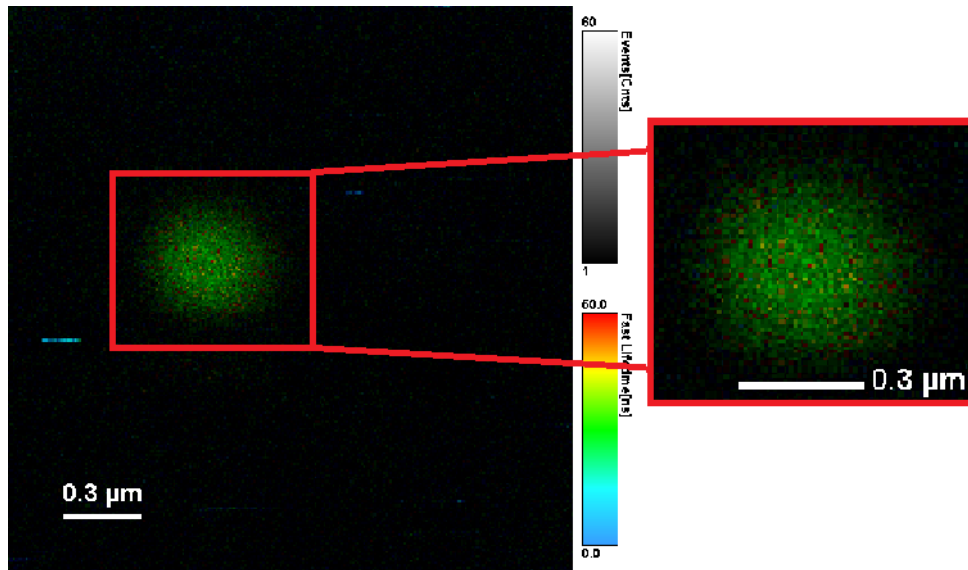


Figure 35: Diffraction-limited FLIM scan of NDs104 (60 nm single crystal). The highlighted area indicates a diffraction limited-spot which represents observed ND particle.

In this experiment, from the image alone, it cannot be concluded whether the fluorescence originates from a single diamond nanoparticle or from a cluster of several nanodiamonds with one or multiple NV defects, particularly in case of the NDs104 (60 nm). To determine the number of independent emitters or whether the single particle contains only one NV centre in the focal volume the emission statistics of the NV fluorescence can be done through observation of photon antibunching via cross-correlation measurement (see 4.1.). Another way to determine the number of fluorescent NDs and solve this uncertainty, is using simultaneous FLIM-AFM (AFM – Atomic Force Microscopy) acquisition^[15]. The combination of FLIM with AFM was not performed because our system is not equipped with a module for simultaneous measurement and doing this without the module is a difficult and a considerably time challenging task (which includes difficult positioning of separately recorded scans from two different systems). Also, only a certain amount of NDs emit fluorescence signal strong enough to be displayed on FLIM scans and therefore, only NDs with stronger emission can be used for identification of measured particles and orientation in the overlap of AFM and FLIM scans. Another advantage of using FLIM+AFM is that it enables to examine the dependence of NV photoluminescence on the shape or size of the particle, which is suggested as following of the work presented in this thesis. Rather than above mentioned techniques, this work focused more on the photon statistics of as large set of measurements as possible.

3.4.1.4. Determination of excitation frequency

The correct choice of excitation frequency is a vital step and goes hand in hand with the time of acquisition, with respect to the particle drift (described earlier), during TCSPC measurement. In a fluorescence decay acquisition and analysis, the repetition rate directly influences excitation and relaxation of the sample (quantum system) and therefore it affects the decay itself (Figure 36). There is a desire to detect as many fluorescence photons as possible and accurately estimate the fluorescence lifetime, which are subjected to the high repetition rate, but, on the other hand, achieve sufficient imaging frame rate and preserving the quality of the data.

When the excitation frequency is selected too high, the quantum system (NV centres) is not allowed to fully relax during its decay before the next excitation pulse is sent and starts another excitation cycle. The repetition rate of a light source is a limitation in the measurement of long decays where the average fluorescence lifetime is comparable to the period between individual excitation pulses.^[47] Consequently, the interval between two excitation pulses is recommended to be up to five times^[37] of the average fluorescence lifetime for the accurate measurement of the lifetime.^[47] Fluorescence decay of such unrelaxed system is shown in Figure 36 and appears as a constant part of the histogram in a few first nanoseconds and also the tail of the histogram should follow the trail of the curve until it reaches and merges with the background signal. Because of the high repetition frequency, slow lifetime components, that are „hidden“ in the tail, would contribute significantly to the current decay curve, which leads to an inaccurate lifetime estimation.^[42] Reduction in the repetition frequency is needed. However, lower excitation frequency will result in an increase of the acquisition time.

In [47], original (unaltered) and measured multi-exponential decay curves were tested, both experimentally and numerically, to determine how does an incomplete decay influences estimated fluorescence lifetime components and corresponding coefficients, using inverse model to predict original lifetime parameters from the measured ones. It was found that for a mono-exponential decay is the incomplete decay the same as the original individual lifetime. For the multi-exponential decay, individual lifetime components are not affected but the average lifetime is underestimated and thus the results must be carefully interpreted.

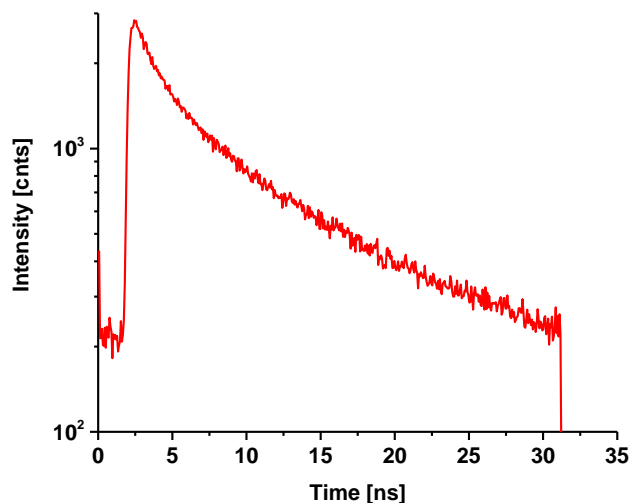


Figure 36: Example of fluorescence decay of not fully relaxed NV centre.

To determine a suitable excitation frequency for the fluorescence decay acquisition, excitation frequencies 20 MHz, 5MHz and 1MHz were examined as a dependence of fluorescence intensity on excitation power for three NDs from all three used kinds of NDs. Example of obtained results for the frequency 1 MHz is shown in Figure 37. Excitation powers were chosen from the range 0 – 2000 au (12,4 μ W) where 2000 au is the highest possible excitation power achievable at 1 MHz. Distinctions in linearity and intensities between each kind of sample were observed. Second aim was to use following results to evaluate possible effect of different environments on fluorescence emission and saturation.

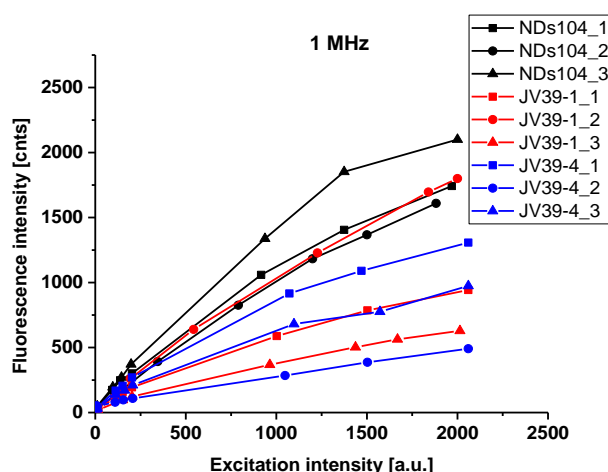


Figure 37: Comparison of dependencies of fluorescence intensity on excitation power for excitation frequency 1 MHz.

No major differences in intensities (including saturation) in the linear range for investigated excitation frequencies were found. Also, any direct effect of examined environments on the fluorescence emission of NDs cannot be concluded from presented data. This is probably due to the short observed range of intensities and a small set of examined populations of NDs.

Assuming the condition about period between excitation pulses with respect to the lifetime, Figure 37 shows that it is safe to use excitation frequency 1 MHz at its highest excitation power because it is sufficiently low and should not disturb decay histogram, while providing acceptable signal and relaxation conditions for NV centres.

The effect of excitation frequency on fluorescence lifetime was also investigated through FLIM lifetime histograms. Uncoated nanodiamonds NDs104 and fluorescent suspension beads (TetraSpeck, ThermoFisher) were investigated. Uncoated NDs were chosen with purpose to neglect additional effect of environment (silica shell). Fluorescent beads were stained throughout with four different fluorescence dyes, displaying four separated excitation and emission peaks from 360 – 680 nm. Fluorescence lifetime histograms (Figure 38) were obtained as Regions Of Interest (ROI) for all individual displayed circular objects (beads, NDs). Using ROI enables to minimize overall contribution from the background to displayed histograms and obtain information only from measured objects. Excitation frequencies were 10, 20, 32 MHz with the time resolution 256 ps. Excitation power used for excitation of beads was 5000 au (31 μ W) and 20000 au (124 μ W) for NDs. Lower excitation power for beads was used to prevent photobleaching. NDs were excited with higher excitation power because NDs need strong excitation to emit satisfactory fluorescence signal and for better FLIM resolution. Also, the magnitude of excitation does not affect fluorescence lifetime, so there should not be any negative effects influencing lifetime histograms.

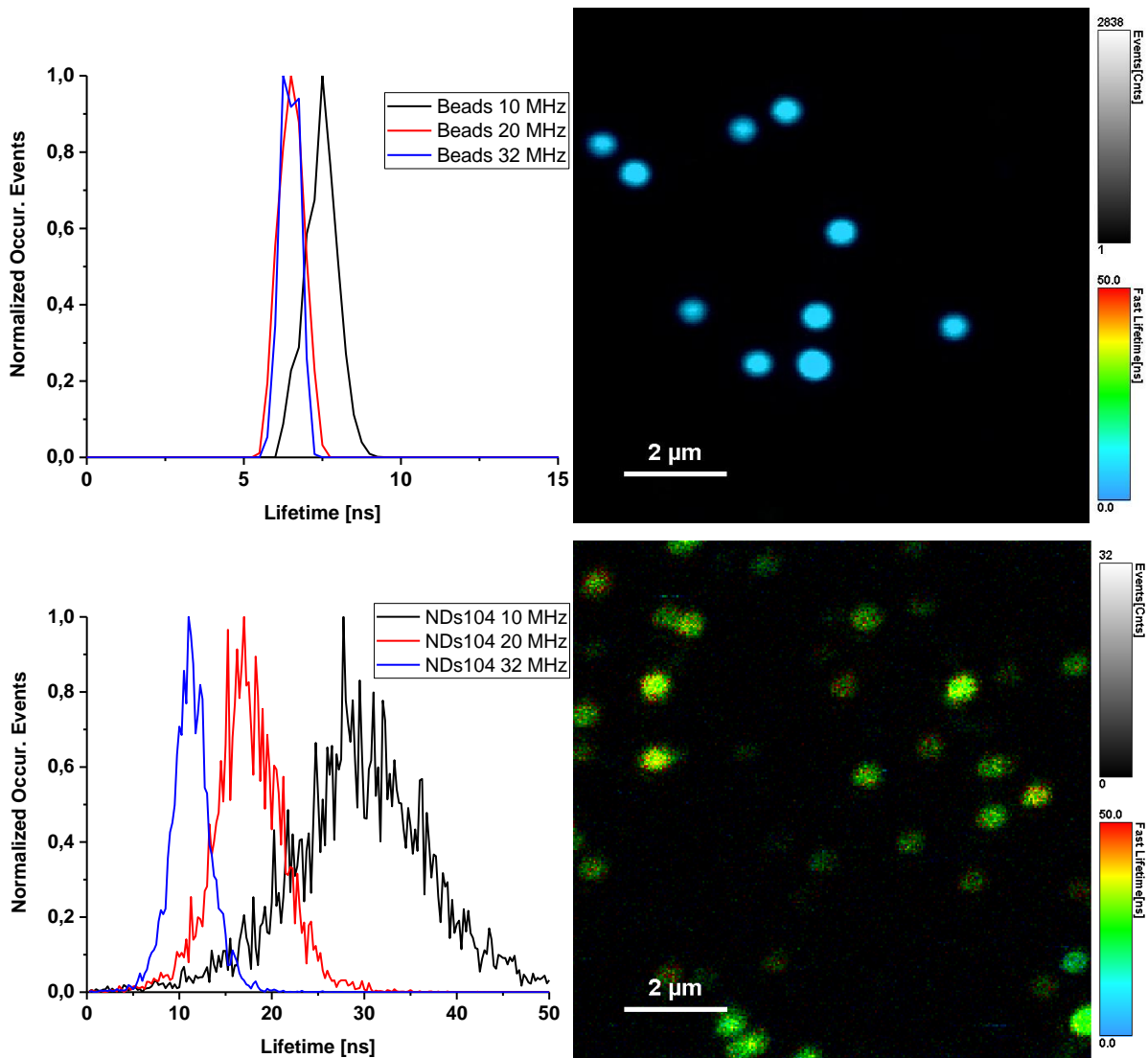


Figure 38: Fluorescence lifetime histograms of fluorescent beads and uncoated diamonds NDs104 for selected excitation frequencies. Upper figures represent lifetime histogram and FLIM image of fluorescent beads, lower figures represent the same for multiple ND (NDs104).

Figure 38 shows that apparent fluorescence lifetime depends strongly on the repetition rate. With increasing repetition rate lifetime histograms are shifted to lower lifetime values. This is in agreement with [42] and supports the claim that repetition rate needs to be kept as low as possible with respect to the time of acquisition and rule about excitation intervals and fluorescence lifetime of the sample.

Considering above, conclusion about correct excitation frequency can be reached. Assuming 25ns fluorescence lifetime, as a higher estimated value of fluorescence lifetime declared for NV centres (range of τ up to 25 ns)^[5,7], and the recommendation of at least five times longer interval between two excitation pulses than average fluorescence lifetime,

the repetition rate 20 MHz cannot be used. Excitation frequencies 5 MHz and 1 MHz meet the requirements but, as precaution, 1 MHz was chosen for point measurements since it provided a sufficient signal and a satisfactory time of the decay acquisition. Frequencies 20 MHz and more would be preferred for imaging (scanning) and displaying NDs because scanning with low excitation frequency (1 MHz) provide weak signal. Based on above, FLIM scans and lifetime histograms obtained from scanning with high excitation frequency are not reliable to use for study of dependence of ND fluorescence lifetime on the environment. This confirms that point measurements at low repetition frequencies are the correct method for accomplishing stated aims.

3.4.1.5. Instrument Response Function acquisition

The meaning of Instrument Response Function (IRF) and its importance in TCSPC analysis was introduced in 3.1.4.3.. The IRF is the best approximation to a temporally infinitely short process possible to measure with a given instrument often referred to as a „lamp function“. The temporal profile of the excitation features or response of the detector are the main contributions to the IRF.^[48]

The IRF was recorded as a response of the instrumentation on the scattered excitation light. However, recording of IRF was preceded by a maintenance^[39] which was carried out before each measurement session to ensure proper adjustment of the main optical unit for the highest possible correctness and precision of the process.

The maintenance of the main optical unit comprises of a quick check of the optical hardware and evaluation of the overall system performance. As a test sample was chosen a thin polished silicon plate glued to the microscope slide. The slide was put on the sample holder with the metal plate downwards facing the microscope objective (inverse confocal microscope) so that the excitation light is directly scattered from the metal plate. Immersion was added on the objective and then the objective was carefully moved close to the sample in order not to create bubbles which would have otherwise impaired the result. A z-position was verified through the video camera by opening the excitation shutter and illuminating the metal plate. After that the objective was raised until the back reflection was visible with the video camera. The beam spot of the back-scattered light on the video camera should be visible as a circular and symmetrical pattern which indicates a correct alignment (the excitation beam runs through centres of the objective lenses) (see Figure 39).

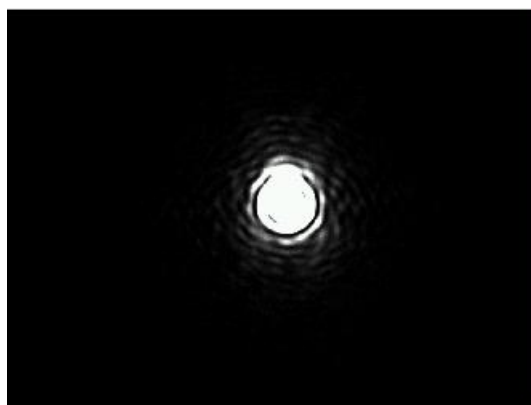


Figure 39: The on-axis beam spot of the back scattered light displayed on the video camera.

Next was the alignment of the lateral position of the pinhole. First step was the selection of the OD3 neutral filter (OD = optical density, grey filter) with 0,1% transmission instead of LP filter, then removal of BP filter before the detector, and observing the time trace signal (cnt/s) on the detector with opened shutter and binning 30 ms while aligning the pinhole. The pinhole was aligned moving the knobs of its holder back and forth until the maximum count rate is reached while observing the changes in time trace signal from minimum to maximum. After that the width and the time-position of the IRF was checked in the TCSPC histogramming mode. While monitoring the IRF, the SPAD lens was fine-tuned to ensure the narrowest IRF and moved as much as possible to the left (0 on x axis).

The last part of maintenance can be used also for measurement of the IRF. IRF recording was performed with the excitation power 12,4 μW (2000 au), excitation frequency 1 MHz, and binning 64 ps, until the peak value reached at least 10^4 counts. It is important to record IRF under the same conditions as fluorescence decay, e.g. same TAC settings and same number of time channels (if possible), acquisition due to subsequent data analysis. An example of recorded IRF is in Figure 40.

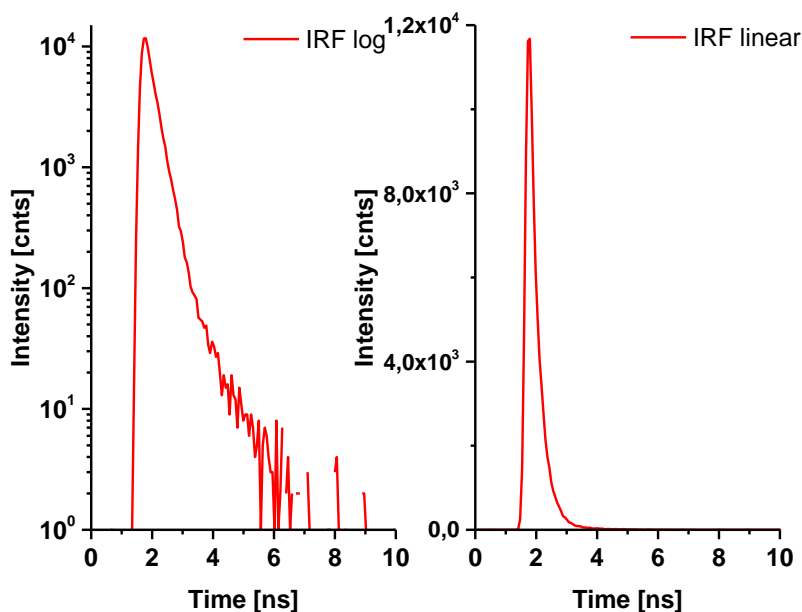


Figure 40: Example of instrument response function for the MicroTime 200 system (see 3.2.). Left: semi-logarithmic scale, right: linear scale.

3.4.1.6. Fluorescence decay measurement

Nanodiamonds and „environments“ used for fluorescence decay measurements were 30 untreated source nanodiamonds (NDs104, 60 nm), 30 silica (TEOS, refractive index $(n) = 1,46$)^[49] coated nanodiamonds with thinner (JV39-1, 160 nm) shell and 30 with thicker (JV39-4, 260 nm) shell, and 10 source nanodiamonds NDs104 measured on air and covered with deionized water ($n = 1,315$)^[50]. Sample preparation and related characteristics of nanodiamonds were described earlier in 3.3.. Excitation power used for fluorescence decay acquisition was 2000 au (12,4 μw) with excitation frequency 1 MHz. To avoid the motion drift of measured particles, acquisition time had to be kept under approximately 12 minutes. To ensure adequate fluorescence signal and time of acquisition from measured particles, a threshold value of detected count rate was determined as 1000 counts/s. Measurements were finished when the number of fluorescence counts reached 10^3 . The upper value 10^3 counts was determined as sufficient for the statistical analysis in terms of reconvolution fitting, since 10^3 counts and chosen measurement parameters, together with above listed countermeasures (e.g. repetition rate), ensured recording of complete decay curves. NDs were visualized using the confocal setup described previously. Results are shown in 4.2.2..

3.4.2. Photon antibunching

Antibunching is a characteristic of light with sub-Poissonian statistics. Antibunching reveals, to a certain level of precision, whether there is only a single photon emitter in the sample. It is done by means of photon coincidence correlation. This information is revealed from the antibunching dip or „zero peak“ (if pulsed light source is used) of the correlation function. This technique is thus often used for characterization of single quantum emitters such as nanodiamonds. The whole experiment is based on the fact that every single quantum emitter can emit only one photon at a time. This is due to a finite amount of time the molecule spends on the excited energy state before it emits photon and relaxes to the ground state. Therefore, when only one photon is emitted, the dip of the correlation function decreases to the zero value because one photon can be detected by only one detector at a time.^[43]

Typical experimental setup (Figure 41) for probing photon antibunching comprise of interferometer with 50/50 beam-splitter, two single photon sensitive detectors (one at each branch) connected to a TCSPC module. Excitation can be performed by either continual or pulsed laser source.

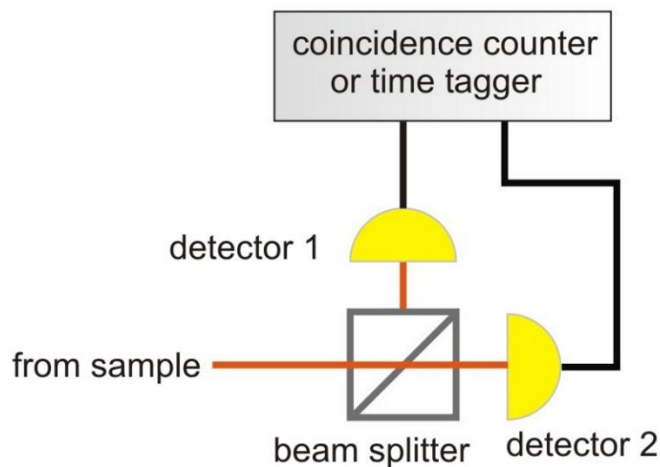


Figure 41: Typical setup for antibunching measurements.^[43]

Measurements were done on NDs104 sample on the confocal and TCSPC setup described in 3.2.. NDs104 was chosen because it was also the source material used for creation of samples JV39-1 and JV39-4. Photon coincidence was measured with emission filter LP 550 nm on both detectors with optical filters 641 ± 75 nm and excitation frequency 10 MHz. The time

of acquisition was chosen with respect to the required amount of data in the range 3 – 10 minutes. Results are shown in section 4.1..

3.4.3. Measurement of single particle saturation intensity

For fluorescence saturation measurements, scanning was performed with a range of excitation powers 6,2 – 558 μW at a wavelength 532 nm to study the quantitative changes in the emission properties of uncoated, silica coated and water enveloped nanodiamonds NDs. Different repetition frequencies of the excitation laser were tested. At first, frequencies 1, 5, 20 MHz were chosen to study an effect of excitation frequency on fluorescence emission of the sample and to observe enhancement/reduction of fluorescence emission caused by the given environment (Figure 37). The chosen range of excitation frequencies was later extended by additional frequency 32 MHz (maximal repetition frequency of the laser). Particles for this measurement were selected according to their fluorescence count rate. The threshold value was selected as 1 000 counts/s in order to acquire a sufficient signal during the decay measurements performed on same particles before measurements of related saturation curves (see example on Figure 43). Photons emitted by the particle were recorded for 3 seconds for each set excitation.

4. Results and discussion

Results described in this chapter were obtained by application of developed experimental methodology for measurement and evaluation of heterogeneity of luminescence properties of nanodiamonds using single-particle time-resolved luminescence measurements.

This chapter deals with determination of the number of NV centres in examined diamond nanoparticles. Results also include assessment and discussion of dependence of ND luminescence lifetime and intensity on refractive index of the surrounding environment.

4.1. Number of NV centres in measured particles

The number of nitrogen-vacancy centres in measured particles is an important information. Small amount of NV centres or even one NV centre in the ND particle are noticeably reducing possible factors which could interfere and alter observed fluorescence. One such side effect that arises from the multi-NV presence is that energy coupling/transfer between individual NV defects might occur. This often comes hand in hand with the energy transfer between NV and other present energy acceptors/donors, such as other defects (NV, H2, H3, etc.) or nitrogen atoms resulting in quenching of NV fluorescence and decrease of fluorescence lifetime.^[11] Therefore, many experiments, which focus on characterisation of fluorescence features of NVs, are carried out with an effort to observe manifestation of only particles with one NV centre, as for example in [14] and [15].

For our purposes, it would be also beneficial to work with nanodiamonds which contain only single NV centre in a single particle. Based on technical specifications and parameters used for fabrication of NV centres (see 3.3.1.2.) in NDs104 (source diamond), a relatively high irradiation energy and subsequent annealing temperature most likely led to creation of numerous NV centres rather than only one inside the diamond. This adds additional limitations that need to be considered during data analysis and interpretation of the results. Number of nitrogen-vacancy centres (single photon emitters) can be determined by observations of photon antibunching (3.4.2.).

To investigate how many NV centres are hosted in NDs used in this work an experiment based on measurement of cross-correlation function (second-order intensity correlation function) was performed. Examples of results are shown on Figure 42.

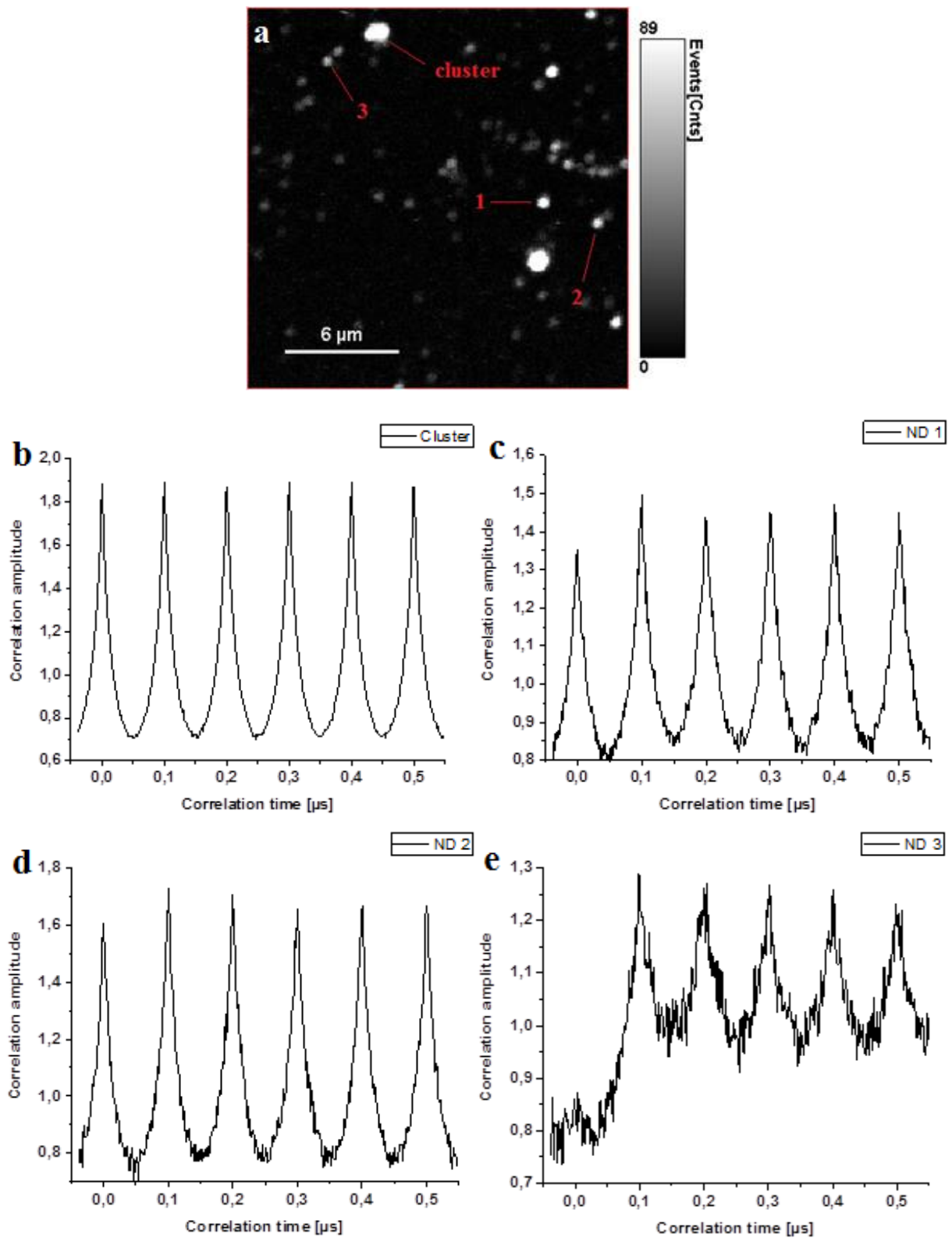


Figure 42: a) FLIM scan of NDs104 diamonds with marked measured particles. Second order correlation curve measured for b) cluster of nanodiamonds, c) + d) nanodiamonds with stronger emission, e) nanodiamond with weaker emission.

To compare the number of NV centres in particles with different fluorescence behaviour a cluster of particles and three arbitrarily chosen diamond nanoparticles with various count rates were investigated (Figure 42a). Cluster of nanodiamonds (Figure 42b) is represented by an approximately 0,7 μm large circular spot with a high number of counts. Size and count rate indicate that the cluster contained more nanodiamonds. Particles ND 1 and ND 2 emitted with count rate around 4-6 kcounts/s while the emission of ND 3 was much weaker around 2 kcounts/s. Thus for ND 3 it is expected that less NV centres are present. This information is provided by the second-order intensity correlation curves on Figure (42b-e). These show that the zero peaks (0 μs) did not decrease below correlation amplitude 0,8. From all measured particles maximum correlation intensity in zero peak was found for cluster (1,9), as expected for case with the highest occurrence of emitters, and the lowest for ND 3. It can be assumed that a particle contains single NV centre if the correlation amplitude drops below 1/3 of the maximum^[14] or in ideal case simply drops to 0 at zero delay time. Therefore, all measured particles likely contained more than 1 NV centre. However, the zero peak decreased as the signal of the particle weakened which indicates less single photon emitters (NV centres).

It can be concluded that occurrence of ND particles with multiple NV centres rather than single ones is more likely. This information is of crucial importance because it may provide partial explanation of notably multiexponential fluorescence „behaviour“ of examined nanodiamonds as well as the heterogeneity of their fluorescence lifetimes. Another point is the orientation of NV centres or how deep in the crystal NV centres are with respect to the surface due to their surface sensitivity which directly affects their fluorescence behaviour.

4.2. Assessment of heterogeneity of fluorescence lifetime

This section is dedicated to the analysis of fluorescence lifetime heterogeneity of nanodiamonds in dependence on refractive indexes of various environments. Photophysics of nanodiamonds, especially their fluorescence decay, is a complicated problematic which has been studied for a long period of time. Finding a certain „behavioural pattern” of NV fluorescence decay based on fluorescence lifetime, with respect to the variable monitored surroundings of the particle which contains NV defects, could lead not only to a better understanding of ongoing processes in NV centres but also to a step forward towards creation of a versatile diamond biosensor.

4.2.1. Single-particle fluorescence decay analysis

This section presents typical fluorescence decay of one diamond nanoparticle NDs104. In vast majority of decay measurements, the best results were obtained fitting the data with four-exponential model. However, exceptions were found for which simpler two- or three-exponential models were sufficient to obtain satisfactory fit of the experimental data. Example of the real fluorescence decay of NDs104 fitted with four exponential model is shown in Figure 43 with related parameters of the fit shown in Table 1. Decay curve and fit parameters are shown in order to demonstrate a significant multi-exponentiality of fluorescence decays of investigated nanodiamonds, in general.

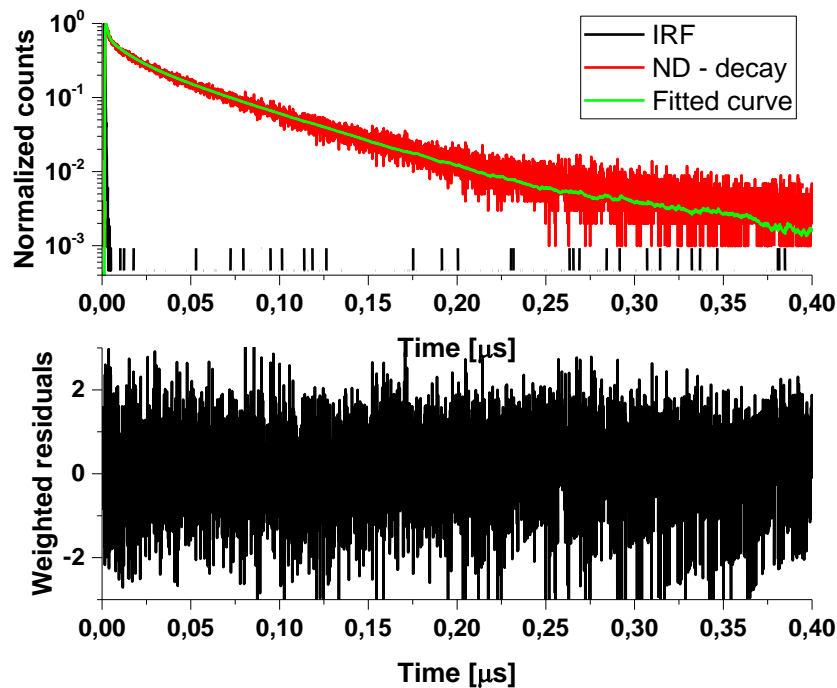


Figure 43: Example of fluorescence decay of NDs104

Table 1: Parameters of the fit shown in Figure 20.

Sample	χ^2	τ_{AVG}^A [ns]	τ_{AVG}^I [ns]	τ_1 [ns]	τ_2 [ns]	τ_3 [ns]	τ_4 [ns]
NDs104	1,1	$17 \pm 0,9$	$50 \pm 0,5$	84 ± 11	$9,2 \pm 2,6$	$0,9 \pm 0,2$	$42 \pm 6,6$
Fractional contribution				f_1 [%]	f_2 [%]	f_3 [%]	f_4 [%]
				30,7	10,2	2,9	56,2

* τ_{AVG}^A and τ_{AVG}^I are amplitude and intensity average lifetimes, f_i are fractional contributions of lifetime components, τ_i are lifetime components

From Table 1, we can see that individual lifetime components are significantly different and that main contribution in measured decay curve comes from long lifetime components. This is also why the intensity average lifetime is so long ($50 \pm 0,5$ ns) and differs from amplitude average lifetime ($17 \pm 0,9$) (see 4.3.1).

Single or two exponential tail-fitting is sometimes a solution for fitting fluorescence decay. The reason for such approach are artefacts and fast-decayed background in first several nanosecond of the decay curve.^[51] We rather use reconvolution of the decay with IRF and more complex fitting model for estimation of average fluorescence parameters and eventually FLIM lifetime histogram (using ROI) as a rough estimation of NV fluorescence lifetimes.

4.2.2. Analysis of fluorescence decay heterogeneity of nanodiamonds

This section was created for a purpose of comparison of fluorescence decays of individual measured nanoparticles within selected populations and to investigate the dependence of fluorescence lifetime on refractive index of surrounding environments. With this, determination of the „behavioural pattern” of NV fluorescence could be achieved.

Fluorescence decay curves were measured for approximately 30 particles of each kind of ND samples in order to have a sufficient amount of data and reliable statistics. Recorded fluorescence decay curves were analysed with non-linear least squares analysis and fitted by a multi-exponential model for estimation of fluorescence lifetimes. Due to complexity of the ND fluorescence decay, multi-exponential fits from two to four-exponential models were

tested and evaluated according to goodness-of-fit parameters (χ^2) and weighted residuals calculated by the software SymphoTime64 (PicoQuant).

Individual decay curves and mean decay curves were used for comparison of heterogeneity of fluorescence decays and lifetimes between measured diamond samples.

4.2.2.1. Fluorescence decay analysis of uncoated nanodiamonds NDs104

Heterogeneity of fluorescence lifetime was first investigated for uncoated nanodiamonds in order to obtain reference results for a direct comparison with silica-coated nanodiamonds. Environmental effect was investigated for air which was considered to be the simplest and basic case. Recorded decay curves are shown in Figure 44.

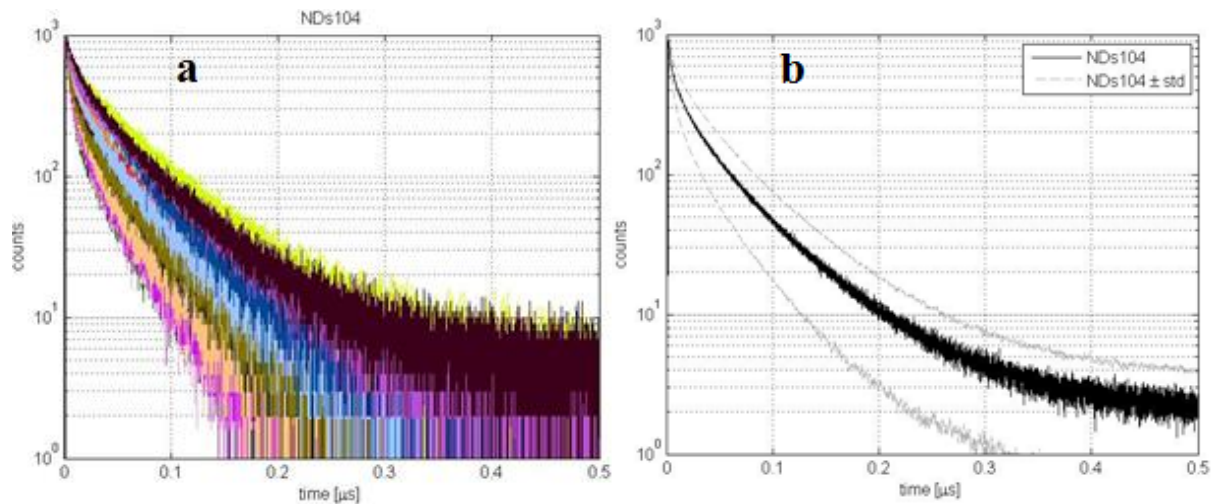


Figure 44: Fluorescence decay heterogeneity a) and mean decay curve b) with indicated standard deviations of NDs104.

Fluorescence decay curves shown in figure 44a exhibit a significant variance which directly indicates that wide range of lifetime values can be expected. This is clearly visible on the range of standard deviations around the mean decay curve plotted in Figure 44b. Fluorescence lifetimes were calculated from each measured decay curve presented in Figure 44a. Resulting values obtained from the analysis were amplitude average lifetimes ranging from 10 to 29 ns with the average value $15,7 \pm 6,7$ ns calculated from individual lifetimes. Such range of fluorescence lifetimes corresponds well with [5,6].

4.2.2.2. Fluorescence decay analysis of silica coated nanodiamonds JV39-1

In this chapter, fluorescence lifetime heterogeneity of nanodiamonds JV39-1 (NDs104 embedded in 50 nm thick silica shell) were investigated. Here the conditions change with silica entering the process. Refractive index of environment therefore increased from $n = 1$ to $n = 1,46$ (Figure 45).

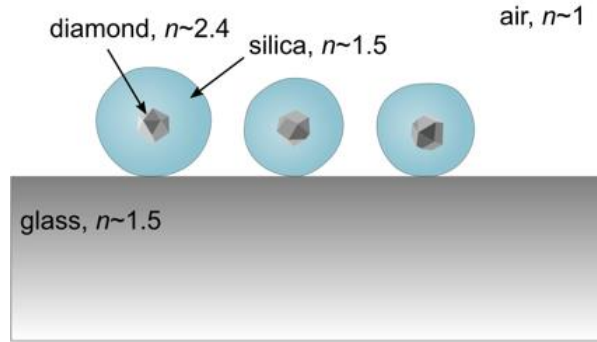


Figure 45: Structured arrangement of silica embedden nanodiamonds JV39[courtesy of Dalibor Panek]

Obtained results from fluorescence decay measurements are shown on Figure 46.

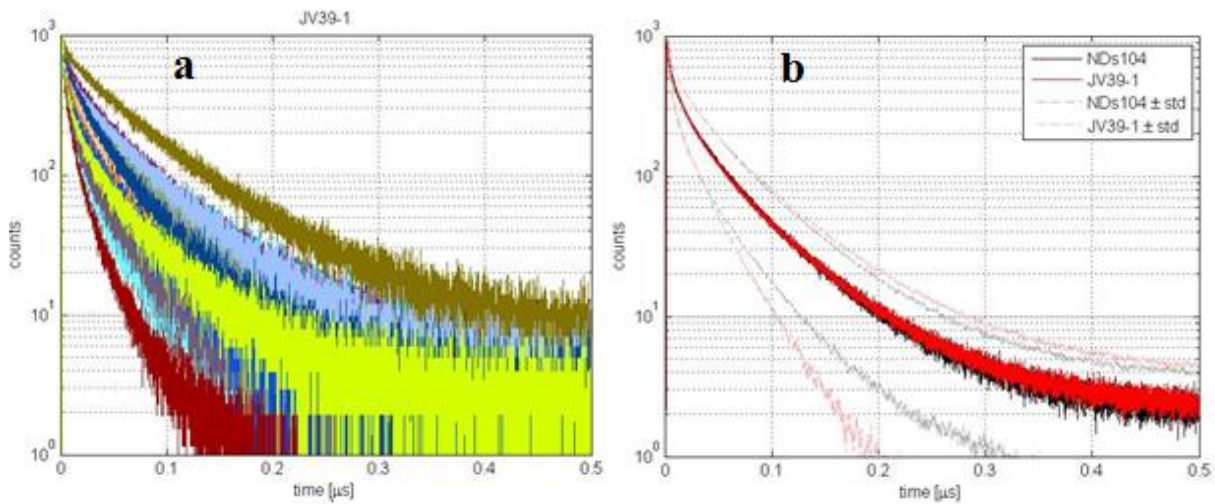


Figure 46: Fluorescence decay heterogeneity a) and mean decay curve b) with indicated standard deviations of JV39-1.

Fluorescence decay curves of coated nanodiamonds (Figure 46a) exhibit significant heterogeneity as well. Fluorescence lifetimes were shorter than observed in 4.2.2.1. with amplitude average lifetime values, calculated from individual decay curves, ranging

from 4,6 to 25 ns and average lifetime $13,3 \pm 6$ ns. Nanodiamonds surrounded by the environment with higher refractive index, represented by the 50 nm silica shell, therefore exhibited decrease in fluorescence lifetime. This is clearly demonstrated by the shift of standard deviation in figure 46b to shorter times.

In figure 46b, mean decay curves are very similar which means that average fluorescence lifetimes calculated from them should be also of similar values. The difference between lifetimes of uncoated and coated NDs could be compared in two ways applicable for measurements involving investigation of environmental effects of ND fluorescence. First, we can compare average lifetimes, calculated from amplitude average lifetimes related to individual measured decay curves, or amplitude average lifetimes, calculated from mean decay curves (Figure 46b).

The difference in average lifetimes, calculated from average amplitude lifetimes, between uncoated and coated nanodiamonds is approximately 2,4 ns.

4.2.2.3. Fluorescence decay analysis of silica coated nanodiamonds JV39-4

This section focuses on investigation of nanodiamonds NDs104 embedded in 100 nm thick silica shell. In previous section, decrease of ND fluorescence lifetime in presence of the higher refraction index environment was presented. Here, the effect of thickness of the shell, which envelopes diamond particles, on fluorescence lifetime can be also examined.

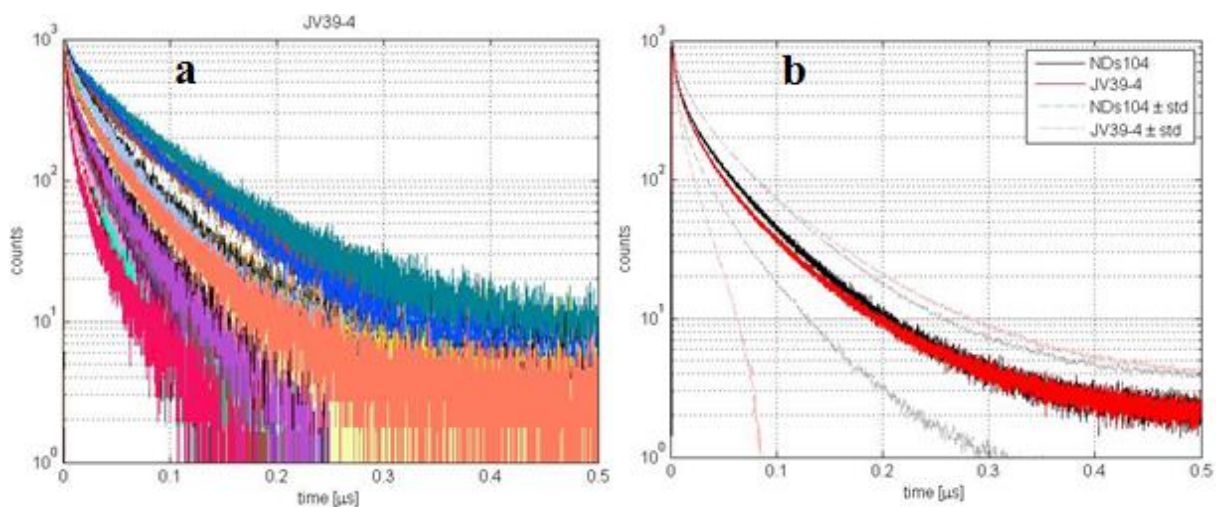


Figure 47: Fluorescence decay heterogeneity a) and mean decay curve b) with indicated standard deviations of JV39-4.

From the behaviour of decay curves in figure 47a, it is clear that the heterogeneity is in this case more significant than in previous two measurements. Standard deviation (Figure 47b) is even more left shifted than it was for JV39-1.

Average fluorescence lifetime calculated from individual amplitude average lifetimes, ranging from 5,4 – 24 ns, is $13,6 \pm 5,2$ ns. Here, the lowest value of standard deviation was found. The difference between average lifetimes of NDs104 and JV39-4 is 2,1 ns.

To discuss possible influence of the thickness of the shell on NV luminescence, a comparison of fluorescence decays of silica coated nanodiamonds JV39-1 and 4 was done in Figure 48.

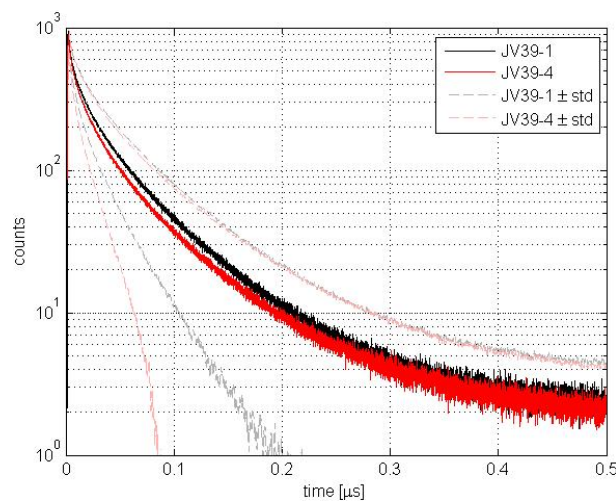


Figure 48: Comparison of fluorescence decays of silica coated nanodiamonds (JV39-1, JV39-4)

Figure 48 shows that the resemblance of fluorescence decays of compared samples is significant. Fluorescence lifetimes of thinner and thicker coated nanodiamonds were $13,3 \pm 6$ ns and $13,6 \pm 5,2$ ns respectively. This similarity might be due to high thickness of the shell which is for JV39-1 almost the size of the source diamond (60 nm) and for JV39-4 almost twice the size. It is possible that the shell is so thick that the „thickness effect“ is no more reflected by fluorescent (lifetime) behaviour. The effect could probably be described easier using ND fractions with various shell thicknesses (single digits nm up to size of the particle) which is easily achievable via controlled growth conditions^[52], e.g. changing amount of silyesters during silication^[53].

To conclude, the effect of surrounding refractive index is difficult to determine this way. The reason is probably that every particle in examined ensembles of NDs contained different amount of NV centres. It was found that fluorescence decay heterogeneity was significant

within measured populations of each kind of nanodiamonds. Average fluorescence lifetimes obtained for silica-embedded nanodiamonds were found to be similar and lower than lifetimes obtained for NDs104. Due to the same core material, despite various content of NV centres, it can be assumed that higher refractive index around the ND particle causes decrease in fluorescence lifetime. However, more promising approach seems to be performing the research on one single „unique” particle first in air environment and vary the environment afterwards, as was performed for nanodiamonds NDs104 measured in air and water environment (4.3.). The shell effect could not have been exactly concluded due to significant heterogeneity of fluorescence decays of NDs104 and JV39-1/4 and similarity of average fluorescence lifetimes of silica embedded JV39-1/4.

4.2.3. Absorption cross section estimation

Emission saturation curves were measured with the aim to estimate the absorption cross section of single NDs in populations of investigated kinds of nanodiamonds in order to determine which of examined environments has the highest probability of light absorption and to explore possible effect of environment on ND saturation.

Through fitting saturation curves, saturation intensity can be calculated. Saturation occurs when the absorption rate equals to the fluorescence decay rate and this is the value of excitation power where the emission ceases to be linearly dependent on excitation. Data from fluorescence saturation measurements were used for estimation of absorption cross section.

Example of data from fluorescence saturation measurements is in Figure 49.

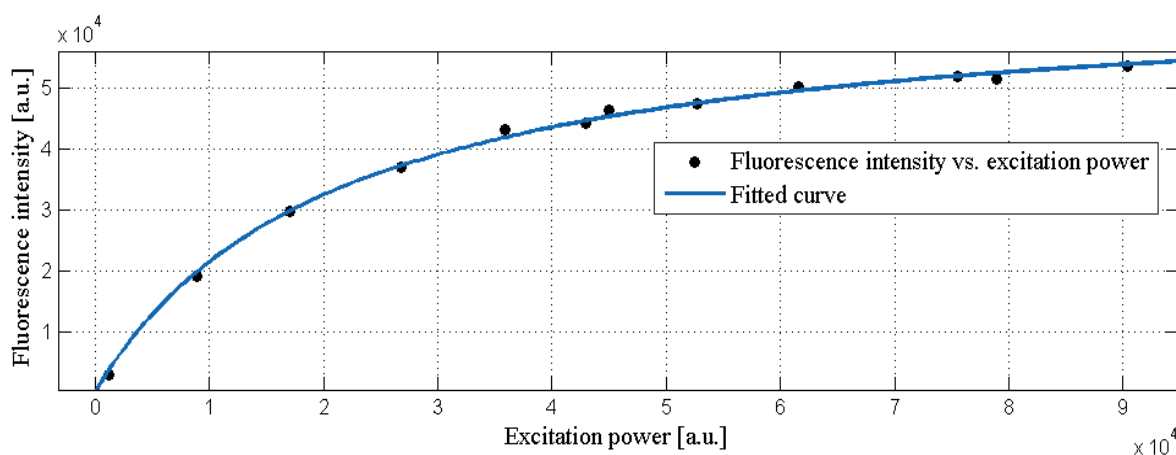


Figure 49: Example of measured saturation curve data for JV39-4 with fitted curve.

Data from saturation measurements were fitted in MATLAB using curve fitting tool *cftool* with the following model^[14,15]:

$$I(P) = I_{MAX} \left(\frac{P}{P + P_{SAT}} \right), \quad (14)$$

where $I(P)$ represents count rates for the given emitter, I_{MAX} is the maximum obtainable intensity count rate, P is excitation power and P_{SAT} is the power where counts saturate.

Fitting model used on example of data in Figure 49 exhibited coefficient of determination $R^2 = 0,9975$ which highly corresponds to measured data. Calculated saturation power was $2,1 \cdot 10^4$ a.u. ($130 \mu\text{W}$).

For the conversion of *arbitrary units* to *watts* was used a calibration curve obtained from the measurement of the laser power on the side of the objective (see Figure 50).

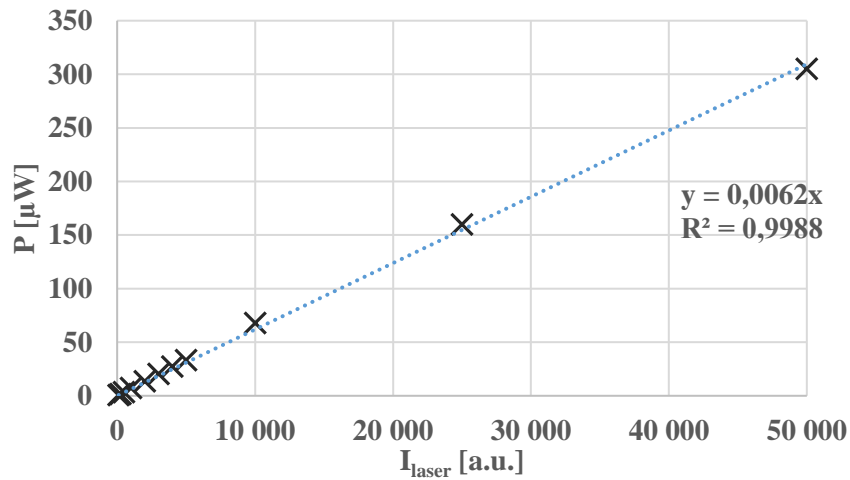


Figure 50: Plot of dependence of laser power (532 nm, 20 MHz, 99%) on intensity [au].
[courtesy of Katerina Zambochova]

With known saturation intensity in *watts* absorption cross section could have been calculated. At first, number of excitation photons was calculated from the equation (15):

$$P = \frac{E_{photon} \cdot N}{t}, \quad (15)$$

where P is the power of the excitation laser beam [W], t is time of acquisition [s], N is number of detected photons per unit time and E_{photon} is energy of single photon given by $E = \frac{h \cdot c}{\lambda}$ (h is Planck's constant, c is the speed of light in vacuum, λ is excitation wavelength).

From the known number of excitation photons it was possible to recalculate related saturation intensity P_{SAT} [photons·m⁻²·s⁻¹] by dividing number of photons by laser beam cross section [m⁻²].

Absorption cross section was then calculated using equation (16):

$$P_{SAT} = \frac{k_e}{\sigma_A}, \quad (16)$$

where k_e is the decay rate of the excited state [s⁻¹] calculated as $k_e = \frac{1}{\tau_e}$ (τ_e – fluorescence lifetime), and σ_A is absorption cross section [m²].

A set of examples of calculated absorption cross sections for seven chosen nanodiamonds of each kind is shown in the following table.

Table 2: Calculated absorption cross sections for different environments.

NDs104 σ_A [m²]	8,66·10 ⁻²¹	4,55·10 ⁻²⁰	3,43·10 ⁻²⁰	1,55·10 ⁻²⁰	1,28·10 ⁻²⁰	1,84·10 ⁻²⁰
JV39-1 σ_A [m²]	8,59·10 ⁻²⁰	7,80·10 ⁻²⁰	8,83·10 ⁻²¹	8,16·10 ⁻²¹	1,32·10 ⁻²⁰	2,69·10 ⁻²⁰
JV39-4 σ_A [m²]	3,57·10 ⁻²⁰	6,08·10 ⁻²⁰	4,14·10 ⁻²⁰	4,71·10 ⁻²⁰	2,76·10 ⁻²⁰	5,15·10 ⁻²⁰
NDs104&Air σ_A [m²]	3,99·10 ⁻²⁰	1,45·10 ⁻²⁰	2,17·10 ⁻²⁰	4,80·10 ⁻²⁰	2,35·10 ⁻²⁰	5,20·10 ⁻²⁰
NDs104&H₂O σ_A [m²]	4,90·10 ⁻¹⁹	3,08·10 ⁻¹⁹	1,15·10 ⁻¹⁹	4,70·10 ⁻¹⁹	2,26·10 ⁻¹⁹	3,85·10 ⁻¹⁹

*Parameters used for calculations were: $t = 3s$, laser beam cross section $7,07 \cdot 10^{-14} \text{ m}^2$ ($R = 150 \text{ nm}$).

Values of absorption cross sections correspond well with its typical values for NV found in literature^[54]. The highest values of absorption cross sections were found for nanodiamonds measured in immersed water (NDs104&H₂O) which indicates the highest probability of absorption and scattering.^[55] Nevertheless, the difference between nanodiamonds measured in water and related nanodiamonds measured on air (NDs104&Air) was not so significant to assign the difference to the influence of the environment.

A comparison of saturation curves obtained for all 30 measured nanodiamonds of each kind related to different environments was also done to observe possible changes in saturation. No significant differences in the behaviour of saturation curves in all measured cases were observed. This was due to inconsistency of the saturation data trend in individual measurements.

It should be noted that determining the effect of the environment on NV emission is very difficult without being able to characterize the same particle before and after the change of environments and controlling this process. If NDs104 and any JV39 nanodiamonds are compared in terms of their emission, it would be relevant only in case where all compare particles would contain same number of NV centres and their fluorescence decays would not differ significantly (dependent on the size of the particle, distance of NVs from the particle's surface and orientation of NV with respect to the surface of the substrate,..).

In general, the problematics of the influence of different refractive index environments on NV emission is a very complicated matter due to many various and differently influencing factors.

4.3. Effect of the change of refractive index of surrounding media on fluorescence lifetime and intensity

As was presented in 4.2.2. the effect of the surrounding refractive index on fluorescence lifetime or intensity of nanodiamonds cannot be exactly concluded due to decay heterogeneity of NDs104 and JV39-1/4. To investigate and determine this effect, it was necessary to perform decay measurements on single „unique“ particles in controlled conditions.

Here, 10 nanodiamonds NDs104 were measured in air and water environment (Figure 51). Nanodiamonds were first measured on air and later in water. At first, sets of two or three nanodiamonds were measured on air and each particle was marked (red arrows in Figure 52) in FLIM scans taken after each measurement. After the measurement of the given set of particles was finished, drop of deionized water (approx. 50 μ l) was added onto the observed area. Measurements in water followed. This was repeated until data from 10 particles for both air and water were obtained. Individual recorded decay curves from measurements in both environments are shown in Figure 53.

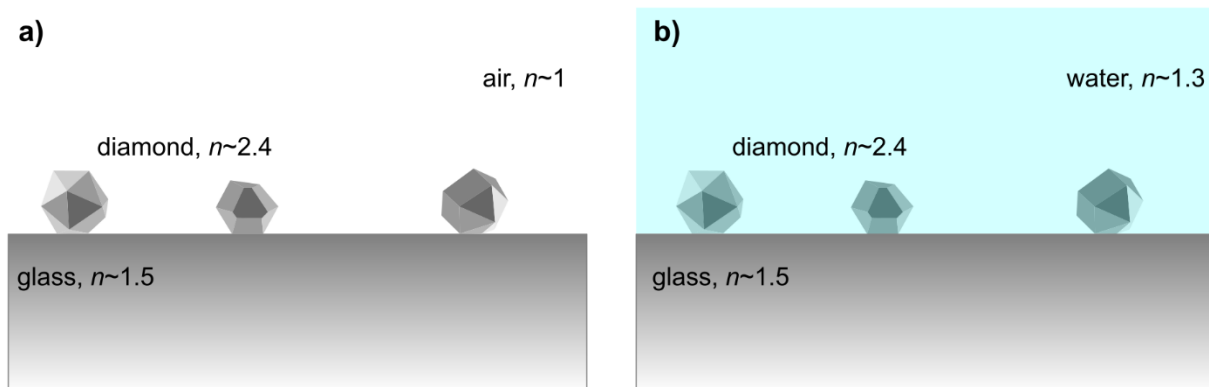


Figure 51: Structured arrangement of NDs104 in a) air and b) water environment. [courtesy of Dalibor Panek]

In some cases, addition of water on top of the sample worsened the resolution and complicated focusing on the sample. Higher excitation power during the scanning was therefore needed to compensate this effect. A possible explanation of this issue might come from optical properties of water and diamonds which are highly scattering media and therefore might have caused scattering of emitted fluorescence.

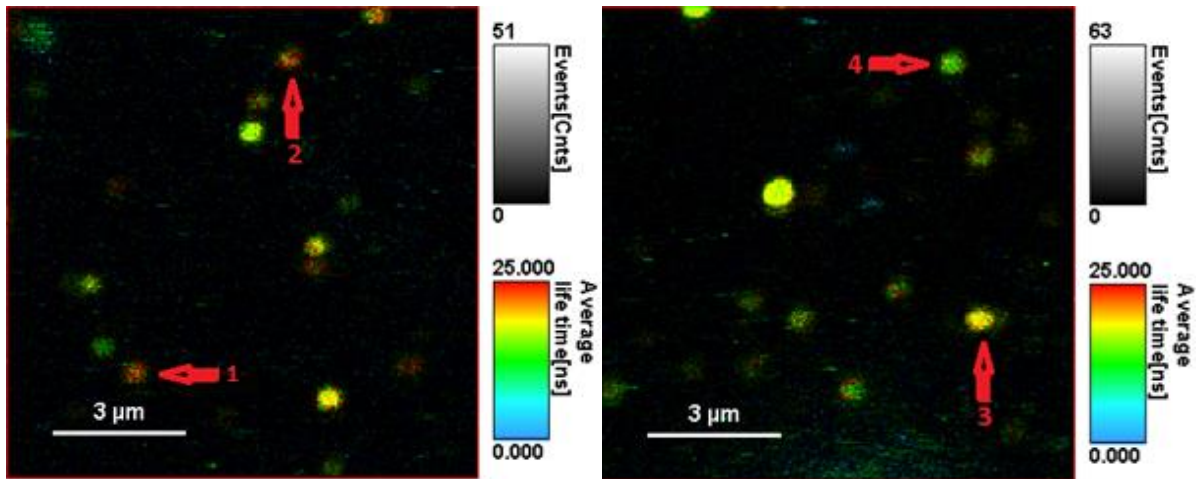


Figure 52: Example of FLIM scans with marked ND particles measured on air and later in water. Each measured particle marked with red arrow and related number was measured in air and later in water.

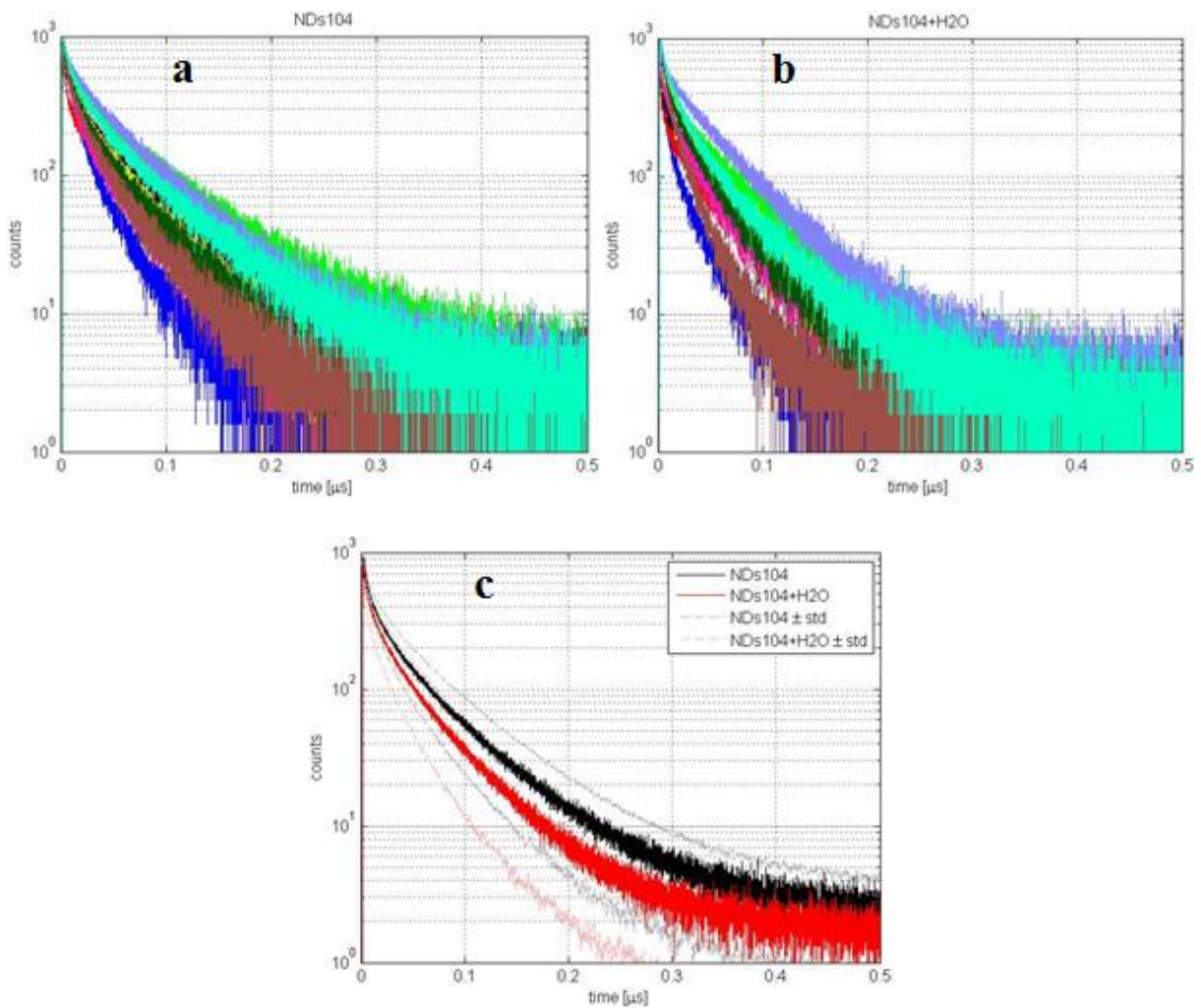


Figure 53: Fluorescence decay curves of ND particles and mean decay curves. Individual fluorescence decay curves for NDs104 measured on air a) and in water b) with plot of mean decay curves c) with indicated standard deviations.

Average fluorescence lifetime of NDs104 (air) (Figure 53a) calculated from individual amplitude average lifetimes was $18,6 \pm 8,2$ ns. Behaviour of decay curves in Figure 53c indicates that lower fluorescence lifetimes can be expected for measurements of NDs in water. Average lifetime obtained from water measurements (Figure 53b) was $12,6 \pm 4,1$ ns. The difference between average lifetimes of NDs104 and NDs104 in water is 6 ns.

Results of comparison of fluorescence signals obtained from NDs104 particles, measured in controlled conditions with different surrounding refractive indexes, follow in Figure 54. Comparison of time trace signals of NDs measured on air and in water were performed in order to determine effect of the surrounding refractive index on NV fluorescence intensity.

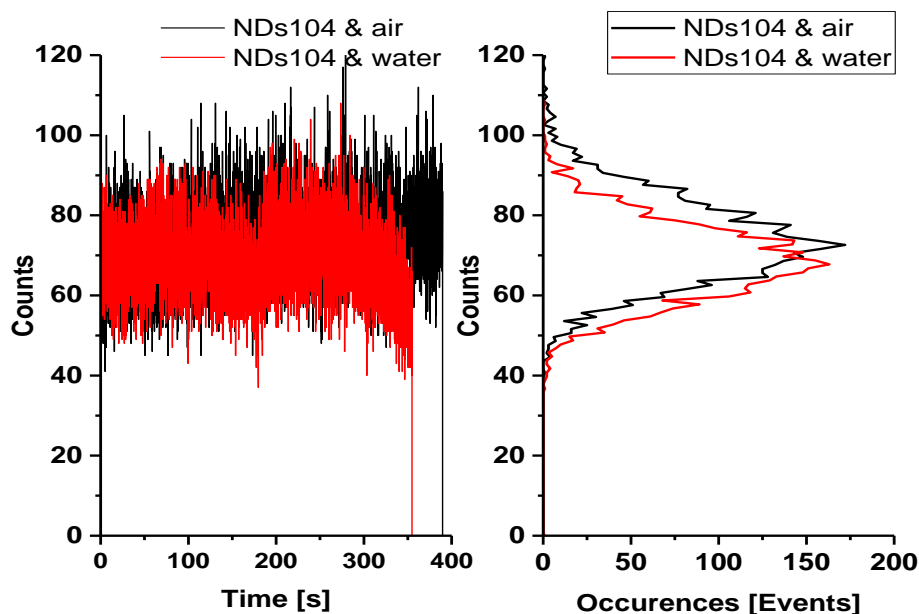


Figure 54: Time trace signals of diamonds NDs104 measured on air and in water.

In figure 54, enhancement of NV luminescence was expected due to higher refractive index environment surrounding measured diamonds containing NV centres.^[14-16] However, here, were observed very similar time trace signals measured for the water environment as for NDs measured on air. This was probably caused due to scattering of both the excitation laser beam and emitted NV fluorescence in the drop of water before the NV fluorescence was collected. The geometry of the light pathway might also play its role in this. Even though used confocal system is mounted with immerse objective, a certain amount of NV luminescence might be lost while fluorescence passes through the polymer layer and glass coverslip.

Also, measured particles are bound to the layer of positively charged PEI which can cause decrease of NV^- photoluminescence depending on the amount of polymer attached to the surface of the ND particle.^[56] This is due to changes in surface charge density caused by PEI which means changes in electron occupation of NV^- and NV^0 states reaching up to 20nm depth.^[9] It was presented that background fluorescence, of which PEI is large contributor, can be photobleached using high laser power. What remains unknown is the level of photodegradation of PEI and actual amount of the polymer which resides attached to the particle and still affects its fluorescent behaviour. This counts even for silica shells where there was not possible to exactly determine the influence of high excitation power on the shell and to verify the amount of silica remaining on the particle (JV39-1 and 4) if subjected to photodegradation. Nevertheless, PEI was present in both cases and addition of water did not induce any significant changes in emission.

A planar glass surface of the substrate of different refraction index then examined environment has also its effect on NV fluorescence lifetime and must be considered. Its influence resides in existence of evanescent waves which are reflected from the substrate and occur (emitted by the dipole) when the relative refraction index ratio $n_{substrate}/n_{environment} > 1$, where medium envelops encapsulated particle (air, water, silica).^[16] Reflected evanescent waves create additional channel for the dipole to radiate its power into and causes rise of power for NDs in a close proximity from the surface of the substrate.^[44] This is coupled to the encapsulation of the electric dipole (and its direction) by the nanoparticle where the radiative power is dependent on the ratio $n_{particle}/n_{environment}$ and decreases with higher refractive indexes of nanoparticle.^[16,44] It could be also said that emission enhancement increases (and thus fluorescence lifetime decreases) with decreasing difference in refractive indexes of the particle and surrounding environment. This corresponds well with presented lifetime results. Considering even the refractive index of the substrate, the fluorescence emission should decrease with the decrease of contrast between refractive index of the substrate and the environment with the particle within.^[15]

Substrates reflectivity and distance of particle from the highly reflective substrate also play a significant role in emission enhancement. If the dipole is in the close proximity to the highly reflective surface, the emission is enhanced.^[16] This is because the higher the difference in refractive indexes between the substrate and the upper media, the more light will be reflected. However, this was stated for a direct observation from above the sample. In this work, the inverse confocal system was used. The refractive index contrast between coating, ND and

substrate, the unknown NV dipole orientation (with respect to the interface)^[15,18] and the size of ND (depth of NV)^[15] are key parameters in determining ND emission in such a structured environment. Absorptivity of the material enveloping nanoparticles and PEI layer is also a question. Unknown dipole-moment orientation makes almost impossible to determine with certainty whether the environmental effect is present or not.^[18] In [18] are proposed two hypotheses for possible absence of the environmental effect. These are, first, that the quantum efficiency of diamond is low, or second, that the very high refractive index material of ND encapsulating emitting NV centre prevents it from responding to moderate changes in surrounding environment it is supposed to probe. However, the latter explanation was tested by numerical simulations and was not confirmed.

To conclude, investigation of the influence of refractive indexes of the surrounding chemical environment enveloping nanodiamonds showed that the change of environment for the one with higher refractive index caused decrease in fluorescence lifetimes (hence quantum yield) of NV centres. This is in good agreement with [14-18,44]. The decrease in average fluorescence lifetime was approx. 2,4 ns (thinner silica shell) or 2,1 (thicker silica shell) and 6 ns (water). These changes may not seem as such a significant difference in case of highly heterogeneous decays. Nevertheless, this difference would probably have a greater meaning for single NV nanodiamonds. Presented lifetime differences could be caused either by surface charge sensitivity or chemistry sensitivity of NV luminescence based on electronic chemical potential^[56] which counts also for the effect on fluorescence intensity. Another factor which can contribute to the fluorescence decay heterogeneity is possible energy transfer between NV centre and nitrogen because nitrogen atoms exhibit absorption continuum (starting at 1,9 eV) which overlaps emission band of NV⁻ (1,4 – 2 eV)^[11].

The complexity of NV fluorescence decays seems to be a complicated problematic with many multiexponential contributors such as short-lived multiexponential decays which originate from the surface defects and dangling bonds.^[32]

Additionally, an improvement of the experimental part of the methodology might be suggested. It is recommended to create a grid or a coordinate system on the substrate's surface which would enable to measure same particles repeatedly. With this approach particles could be measured firstly on air (no side effects from the chemical environment) and then they could be covered by various polymer layers or solutions (environments).

To discuss the relevancy of measured ND material, from the essence of the experiment, used ND samples are probably not suitable for this kind of investigated problematic.

Complicated fluorescence behaviour and high presence of NV defects (see 4.1.) make determining NV lifetime heterogeneity highly difficult. In imaging techniques, presence of multiple NV centres would be preferred because the bright emission is required.

4.3.1. The correct choice of „Average“ fluorescence lifetime

This section is dedicated to solving the question of correct choice of average fluorescence lifetime. Average fluorescence lifetimes, results of fluorescence decay analysis, provided by the software SypmhoTime64, were the amplitude and the intensity average lifetime. In fluorescence decay analysis, fluorescence decay is mostly multi-exponential and should not be always approached as a simple system even though the complex fluorescence behaviour can be described by an average fluorescence lifetime. In most papers, there is only a mention of average fluorescence lifetime but no clear identification whether this average lifetime is amplitude or intensity weighted. Moreover, it is sometimes difficult to decide which one is to be used in the given situation. Only a very few studies deal with this problem [37,57].

To investigate this matter further and decide which average parameter should be used for presented NV analysis, a brief introduction of average amplitude and intensity lifetimes will be made, including analysis and justification of appropriateness of their use.

Intensity average fluorescence lifetime can be defined as the average fluorescence lifetime of a collection of different excited-state populations, where the lifetime of each population is weighted by the relative contribution of that population to the total fluorescence. Intensity average fluorescence lifetime is obtained by averaging t over intensity decay:

$$\tau_{\text{AVG}}^I = \frac{\sum \alpha_i \tau_i^2}{\sum \alpha_i \tau_i} = \frac{\int_0^{\infty} t \sum \alpha_i e^{-t/\tau_i} dt}{\int_0^{\infty} \sum \alpha_i e^{-t/\tau_i} dt} \quad (17)$$

The intensity average lifetime is for a single exponential decay equal to the lifetime τ . This is not true for more complex decay laws; multi- or non-exponential decays. Equation 17 can be used for calculation of the average lifetime. This average lifetime, however, can be a complex function and it is necessary to interpret it carefully.^[37]

Amplitude average fluorescence lifetime is the lifetime a fluorophore would have if it had the same steady-state fluorescence as a fluorophore with several lifetimes^[57]:

$$\tau_{\text{AVG}}^A = \frac{\sum \alpha_i \tau_i}{\sum \alpha_i} \quad (18)$$

In most cases, including system of one fluorophore with several lifetimes or a multiple fluorophore system (extinction coefficients of individual fluorophores must be considered) with multiple lifetimes, it is recommended to use amplitude average lifetime. Intensity average lifetime can be used in case that all fluorophores in the system have the same extinction coefficients.^[57]

Here, assuming diamond as a system with multiple emitter with multiple lifetimes, where only NV centres emit from inside nanodiamonds, extinction coefficients of NV defects could be the same and therefore, intensity average lifetime can be used. However, diamond material must be considered and its optical properties. On the other hand, amplitude average lifetime is proportional to steady-state intensity^[37] and fluorescence intensity in diamond is directly proportional to the number of NV centres within.

Another support for using amplitude average lifetime comes from the centre of mass (CoM) calculated from the decay, histogrammed from the data provided by the region of interest function. As described in 3.4.1.4. excitation frequency has a crucial impact on fluorescence decay histogramming. Fluorescent particles in the area of interest undergo excitation during each scanning. This excitation consecutively affects their fluorescence lifetime and therefore, directly influences the form and time-position of lifetime histogram for the given FLIM scan. If the ROI function is applied on individual fluorescent particles (NDs), lifetime histogram is formed without the contribution of the background.

CoM is calculated from detected photons in each pixel and is used for the lifetime histogram provided by SymphoTime64 for each scan:

$$CoM = \frac{\sum_i n_i t_i}{\sum_i n_i}, \quad (19)$$

where n_i is the number of detected photons in the time channel t_i .

If we desire a complete relaxation of the given system, excitation frequency must be in accordance with requirements and recommendations („as low as possible“) mentioned in 3.4.1.4.. As shown on Figure 38, high repetition rate shifts the lifetime histogram to lower lifetimes. Therefore, by scanning with lower frequency which still provides satisfactory resolution as well as sufficient contrast, lifetime histogram should be approaching real lifetime

values. These values often corresponded well with amplitude average lifetimes obtained from the decay analysis. For low repetition frequencies CoM provided similar values of lifetimes as amplitude average lifetime from the decay analysis. Hence, it is possible that CoM-calculated lifetime histograms could serve as a rough-estimation tool for determining lifetimes and support that using amplitude average lifetime for interpretation of results from the decay analysis is the correct approach.

Intensity average lifetimes were (with a few exceptions) mostly in scale of 30 – 60 ns which are considerably longer than stated in literature for fluorescence lifetimes of nitrogen-vacancy centres in diamond. This is caused by components with low amplitude and a considerably long lifetime. Intensity of the given component in overall intensity is represented by the area under curve of the component to the area under decay curve. Therefore, because of low amplitudes of long lifetime components, the estimation of related lifetimes might be often inaccurate which makes inaccurate also intensity average lifetimes. The significance of the difference between two discussed lifetimes is shown in Table 3 on the example of NDs104 lifetimes measured on air and in water.

Table 3: Examples of amplitude and intensity average fluorescence lifetimes for NDs104 measured on air and in water.

NDs104&air		NDs104&H₂O	
τ_{AVG}^A [ns]	τ_{AVG}^I [ns]	τ_{AVG}^A [ns]	τ_{AVG}^I [ns]
19	42	15	37
17	43	12	34
35	55	17	49
17	33	10	19
13	36	9,6	31

Table 3 shows that both amplitude and intensity average lifetimes follow the trend of decreasing lifetime in high refractive index environment.

With respect to the above and high values of intensity average lifetimes, amplitude average lifetimes have been used in this work.

5. Conclusions and perspective

Main aims of this thesis were to develop a methodology for evaluation of heterogeneity of luminescence properties of nanodiamonds using single-particle time-resolved luminescence measurements and to discuss the dependence of the ND luminescence lifetime on the surrounding environment.

The thesis has introduced the methodology developed for measurement and evaluation of heterogeneity of luminescence properties of nanodiamonds using single-particle time-resolved luminescence measurements based on Time Correlated Single Photon Counting (TCSPC). The research was performed on fluorescent nanodiamonds NDs104 (60 nm) and their core-shell modifications JV39-1 (50 nm thick silica shell) and JV39-4 (100 nm thick silica shell) which enabled a mutual comparison of results. This allowed to explore the dependence of fluorescence lifetime of nitrogen-vacancy centres on refractive indexes of various surrounding chemical environments and thickness of the shell in which nanodiamonds are embedded in.

Optimal methodology of sample preparation and substrate purification is demonstrated. Several purification procedures were discussed and it was found that the most successful purification can be achieved combining sonication and etching of the substrate with 20% sodium hydroxide which eliminated most of the short-lived fluorescent impurities and provided additional advantageous effects such as high hydrophilicity of the substrate. Further, optimal substrate modification for single nanodiamond crystal distribution, based on Polyethylenimine-coated substrate, was found and successfully tested. Polyethylenimine exhibited high wettability of the substrate as well as no significant cluster formation in the final sample.

Technical part of the research focused on the investigation, discussion and technical troubleshooting of influence of the used instrumentation on measured fluorescence of nanodiamonds. It was found that correct choice of optical filter has a crucial impact on the fluorescence decay acquisition where the decay histogram suffered from distortion caused by the scattering of light on nanodiamonds. It has been also demonstrated how the motion drift of the particle may affect recorded signal as well as decay curve. Possible ways to prevent these side effects have been suggested.

It was found that diffraction-limited resolution of the confocal microscope makes difficult to determine the number of measured diamond nanoparticles with respect to their actual size. This information and presence of single photon emitter can be obtained from the observation

of antibunching. Antibunching measurements showed that measured particles contained multiple NV centres. Using combination of FLIM and AFM for simultaneous measurement which would provide information about not only size of the particle but also its shape has been suggested. Additionally, this would allow to investigate the dependence of ND fluorescence on their shape or size in given conditions.

Excitation parameters and their effect on the fluorescence lifetimes of NV centres were also investigated. It was found that fluorescence lifetime of NV centres strongly depends on the excitation frequency and that high excitation frequency shifts NV fluorescence lifetime to shorter values which negatively affects decay analysis. Optimal excitation frequency was found to be 1 MHz.

Instrument response function acquisition has been presented. Recorded instrument response function met presented requirements and could have been used for fluorescence decay analysis.

Study of effect of surrounding refractive index on fluorescence intensity of nanodiamonds showed that no significant differences in saturations of examined nanodiamonds were found and that direct comparison was possible on nanodiamonds measured on air and in water. It was found that fluorescence intensities of diamonds measured on air and in water exhibited similar behaviour, probably due to the loss of light caused by scattering in water or the geometry of the light pathway. Estimation of absorption cross sections was performed, too. The results showed the highest values of absorption cross section to be 10^{-19} m^2 for nanodiamonds measured in water and $10^{-20} - 10^{-21} \text{ m}^2$ for silica and air enveloped nanodiamonds.

Additionally, this work has presented the study of fluorescence lifetime heterogeneity of diamond nanoparticles. It was found that fluorescence lifetimes of measured samples were highly heterogeneous. Average values of lifetimes of uncoated NDs104 were found to be $15,7 \pm 6,7 \text{ ns}$, for JV39-1 $13,3 \pm 6 \text{ ns}$, for JV39-4 $13,6 \pm 5,2 \text{ ns}$ and for 10 NDs104 measure in air and water $18,6 \pm 8,2 \text{ ns}$ and $12,6 \pm 4,1 \text{ ns}$ respectively. These changes indicate decrease in fluorescence lifetime with increasing refractive index of the surrounding environment. Regarding the effect of the thickness of the shell on NV luminescence, fluorescence decays and lifetimes were similar for both coated samples and therefore, no exact pattern in fluorescent behaviour with respect to the shell thickness was found.

Finally, the thesis has presented arguments for the use of amplitude average fluorescence lifetime in decay analysis of measured nanodiamonds.

To conclude, all of the stated goals have been fulfilled.

Obtained results extend the knowledge about fluorescent behaviour of core-shell nanodiamond systems and bring a valuable insight into their Photophysics. This knowledge will move potential application of nanodiamond probes for sensoric application in biomedicine based on fluorescence lifetime one step closer toward the practical use. Further experimental investigations are needed to verify the effect of Polyethylenimine on attached nanodiamonds. Important benefit in Photophysics of nanodiamonds could also be investigation of effect of the size and shape of nanodiamonds on their luminescence properties. For future investigations of nitrogen-vacancy lifetime heterogeneity, it is recommended to dedicate part of the research to the fabrication process or the choice of suitable nanodiamond samples which would contain single NV centres.

References

- [1] MICHALET, X., et al. Quantum dots for live cells, in vivo imaging, and diagnostics. *science*, 2005, 307.5709: 538-544.
- [2] WILLIAM, W. Yu, et al. Water-soluble quantum dots for biomedical applications. *Biochemical and biophysical research communications*, 2006, 348.3: 781-786.
- [3] SCHRAND, Amanda M., et al. Are diamond nanoparticles cytotoxic?. *The journal of physical chemistry B*, 2007, 111.1: 2-7.
- [4] YU, Shu-Jung, et al. Bright fluorescent nanodiamonds: no photobleaching and low cytotoxicity. *Journal of the American Chemical Society*, 2005, 127.50: 17604-17605.
- [5] MOCHALIN, Vadym N., et al. The properties and applications of nanodiamonds. *Nature nanotechnology*, 2012, 7.1: 11-23.
- [6] ŠLEGEROVÁ, Jitka a Petr CÍGLER. Nanodiamanty – fluorescenční a zobrazovací nanosondy. *Chemické listy*. 2015, **2014**(108), 7.
- [7] SCHIRHAGL, Romana, et al. Nitrogen-vacancy centers in diamond: nanoscale sensors for physics and biology. *Annual review of physical chemistry*, 2014, 65: 83-105.
- [8] FU, Chi-Cheng, et al. Characterization and application of single fluorescent nanodiamonds as cellular biomarkers. *Proceedings of the National Academy of Sciences*, 2007, 104.3: 727-732.
- [9] PETRAKOVA, V., et al. Imaging of transfection and intracellular release of intact, non-labeled DNA using fluorescent nanodiamonds. *Nanoscale*, 2016, 8.23: 12002-12012.
- [10] LIAUGAUDAS, G., et al. Luminescence lifetimes of neutral nitrogen-vacancy centres in synthetic diamond containing nitrogen. *Journal of Physics: Condensed Matter*, 2012, 24.43: 435503.
- [11] LIAUGAUDAS, Gediminas, et al. Luminescence-lifetime mapping in diamond. *Journal of Physics: Condensed Matter*, 2009, 21.36: 364210.
- [12] PETRÁKOVÁ, Vladimíra, et al. Luminescence of nanodiamond driven by atomic functionalization: towards novel detection principles. *Advanced Functional Materials*, 2012, 22.4: 812-819.

- [13] KRATOCHVÍLOVÁ, Irena, et al. Tuning of nanodiamond particles' optical properties by structural defects and surface modifications: DFT modelling. *Journal of Materials Chemistry*, 2011, 21.45: 18248-18255.
- [14] INAM, Faraz A., et al. Emission and nonradiative decay of nanodiamond NV centres in a low refractive index environment. *ACS nano*, 2013, 7.5: 3833-3843.
- [15] KHALID, Asma, et al. Lifetime Reduction and Enhanced Emission of Single Photon Color Centres in Nanodiamond via Surrounding Refractive Index Modification. *Scientific reports*, 2015, 5.
- [16] CHUNG, Kelvin; TOMLJENOVIC-HANIC, Snjezana. Emission Properties of Fluorescent Nanoparticles Determined by Their Optical Environment. *Nanomaterials*, 2015, 5.2: 895-905.
- [17] BEVERATOS, Alexios, et al. Nonclassical radiation from diamond nanocrystals. *Physical Review A*, 2001, 64.6: 061802.
- [18] MOHTASHAMI, Abbas; KOENDERINK, A. Femius. Suitability of nanodiamond nitrogen–vacancy centers for spontaneous emission control experiments. *New Journal of Physics*, 2013, 15.4: 043017.
- [19] BEAMS, Ryan, et al. Nanoscale fluorescence lifetime imaging of an optical antenna with a single diamond NV center. *Nano letters*, 2013, 13.8: 3807-3811.
- [20] STRICKLER, S. J.; BERG, Robert A. Relationship between absorption intensity and fluorescence lifetime of molecules. *The Journal of chemical physics*, 1962, 37.4: 814-822.
- [21] CHUNG, Pei-Hua; TREGIDGO, Carolyn; SUHLING, Klaus. Determining a fluorophore's transition dipole moment from fluorescence lifetime measurements in solvents of varying refractive index. *Methods and Applications in Fluorescence*, 2016, 4.4: 045001.
- [22] PIERSON, Hugh O. *Handbook of carbon, graphite, diamonds and fullerenes: processing, properties and applications*. William Andrew, 2012.
- [23] BREEDING, Christopher M.; SHIGLEY, James E. The “type” classification system of diamonds and its importance in gemology. *Gems & Gemology*, 2009, 45.2: 96-111.
- [24] COLLINS, Alan T. Optical centres produced in diamond by radiation damage. *New Diamond Front. Carbon Technol*, 2007, 17.2: 47.

- [25] WILLIAMS, Oliver A.; NESLÁDEK, Miloš. Growth and properties of nanocrystalline diamond films. *physica status solidi (a)*, 2006, 203.13: 3375-3386.
- [26] BOVENKERK, H. P., F. P. BUNDY, H., T. HALL, H. M. STRONG a R. H WENTORF. PREPARATION OF DIAMOND. *Nature*. 1959, (184), 1094-1098.
- [27] STEHLIK, Stepan, et al. Size and Purity Control of HPHT Nanodiamonds down to 1 nm. *The Journal of Physical Chemistry C*, 2015, 119.49: 27708-27720.
- [28] JELEZKO, F., et al. Spectroscopy of single NV centers in diamond. *Single Molecules*, 2001, 2.4: 255-260.
- [29] ZAITSEV, Alexander M. *Optical properties of diamond: a data handbook*. Springer Science & Business Media, 2013.
- [30] ADELTA, Milan et al. Study of time-resolved characteristics of nitrogen-vacancy centres in nanodiamond for biosensoric applications. *Instruments and Methods for Biology and Medicine 2016*. **2016**, 3-9. ISBN 978-80-01-06017-9.
- [31] SAY, J. M., et al. Fluorescent nanodiamonds for biological applications. In: *Quantum Electronics Conference & Lasers and Electro-Optics (CLEO/IQEC/PACIFIC RIM), 2011*. IEEE, 2011. p. 1708-1710.
- [32] SMITH, Bradley R., et al. Five-Nanometer Diamond with Luminescent Nitrogen-Vacancy Defect Centers. *Small*, 2009, 5.14: 1649-1653.
- [33] Introduction to Confocal Microscopy. *Olympus Microscopy* [online]. Olympus, 2012 [cit. 2017-04-25]. Available from:
<http://www.olympusmicro.com/primer/techniques/confocal/confocalintro.html>
- [34] YUAN, Yuehua; LEE, T. Randall. Contact angle and wetting properties. In: *Surface science techniques*. Springer Berlin Heidelberg, 2013. p. 3-34.
- [35] ADELTA, Milan. *Spectroscopy of NADH*. Kladno, 2015. Bachelor thesis. Czech Technical University of Prague.
- [36] HOFER, Ctirad. Barevné principy absorpce a fluorescence. *Masarykova univerzita* [online]. 2011 [cit. 2014-10-25]. Available from:
<http://is.muni.cz/el/1431/podzim2011/Bi7230/um/6053971/6056654/02_principy.pdf>

- [37] Time-Domain Lifetime Measurements. LAKOWICZ, Joseph R. *Principles of Fluorescence Spectroscopy*. 3rd. Singapore: Springer US, 2006, s. 98-157. ISBN 978-0-387-46312-4.
- [38] WAHL, Michael. *Time-Correlated Single Photon Counting*. Berlin, PicoQuant. 2014.
Available from:
https://www.picoquant.com/images/uploads/page/files/7253/technote_tcspsc.pdf
- [39] PICOQUANT. *MicroTime 200: User's Manual and Technical Data*. Version 5.1. Berlin
- [40] Fluorescence Lifetime Imaging (FLIM) in Confocal Microscopy Applications: An Overview. *PicoQuant* [online]. Berlin: PicoQuant [cit. 2017-04-25]. Available from:
https://www.picoquant.com/images/uploads/page/files/7350/appnote_flim_overview.pdf
- [41] Fluorescence Lifetime Imaging (FLIM): Imaging technique based on differences in the excited state decay rate. *PicoQuant* [online]. Berlin: PicoQuant [cit. 2017-04-26].
Available from: <https://www.picoquant.com/applications/category/life-science/fluorescence-lifetime-imaging-flim>
- [42] GERRITSEN, Hans C.; VAN DEN HEUVEL, Dave J.; AGRONSKAIA, Alexandra V. High-speed fluorescence lifetime imaging. In: *Biomedical Optics 2004*. International Society for Optics and Photonics, 2004. p. 77-87.
- [43] Antibunching. *PicoQuant* [online]. PicoQuant, 2016 [cit. 2017-04-22]. Available from:
<https://www.picoquant.com/applications/category/metrology/antibunching#description>
- [44] KHALID, Asma, et al. Synthesis and characterization of biocompatible nanodiamond-silk hybrid material. *Biomedical optics express*, 2014, 5.2: 596-608.
- [45] BECKER, Wolfgang; BERGMANN, Axel. Lifetime imaging techniques for optical microscopy. *Technical report, Becker & Hickl GmbH*, 2003.
- [46] Fit fluorescence intensity decays. *FluorTools* [online]. Copenhagen: FluorTools, 2015 [cit. 2017-04-26]. Available from:
<http://www.fluortools.com/software/decayfit/documentation/fit>
- [47] LEUNG, Regina Won Kay; YEH, Shu-Chi Allison; FANG, Qiyin. Effects of incomplete decay in fluorescence lifetime estimation. *Biomedical optics express*, 2011, 2.9: 2517-2531.

- [48] IRF. *Time Correlated Single Photon Counting Wiki* [online]. 2014 [cit. 2017-03-26]. Available from: <http://www.tcspc.com/doku.php/glossary:irf>
- [49] Fundamentals of Semiconductor Fabrication. *Fundamentals of Semiconductor Manufacturing and Process Control*. Hoboken: John Wiley, 2006, s. 158. ISBN 0471790273.
- [50] HALE, George M.; QUERRY, Marvin R. Optical constants of water in the 200-nm to 200- μ m wavelength region. *Applied optics*, 1973, 12.3: 555-563.
- [51] SCHELL, Andreas W., et al. Scanning single quantum emitter fluorescence lifetime imaging: quantitative analysis of the local density of photonic states. *Nano letters*, 2014, 14.5: 2623-2627.
- [52] GONG, Jianxiao; STEINSULTZ, Nat; OUYANG, Min. Nanodiamond-based nanostructures for coupling nitrogen-vacancy centres to metal nanoparticles and semiconductor quantum dots. *Nature communications*, 2016, 7.
- [53] REHOR, Ivan, et al. Fluorescent nanodiamonds embedded in biocompatible translucent shells. *Small*, 2014, 10.6: 1106-1115.
- [54] CHAPMAN, Robert; PLAKHOTNIK, Taras. Quantitative luminescence microscopy on Nitrogen-Vacancy Centres in diamond: Saturation effects under pulsed excitation. *Chemical Physics Letters*, 2011, 507.1: 190-194.
- [55] Absorption Cross Section. *Springer Nature* [online]. New York: Springer [cit. 2017-04-24]. Available from: https://link.springer.com/referenceworkentry/10.1007%2F978-3-642-11274-4_8
- [56] PETRAKOVA, Vladimira. *Interactions of nitrogen-vacancy centers with charged surfaces of functionalized nanodiamond particles for the detection of cellular processes*. Kladno, 2012. Doctoral Thesis.
- [57] SILLEN, Alain; ENGELBORGHS, Yves. The correct use of “average” fluorescence parameters. *Photochemistry and photobiology*, 1998, 67.5: 475-486.